



Terms and Conditions of Use of Digitised Theses from Trinity College Library Dublin

Copyright statement

All material supplied by Trinity College Library is protected by copyright (under the Copyright and Related Rights Act, 2000 as amended) and other relevant Intellectual Property Rights. By accessing and using a Digitised Thesis from Trinity College Library you acknowledge that all Intellectual Property Rights in any Works supplied are the sole and exclusive property of the copyright and/or other IPR holder. Specific copyright holders may not be explicitly identified. Use of materials from other sources within a thesis should not be construed as a claim over them.

A non-exclusive, non-transferable licence is hereby granted to those using or reproducing, in whole or in part, the material for valid purposes, providing the copyright owners are acknowledged using the normal conventions. Where specific permission to use material is required, this is identified and such permission must be sought from the copyright holder or agency cited.

Liability statement

By using a Digitised Thesis, I accept that Trinity College Dublin bears no legal responsibility for the accuracy, legality or comprehensiveness of materials contained within the thesis, and that Trinity College Dublin accepts no liability for indirect, consequential, or incidental, damages or losses arising from use of the thesis for whatever reason. Information located in a thesis may be subject to specific use constraints, details of which may not be explicitly described. It is the responsibility of potential and actual users to be aware of such constraints and to abide by them. By making use of material from a digitised thesis, you accept these copyright and disclaimer provisions. Where it is brought to the attention of Trinity College Library that there may be a breach of copyright or other restraint, it is the policy to withdraw or take down access to a thesis while the issue is being resolved.

Access Agreement

By using a Digitised Thesis from Trinity College Library you are bound by the following Terms & Conditions. Please read them carefully.

I have read and I understand the following statement: All material supplied via a Digitised Thesis from Trinity College Library is protected by copyright and other intellectual property rights, and duplication or sale of all or part of any of a thesis is not permitted, except that material may be duplicated by you for your research use or for educational purposes in electronic or print form providing the copyright owners are acknowledged using the normal conventions. You must obtain permission for any other use. Electronic or print copies may not be offered, whether for sale or otherwise to anyone. This copy has been supplied on the understanding that it is copyright material and that no quotation from the thesis may be published without proper acknowledgement.

Prediction of Fatigue Failure in Engineering Components Using the Finite Element Method

Ge Wang

Submitted in fulfilment of the requirements for the award of the degree of Doctor of
Philosophy to The University of Dublin, Trinity College, October 1999.

Supervisor: Professor David Taylor

The work presented in this thesis was conducted at the Department of Mechanical and
Manufacturing Engineering, University of Dublin, Trinity College Dublin, Ireland.

Table of Contents

<i>Table of Contents</i>	<i>i</i>
<i>Declaration</i>	<i>v</i>
<i>Acknowledgements</i>	<i>vi</i>
<i>Summary</i>	<i>vii</i>
<i>Nomenclature</i>	<i>viii</i>
Chapter 1 Introduction	1
Chapter 2 Review of the Literature	3
2.1 Traditional Approaches for Prediction of Fatigue Failure	3
2.1.1 Stress life method.....	3
2.1.2 Strain life method.....	4
2.1.3 Critical distance methods	5
2.2 Fracture Mechanics Methods	6
2.2.1 Smith and Miller method.....	7
2.2.2 Crack Modelling Method	9
2.3 Consideration of Crack Closure and Defect Effects	11
2.3.1 Newman’s model, considering crack closure.....	11
2.3.2 Murakami and Endo’s model: considering defects and hardness.....	12
2.4 Short Crack Problems	14
2.4.1 Kitagawa and Takahashi Curve	15
2.4.2 ElHaddad Model: parameter a_0	16
Chapter 3 Further Study of the Crack Modelling Method	19
3.1 Introduction	19
3.2 The Focus Path	19
3.2.1 Path orientation, the rule of lowest ΔK_{FE}	19
3.2.2 Minimum distance	26
3.2.2 Maximum distance.....	30

3.3 The Effects of Mesh Density	34
3.4 Conclusions.....	39
Chapter 4 Modification of CMM for the Short Crack Problem.....	40
4.1 Introduction	40
4.2 Method 1 – Comparing with $\Delta\sigma_0$.....	40
4.3 Method 2 –Using a_w as the equivalent crack length.....	44
4.4 Method 3 – Adding a_0 or extrapolating the stress/distance curve	48
4.5 Method 4 – Average of NM & CMM.....	51
4.6 Conclusions.....	54
Chapter 5 A New Method of Prediction	56
5.1 Introduction	56
5.2 Background of the Theoretical Model	56
5.3 New Approach to Find the Critical Distance.....	57
5.3.1 Point Method.....	59
5.3.2 Line Method.....	60
5.3.3 Area Method.....	61
5.4 Application of the Model to Short Cracks	63
5.5 Application of the Model to Notches	65
5.6 Discussion	66
5.6.1 Input parameters needed.....	66
5.6.2 Comparison of the new methods with previous approaches	66
5.6.3 Extension to other loading modes.....	67
5.6.4 Further work.....	68
5.7 Conclusions.....	69
Chapter 6 Notched Specimen Verification.....	70
6.1 Introduction	70

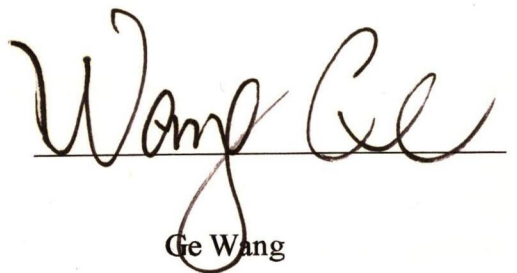
6.2 Experimental Details	71
6.2.1 Steel samples	71
6.2.2 Aluminium alloy samples	73
6.2.3 Cast iron samples	74
6.3 Stress Analysis	75
6.3.1 Element type	75
6.3.2 Load condition	76
6.4 Definition of Prediction Error.....	77
6.5 Prediction Results.....	78
6.5.1 Verification of steel samples	79
6.5.2 Verification of aluminium alloy samples	89
6.5.3 Verification of cast iron samples	92
6.5.4 Summary of verification.....	93
6.6 Discussion	94
6.7 Conclusions.....	97
Chapter 7 Prediction of The Fatigue Failure in Engineering Components	99
7.1 Marine Component.....	99
7.1.1 Fatigue failure description.....	99
7.1.2 Prediction results from CMM, PM and NM	101
7.1.3 Conclusions	102
7.2 Crankshaft.....	102
7.2.1 Introduction	102
7.2.2 Material and experimental data	103
7.2.3 Prediction result	105
7.2.4 Conclusions	106
7.3 Camshaft.....	107
7.3.1 Introduction	107
7.3.2 Experimental details	107
7.3.3 Results	108

7.3.4 Finite element analysis	112
7.3.5 Prediction of fatigue limit.....	113
7.3.6 Discussion	116
7.3.7 Conclusions.....	117
7.4 Al-alloy Components	118
7.4.1 Introduction.....	118
7.4.2 Experimental details	118
7.4.3 Results	123
7.4.4 Estimation of threshold ΔK_{th}	126
7.4.4.1 Short crack effect.....	126
7.4.4.2 Procedure.....	126
7.4.4.3 Prediction results	127
7.4.4.4 Kitagawa and Takahashi curves of LM25	127
7.4.5 Fatigue failure prediction	128
7.4.5.1 Definition of σ - r curve path.....	128
7.4.5.2 Prediction results and discussion.....	131
7.4.6 Conclusions	133
7.5 General Conclusions for the Application to Engineering Components	133
<i>Chapter 8 Discussion, General Methodology and Conclusions</i>	<i>135</i>
8.1 Discussion	135
8.1.1 Overview of Chapters 6 and 7.....	135
8.1.2 Critical distance methods	137
8.1.3 Crack Modelling Method combined with the Notch Method.....	138
8.2 General Methodology	139
8.3 Conclusions.....	143
<i>References</i>	<i>145</i>

Declaration

I declare that the present work has not been submitted as an exercise for a degree at any other University. This thesis consists entirely of my own work except where references indicate otherwise.

I agree that the library of the University of Dublin, Trinity College, Dublin may lend or copy this thesis upon request.


Ge Wang

Acknowledgements

I would like to thank all those who helped in this research. In particular I would like to thank and congratulate my supervisor Professor David Taylor, for his guidance, suggestions, advice, insight and help in creating this thesis. I would also like to thank him for my involvement in the Rover Group and IDAC Ltd, which were beneficial to my research.

I am very grateful to all the technical staff, Frank, John, Ray, Tom, Gabriel, Gerry and Danny for all their help and friendship. A special thanks to Peter and Sean who were always willing to give up their time to help with my research. I am very grateful to Virginia and Joan for their kind help.

The financial support provided by Materials Ireland, Enterprise Ireland and Rover are gratefully acknowledged.

I am also very grateful to all the postgraduates and staff at Trinity College, for it was they who made my stay enjoyable, in particular I would like to thank Conor, Magali, Carlos, Peter, Damien, Liam, Darren, Gavin, Bruce, Suzanne and Linda. I would especially like to thank Jeff Badger and Toman MacGinley for their advice, letter writing abilities, computer skill and their friendship. I would also like to thank Dr. Youhe Zhang for his kind help and friendship.

I would like to convey my deepest appreciation to my mother and father, my parents in law, for their continuous support, encouragement, help, advice and patience.

Finally I would like to thank my one true friend, my wife, Dingqun, without you I would have never have completed this work and thank you for showing me the good side to everything. I would like to thank my lovely daughter, Jue, for her understanding of my going abroad for research at her early age.

Summary

Prediction of fatigue failure in engineering artefacts is becoming increasingly important as we enter the third millennium; more catastrophic fatigue failures will occur as engineers push the limits of design even further due to demands for greater efficiency. This thesis describes a methodology for predicting fatigue failure in engineering components subjected to high cycle fatigue using the finite element analysis method.

The research started from a previous theory known as the “crack modelling method”, which considers the whole stress field and models a geometrical discontinuity as a crack. Further study of the theory was carried out and improvements were made for application to the short crack/notch problem. Because of the difficulty of judging whether a defect in a given component would behave as a short crack or not in practice, a new approach was developed. The method was still based on a consideration of the stress field of the component, but attention was focussed on a small region close to the stress concentration. The method avoids the problem because it inherently allows for short crack effects. The basic theory was formulated and tested, with respect to standard test specimens, for which data was found from the literature. The effect of notch depth, of notch acuity, of notch and specimen type, of load ratio, and of material properties on the notched fatigue limit were considered. The theory showed good predictions. The implication of this research is that there is no fundamental difference between the fatigue limit of an uncracked body and that of a body which already contains a crack. The theory was also tested on real components used in vehicles, including a crankshaft, camshaft, pump bracket and C-shaped bracket. Good predictions were achieved in all cases.

A general methodology was devised which combined the new method, the previous method and traditional methods. It is intended that the methodology will meet every possibility which could occur in engineering applications. The methodology can be incorporated into software which will address the requirement of “design right at first time” for industries.

Nomenclature

Symbol	Unit	Definition
\sqrt{area}	mm	Murakami defect geometrical parameter
a	mm	Crack length
a_o	mm	ElHaddad crack-length constant
a_1, a_2	mm	Taylor and Knott crack length related to short crack
a_{eq}	mm	Equivalent crack length
a_w	mm	Half crack length of a central crack in an infinite plate
AM		Area Method
A_n		Constant whose value depends on the strength and ductility of the material
Ave.		Average Method
C		Constant factor in the Paris equation
CMM		Crack Modelling Method
CMMscr		Crack Modelling Method with short crack correction
CNB		Circumferential notch cylindrical bar
CNP		Centre notch in a flat plate
D	mm	Notch depth
da/dN		Crack growth rate
DENP		Double edge notch in flat plate
d_p		Peripheral density factor
d_r		Radial density factor
ElHaddad		LEFM prediction modified using ElHaddad's correction
F		Geometrical factor in the stress intensity equation
f_v		Volume fraction of graphite
H	mm	Notched specimen height
h	mm	Effective height of plain specimen

H_v		Vickers micro-hardness
$H_{v,gross}$		Gross Vickers hardness value including the contribution of graphite nodules
K	MPa m ^{1/2}	Stress intensity factor
K&L		Klesnil and Lucas Method
K_f		Fatigue notch factor
K_t		Theoretical elastic stress concentration factor
K_t^*		Critical value of K_t
K_ε		Strain concentration factor
K_σ		Stress concentration factor
L	mm	Notched specimen length
l	mm	Effective length of plain specimen
LEFM		Standard crack prediction method following Smith and Miller when applied to notches
LM		Line Method
l_p	mm	Average element length round a fillet or a notch root
l_r	mm	Average element length along the radial direction
n		Empirical exponent in the Paris equation
Nf		Fatigue cycles to failure
NM		Notch Method
PM		Point Method
r	mm	Distance from notch/crack tip or stress concentration
R		Load ratio
r_{min}, r_{max}	mm	Minimum and maximum distance of a stress-distance curve
SENP		Single edge notch in flat plate
W	mm	Notched specimen thickness
ΔF_Y	N	Axial input force applied to a finite element model
ΔK	MPa m ^{1/2}	Range of the stress intensity factor
ΔK_{FE}	MPa m ^{1/2}	Predicted threshold stress intensity factor range using FEA
ΔK_{th}	MPa m ^{1/2}	Threshold stress intensity factor range
ΔM	Nm	Bending moment range

ΔP_{FE}		Load range applied to a finite element model
ΔP_o		Predicted fatigue limit load range
ΔP_T		Experimental value of fatigue limit range
$\Delta \sigma$	MPa	Stress range
$\Delta \sigma_o$	MPa	Fatigue limit of plain specimens
$\Delta \sigma_{oc}$	MPa	Fatigue limit of cracked specimens (nominal stress)
$\Delta \sigma_{on}$	MPa	Fatigue limit of notched specimens (nominal stress)
$\Delta \sigma_{PRED}$	MPa	Predicted fatigue limit
$\Delta \sigma_{th}$	MPa	Threshold stress range
$\Delta \sigma_{gross}$	MPa	Fatigue limit in gross-section
T	mm	Plain specimen thickness
α, β	Degrees	Angle of the path of a stress-distance curve
χ	mm	Distance measured from centre of a hole
δ	mm	Distance between the axis and the point where ΔF_Y is applied
ϕ	mm	Specimen diameter
η		Correcting factor for short crack effect
ρ	mm	Notch root radius
ρ^*	mm	Critical value of ρ
σ	MPa	Stress
σ_{cy}	MPa	Cyclic yield stress
$\sigma-r$		Stress-distance curve
σ_w	MPa	Tensile stress applied to an infinite plate in Westergaard's equation
σ_y	MPa	Yield stress

Chapter 1 Introduction

Fatigue is the most common cause of failure of engineering structures and components. Making reliable fatigue predictions is very difficult because knowledge about fatigue mechanisms in all stages of the fatigue process must be developed much further. Despite the huge volume of research which has been conducted in this area and many hundreds of papers and reports published each year on the problem of fatigue life prediction, it remains the principal limitation on the life prediction of components, especially components such as aircraft, vehicles, medical devices and machine tools.

The aim of the present research has been to develop methods of analysis for the prediction of the high cycle fatigue (HCF) behaviour in engineering components using the finite element analysis (FEA) method. Traditional methods, which compute fatigue life on a point-by-point basis, could not give a satisfied prediction when applied to high stress concentrations (e.g. sharp notches) or to materials of low notch-sensitivity (e.g. cast iron). The reason is that very high stresses can be tolerated by a component provided they are restricted to small regions of the component and then there is no one to one relationship between stress and life.

The crack modelling method developed by Taylor [1996], which considers the whole stress field and models the geometrical feature, such as a notch, a hole and a corner, as a crack, was tried in this thesis. Further study was done on the method, such as the path determination, the minimum and maximum distance. With these improvements the method was tested using some simple specimens from the literature and in-house. The method was also tested on a real engineering component which was used by Rover car company. The results were very promising in many cases.

However, a problem was identified when short cracks/notches occurred. The crack modelling method did not account for the short crack effect in reducing the fatigue strength of the specimens or components. The problems are more significant in low notch-sensitive

materials such as cast irons, cast aluminium alloys. Several attempts were tried to modify the method in order to overcome the difficulties. These included adding a material constant, adding a short crack length in a notched body and combining the method with a traditional stress-life method. Different modifications were made for different situations and the revised method was tested on notched specimens showing short crack effect. The prediction results on the simple geometrical specimens showed a good agreement with the experimental data.

However, a problem arose when faced with real engineering components with complex geometry. The difficulty was how to know whether a given geometrical feature would be a short crack problem or not. We went back to basics and made big modifications to the previous theory. The new theory was devised based on a consideration of the stress field of the component, but now attention was focussed on a small region close to the stress concentration. Three methods were formulated: the point method, the line method and the area method. Each of them has its own advantage. They inherently allowed for the short crack effect, so they should avoid the problem found in the previous approach theoretically.

Ten methods including traditional stress-life methods, the crack modelling method and its revised versions and the new methods were tested on standard test specimens, for which data can be found from the literature. The effect of notch depth, of notch acuity, of notch and specimen type, of load ratio, and of material properties on the threshold stresses were considered. The theory showed good predictions on 90 percent of forty-six data sets. Furthermore, four types of real components were used for testing thanks to Rover Car Company and GEC Ltd. Some of the components had surface effects and for some of them we needed to measure the fatigue threshold. All these difficulties were overcome and good results were obtained, showing that the new methods can be applied to real components.

A general methodology was devised which combined all the methods. It is hoped that the methodology will meet every possibility which could occur in engineering applications. The theory was written into computer software to interface with FEA, to meet the requirement of "design right at first time" from industries. Some problems still remain and need further work.

Chapter 2 Review of the Literature

Engineering structures invariably contain stress concentrations which are the principal sites for the inception of fatigue flaws. The stress and deformation fields in the immediate vicinity of the stress concentration have a strong bearing on how the fatigue cracks nucleate and propagate. Continuum approaches on this topic can be divided into four categories. They are traditional approaches (which include stress-life, strain-life and critical distances), fracture mechanics concepts, crack closure & defect effects and the short crack problem.

The effect of stress concentrators on fatigue limit and high-cycle endurance has traditionally been studied using notches. The simplest approach – using the elastic stress-concentration factor K_t – is reasonably accurate for blunt notches under low applied stress, but K_t is found to diverge from the experimentally measured fatigue strength reduction, K_f , when notches are sharp or when the notch depth, D , is small. Relevant factors include the existence of the plastic zone and the relatively small stressed volume ahead of a sharp notch.

2.1 Traditional Approaches for Prediction of Fatigue Failure

2.1.1 Stress life method

The stress-life approach is used for high-cycle fatigue failures ahead of stress concentrations. High cycle fatigue (HCF) is caused by low, nominally elastic fluctuating stresses. The prediction of fatigue failure is made by appropriately modifying the smooth specimen (unnotched) endurance limit.

The theoretical elastic stress concentration factor K_t , which relates the local stress ahead of the notch tip to far-field loading, is defined as the ratio of the maximum local stress σ_{\max} to the nominal stress σ . K_t is a function only of the component geometry and loading mode and is available from handbooks [Peterson, 1953; 1974]. For the stress at the end of an elliptic hole [Smith, 1982],

$$K_t = 1 + 2\sqrt{D/\rho} \quad (2-1-1)$$

where ρ is the radius at the ends of the ellipse and D is the depth (half width) of the elliptical hole.

The stress-life method is unsuitable for situations where considerable plastic deformation occurs ahead of the stress concentration.

2.1.2 Strain life method

The local strain approach relates deformation occurring in the immediate vicinity of a stress concentration to the remote stresses and strains using the constitutive response determined from fatigue tests on simple laboratory specimens. The method predicts the life expectancy of a machine part which is under low cycle fatigue loads. Low cycle fatigue (LCF) is caused by high, fluctuating stresses and strains. The method has its beginning in the early 1950s. Today it is still in frequent use by machine designers in LCF and HCF analyses and it is recommended by ASME [ASME, 1989], SAE [Rice, 1988] and ASTM [ASTM, 1980].

The strain concentration factor K_ϵ is the ratio of the maximum local strain to the nominal strain. The stress and strain concentration factors are of the same value when only elastic deformation occurs at the tip of the notch. However, once the material yields at the notch tip, the stress and strain concentration factors take different values. Under conditions of plastic deformation, the theoretical elastic stress concentration factor is given approximately by the geometrical mean of the stress K_σ and strain concentration factors K_ϵ . This is the well-known Neuber rule [Neuber, 1961]:

$$K_t = \sqrt{K_\sigma K_\epsilon} \quad (2-1-2)$$

Satisfactory predictions of the fatigue behaviour in notched members of a wide variety of steels were provided by modifying and applying the rule to fatigue loading conditions [Topper et al, 1969; Dowling et al, 1977]. These analyses can be divided into two steps:

First, the local stress and strain histories at the notch tip must be known. Second, the fatigue life that can be expected for the local stress and strain histories must be determined. For the first part, either simple analytical expressions or detailed finite element simulations of the notch tip deformation (using constitutive laws and hardening rules) are developed to relate the local stresses and strains to far-field loading. Alternatively, the notch tip deformation is experimentally monitored with the aid of strain gauges or other displacement/strain measurement techniques.

2.1.3 Critical distance methods

Under fatigue loading conditions, the elastic stress concentration factor is replaced by the so-called fatigue notch factor:

$$K_f = \text{unnotched bar endurance limit} / \text{notched bar endurance limit} \quad (2-1-3)$$

Fatigue experiments suggest that notches produce a lower stress concentrating effect than predicted by theoretical elastic analysis, so $K_f < K_t$; $K_f \rightarrow K_t$ for large notch-root radii and for higher strength materials. K_f is determined empirically from experimental measurements. The critical distance method, which has a long history [Peterson, 1959; Neuber, 1958; Mitchell, 1979], is based on the idea of averaging stresses over some characteristic volume, which is material-dependant. Thus for a notch, especially if it is sharp and/or small in size, the stress range when averaged in this way will be significantly smaller than the hot-spot value. Normally the approach is simplified so that in practice one examines the stress at a given point (located a fixed distance from the hot-spot) which is assumed to be an estimate of the averaged stress: alternatively the solution can be expressed in terms of the hot-spot stress combined with the local stress gradient [Siebel and Stieler, 1955]. Methods of this kind are popular in industry because they are easy to use and do not require test data except the plain-specimen fatigue limit; also they can be easily adapted to FE analysis [Sheppard, 1991]. The main problem, however, is the size of the critical volume or distance. This is very material dependant, and can only be found using empirical rules, usually based on the material's UTS. Examples of these methods are as follows:

The Peterson equation for ferrous wrought alloys has the form

$$K_f = 1 + \frac{K_t - 1}{1 + A_n / \rho} \quad (2-1-4)$$

... where A_n is a constant whose value depends on the strength and ductility of the material and ρ is the notch-root radius. By considering the threshold condition for a crack of length a_0 at the notch root, Klesnil and Lucas [1980] derived an equation as follows:

$$K_f = \frac{K_t}{\sqrt{1 + 4.5a_0 / \rho}} \quad (2-1-5)$$

where a_0 is the ElHaddad crack-length constant (see Section 2.4.2).

2.2 Fracture Mechanics Methods

The most successful application of the theory of fracture mechanics is in the characterisation of fatigue crack propagation. One of the known methods is the method of linear elastic fracture mechanics (LEFM). It is designated to compute the crack propagation based on the fundamental assumption that the material is linearly elastic. This method basically approaches the crack propagation problems in 2-D space. For more complex cases an adaptation of the basic correlations is used. A very important parameter, called the stress intensity factor (SIF), was introduced, which signifies the relationship of three factors: the geometry of the plate, the loading, and the length of the crack. The stress intensity factor is defined as follows

$$K = F \sigma \sqrt{\pi a} \quad (2-2-1)$$

In the above, F is a compliance function that describes the geometry of the part, σ is a stress in a remote distance which designates the loading and a is the crack length. The crack growth can be expressed in the form of

$$\frac{da}{dN} = C(\Delta K)^n \quad (2-2-2)$$

where C is a constant factor, ΔK is the range of the stress intensity factor and n an empirical exponent. The equation is known as the fatigue crack propagation law [Paris and Endoyan, 1963]. Crack propagation ceases if $\Delta K < \Delta K_{th}$, the threshold value, which depends on the load ratio, R [Taylor, 1989]

2.2.1 Smith and Miller method

Smith and Miller's model [Smith and Miller, 1978] can be used for the prediction of fatigue failure on notched specimens including the prediction of non-propagating cracks. It is illustrated in Fig. 2.2.1, concerning notches with variable radius and constant depth D . We called it the Notch Method (NM). For low K_t (between A and B) the fatigue limit is given by

$$\Delta\sigma_{on} = \Delta\sigma_0 / K_t \quad (2-2-3)$$

where $\Delta\sigma_0$ is the fatigue limit of plain specimens and $\Delta\sigma_{on}$ is the fatigue limit of notched specimens. For high K_t (between B and C) the notch is assumed to behave like a crack, so the fatigue limit is given by

$$\Delta\sigma_{on} = \Delta K_{th} / F\sqrt{\pi D} \quad (2-2-4)$$

Non-propagating cracks will occur if the stress is below this value.

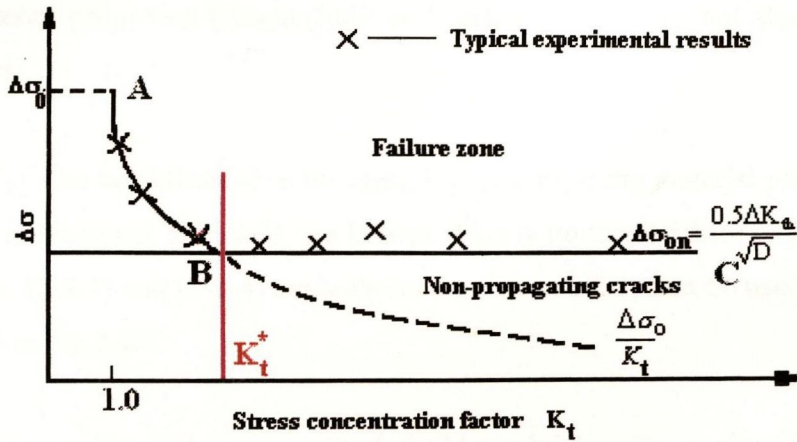


Fig. 2.2.1 The boundary conditions between failure and non-failure of variously notched specimens

This model gives good predictions for many materials such as mild steels and alloy steels [Taylor, 1994] in laboratory tests.

The curve will move up or down in the figure if the notch depth decreases or increases for a component. So there is not a fixed critical value for the varying notch depths. However there will be a critical value of the factor, K_t^* , existing at point B in the figure for a certain notch depth, D . At that point, both Eqs. (2-2-3) and (2-2-4) should give the same predictions. So the critical value can be determined by

$$K_t^* = \frac{\Delta\sigma F \sqrt{\pi D}}{\Delta K_{th}} \quad (2-2-5)$$

So for elliptical notches, for example;

$$\Delta K_{th} = \frac{\Delta\sigma F \sqrt{\pi D}}{1 + \sqrt{D/\rho^*}} \quad (2-2-6)$$

where ρ^* is a critical value of the notch tip ratio for the given D . Eq. (2-2-6) deals not only with the material properties (fatigue limit and material threshold) but also with geometry characteristics.

The value of ρ^* can be defined directly using Eq. (2-2-6), if the material properties, such as fatigue limit and material threshold, are known. This is quite useful for engineering design. Normally Eqs. (2-2-3) and (2-2-4) are both conservative so they can be used simultaneously at the point B in Fig.2.2.1.

A problem that remains is that this method could not be directly employed for components that do not contain notches, but instead have corners or other geometric features where the stress concentration occurs. This is because neither D nor F can be defined in these cases. This greatly reduces the use of this method in engineering applications.

2.2.2 Crack Modelling Method

The crack modelling method [Taylor, 1996] is an extension of the Smith and Miller model. This extension made the model available for the prediction of engineering components not only with notches but also with other geometric features.

The method examines the stress field in the region of the stress concentration, and compares this with the stress field that is known to exist around an ideal crack. Figure 2.2.2 describes the approach schematically. From an FE model of the component, loaded with some system of loads, L , a plot is obtained of stress as a function of distance, r , measured from the point of maximum stress. The curve in the plot was named as the Stress-Distance curve or σ - r curve for short. The curve is compared with the stress-distance plot from an ideal crack; the particular crack geometry chosen is the one examined by Westergaard [1939]: a central, through crack of length $2a_w$, in an infinite plate subjected to a tensile stress σ_w . This stress field is described by

$$\sigma = \sigma_w / [1 - (a_w / (a_w + r))^2]^{1/2} \quad (2-2-7)$$

The values of σ_w and a_w can be varied to obtain a best fit between the stress-distance curve of Eq. (2-2-7) and the curve obtained from FE data. When the best fit has been found, the appropriate K value is given by

$$K = \sigma_w \sqrt{\pi a_w} \quad (2-2-8)$$

This method assumes that if the equivalent ΔK is less than the threshold value of the material, at the appropriate R ratio, fatigue failure will not occur.

The great advantage of the method is that it uses fracture mechanics concepts without introducing a crack into the component. It examines the stress distribution in the region of hot spots just from linear-elastic FE analysis and just uses standard material properties such as the material threshold. No real crack model is needed. No plastic zone analysis is needed. All these greatly reduce the cost of the prediction.

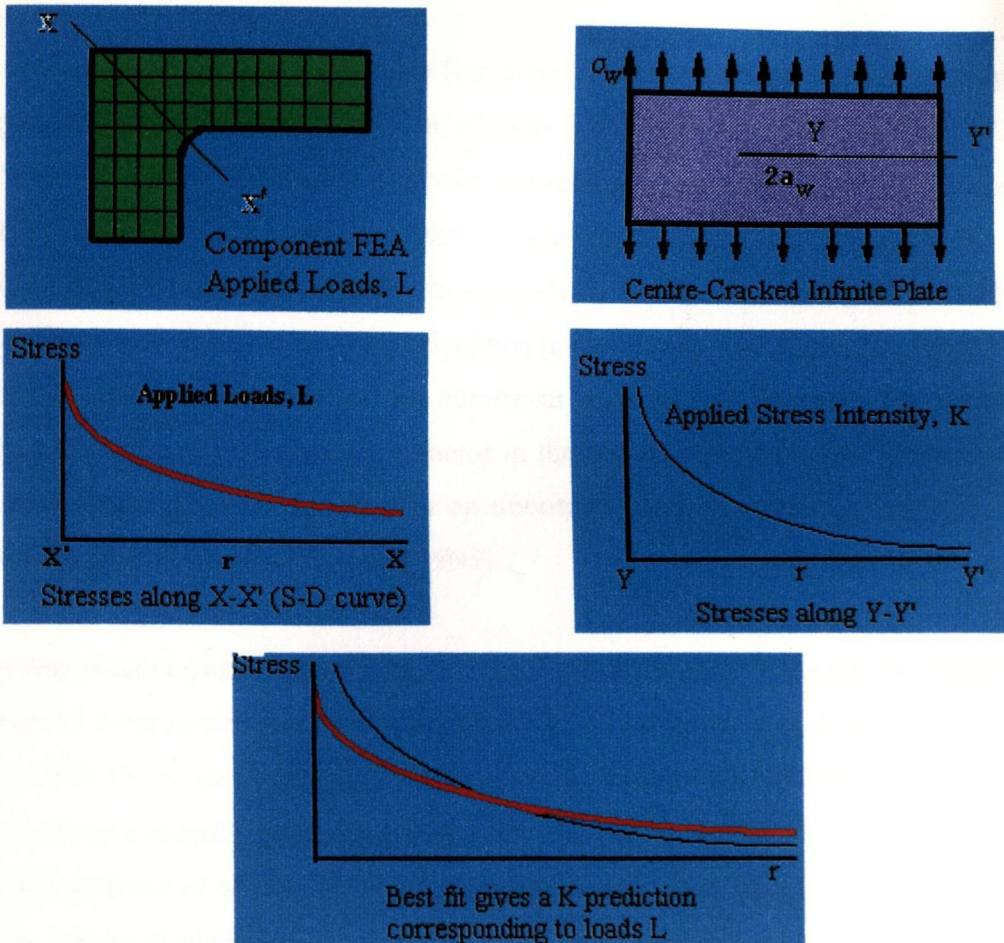


Fig. 2.2.2 Schematic illustration of the methodology used in the crack modelling technique

2.3 Consideration of Crack Closure and Defect Effects

2.3.1 Newman's model, considering crack closure

Fatigue crack closure is understood to play an important role in many aspects of fatigue crack growth (FCG) [Elber, 1968]. Although closure is not equally important in all FCG problems, and although closure does not provide a complete explanation of every problem where it is important, the closure phenomenon is an intrinsic feature of crack tip behaviour that must be considered in many problems. The elastic-plastic finite element (FE) method has been used successfully to study fatigue crack closure for more than twenty-five years [McClung, 1999].

The earliest investigations of closure based on the finite element method were published independently from 1973 to 1977. One of them is Newman's model [Newman, 1974; 1981; 1982; 1994], which is called a plasticity-induced crack-closure model. He believed that crack-closure effects are also one of the key elements in small-crack growth. His model is based on Elber's crack-closure phenomenon [Elber, 1970] and the Dugdale model [Dugdale, 1960]. Crack-opening stresses were calculated in the model. The J -integral [Rice, 1968], one of the commonly used parameters for non-linear crack-growth analyses, was used to define an equivalent plastic stress intensity factor in the elastic-plastic fracture mechanics regime. The model agreed well with test data on unnotched and notched specimens made of two aluminium alloys [Wu and Newman, 1993].

Many real closure problems are 3-D, but the computational expense of FE closure analysis has limited most previous investigations to 2-D. Chermhimi *et al.* [1988; 1989] performed the first 3-D FE closure analysis, studying closure through the thickness of a centre-cracked plate, and more recently publishing some very elementary results for a semi-elliptical surface crack [Chermhimi *et al.*, 1993]. They generally found higher opening levels at the specimen surface, similar to plane stress behaviour, and lower opening levels in the specimen interior, similar to plane strain behaviour. As computational power continues to increase, 3-D FE closure analysis should become more practical, and many important problems are waiting to be solved. However, careful study of 3-D modelling issues will be required before the results can be fully trusted.

2.3.2 Murakami and Endo's model: considering defects and hardness

Murakami and Endo [1983] proposed a model, which considered the defect effect, by introducing a new geometrical parameter \sqrt{area} for two-dimensional and three-dimensional defects. This parameter is based on both microscopic observation of cracking from small surface defects and 3-D numerical stress analysis. From their experiences, they derived the following formula: $\sigma_w^n \sqrt{area} = c$ with $n \approx 6$, where σ_w is the rotating bending or tension-compression fatigue limit; \sqrt{area} is defined as the square root of the defect area obtained by

projecting a defect or a crack onto the plane perpendicular to the maximum tensile stress. n and c are constants that have to be determined through fatigue tests.

The choice of \sqrt{area} comes from stress intensity factor considerations. Its application has been widespread, not only to the fatigue problems of small cracks and holes, but also to those of surface scratches and roughness, non-metallic inclusions, corrosion-pits, carbides in tool steels, second phases in Al-Si eutectic alloys and spheroidal graphites in cast irons.

Murakami and colleagues [Murakami *et al.*, 1990] further revised the model and proposed the following equations:

$$\Delta\sigma_w = 1.43(H_v + 120)(\sqrt{area})^{-1/6} \quad (2-3-1)$$

$$\Delta K_{th} = 3.3 \cdot 10^{-3}(H_v + 120)(\sqrt{area})^{1/3} \quad (2-3-2)$$

Here H_v is the Vickers micro-hardness; ΔK_{th} = threshold stress intensity factor range under the stress ratio $R = -1$ ($\text{MPa m}^{1/2}$); \sqrt{area} is in μm . The extended equation to predict the fatigue limit for various values of stress ratio R is expressed by including a factor, $\left(\frac{1-R}{2}\right)^\alpha$, in Eq. (2-3-1), where $\alpha = 0.226 + H_v \times 10^{-4}$. In predicting $\Delta\sigma_w$ by using Eq. (2-3-1), no fatigue test is necessary. It is sufficient to measure the values of \sqrt{area} and H_v and to estimate R at the place where the defect exists. They reported that the prediction error was less than 15% for $H_v = 100-740$.

In 1991, Endo [1991] proposed a modified equation of this method for nodular cast iron. Instead of introducing a parameter C , he used the matrix hardness and the percentage of graphite to predict the fatigue limit $\Delta\sigma_w$ and ΔK_{th} . This method therefore unifies both effects of defects and matrix structures:

$$\Delta\sigma_w = 1.43 * (H_{v,gross} / (1 - f_v) + 120) * (\sqrt{area})^{-1/6} \quad (2-3-3)$$

where $H_{v, gross}$ is the gross Vickers hardness value including the contribution of graphite nodules and f_v is the volume fraction of graphite. On the other hand, ΔK_{th} is defined as follows:

$$\Delta K_{th} = 3.3 * 10^{-3} * (H_v / (1 - f_v) + 120) * (\sqrt{area})^{1/3} \quad (2-3-4)$$

Murakami and Endo's model is valid over a \sqrt{area} range which is dependent on the material. The valid upper limit of \sqrt{area} is considered to be $\sim 1000 \mu\text{m}$. [Murakami and Endo, 1994].

2.4 Short Crack Problems

The fatigue life of a structure goes through several stages from crack initiation, through crack propagation, to the final failure. Miller [1993] indicated three categories of crack growth regimes for the whole period. They are the micro-structural fracture mechanics (MFM) regime, the elastic-plastic fracture mechanics (EPFM) regime and the linear elastic fracture mechanics (LEFM) regime. In the MFM and EPFM regimes, cracks are short and require a high stress range to propagate. Suresh and Ritchie [1984] suggested the following definitions by which short cracks can be broadly classified: microstructurally small, mechanically small, physically small and chemically small cracks. "Small cracks" and "short cracks" are often used interchangeably. However there is sometimes a distinction between the two cases. The former definition is employed for flaws that are small in all three dimensions. The latter types are taken to denote through-thickness flaws that are small in all but one dimension.

The prediction of fatigue failure for such short cracks results in consistently lower crack growth rates than the experimental data [Suresh, 1991] using standard threshold and Paris growth law concepts. This has been commonly attributed to several factors, including the influence of microstructure, plasticity-induced closure, roughness-induced closure and crack face bridging/interference.

Over the past decade, the propagation of short cracks in fatigue has received considerable attention. The behaviour of short fatigue cracks was reviewed in three books [Miller and de los Rios, 1986; Ritchie and Lankford, 1986; Suresh, 1991]. Quantitative attempts have been used to try to explain the propagation and have achieved some success in the correction of the propagation behaviour.

2.4.1 Kitagawa and Takahashi Curve

Kitagawa and Takahashi [1976] presented a figure similar to Fig. 2.3.1, which shows the boundary between propagating and non-propagating cracks.

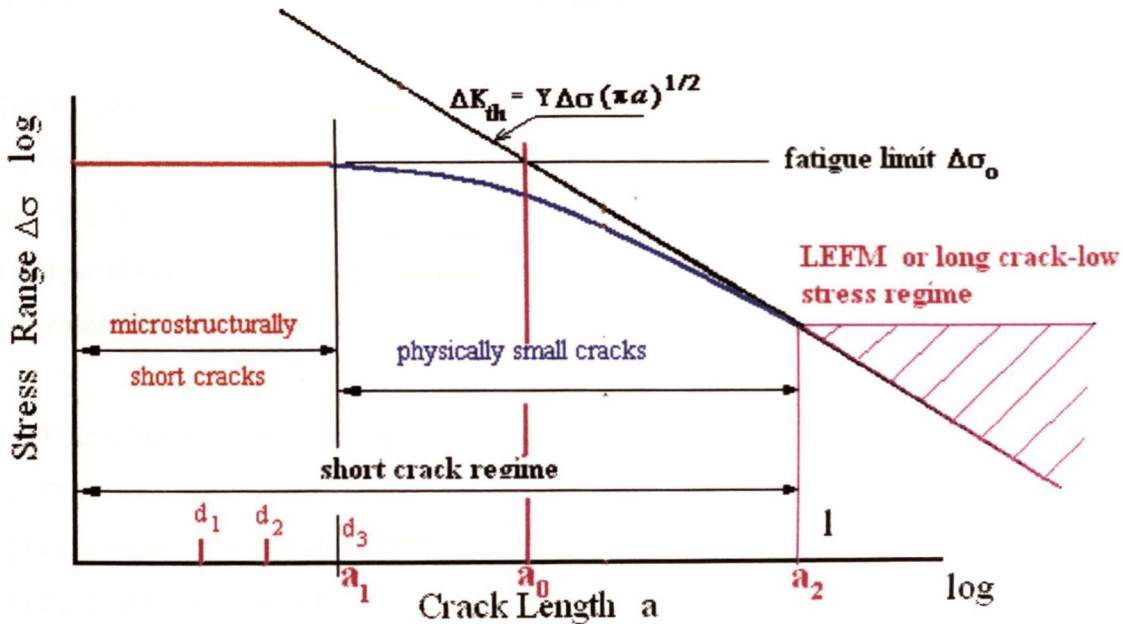


Fig.2.3.1. Schematic of the Kitagawa-Takahashi curve showing the boundary between propagating and non-propagating cracks

The line given by ΔK_{th} represents the threshold condition below which a crack should not grow if LEFM assumptions are valid. Obviously they are invalid when small scale yielding conditions are exceeded and this occurs to a greater or lesser extent when the term $\Delta\sigma$ exceeds about two thirds of the cyclic yield stress, σ_{cy} , in a reversed stress test. A second line on the Kitagawa-Takahashi plot is the fatigue limit itself. Obviously LEFM is not applicable at these levels of stress. An examination of the figure reveals why cracks can grow at levels

less than ΔK_{th} , but it should also be appreciated that cracks have been reported as growing on surfaces of plain specimens at stress levels below the fatigue limit. However, such cracks eventually stop propagating. This has made some people modify the curve in the microstructurally short region.

Several other lines can be drawn on the plot, i.e., d_1, d_2, d_3 , etc., to represent the size of microstructural units such as grain sizes, inclusion spacing, precipitation spacing, surface finish, etc., and these too will be expected to affect crack growth behaviour. The lengths at which the experimental data points merge with the plain specimen limit and the long-crack threshold were defined by Taylor and Knott [1981] as a_1 and a_2 , respectively. The so-called the short crack problem is concerned with any crack length that is within a_1 and a_2 .

But at crack lengths beyond microstructural effects, i.e., $a > a_2$, it is to be expected that a continuum mechanics approach will represent crack growth behaviour. However, LEFM analyses of crack tip fields may not be of sufficient accuracy at these stress levels to describe fatigue crack growth behaviour permitting correspondence between large structures and small laboratory specimens.

Therefore, fatigue cracks fall into three categories:

- (1) microstructurally short cracks: $a < a_1$;
- (2) long cracks sometimes termed as LEFM-type cracks: $a > a_2$;
- (3) transition length cracks: $a_1 < a < a_2$.

The first category of short cracks require high stresses for continuous propagation to failure, i.e., $\Delta\sigma > \Delta\sigma_0$. The second category is essentially for cracks in low elastic stress fields. The third category is essentially the short-crack category.

2.4.2 ElHaddad Model: parameter a_0

ElHaddad *et al* proposed a method for dealing with the short crack problem [ElHaddad *et al.*, 1979; 1980; ElHaddad and Miettinen, 1982]. The following expression was proposed in

which the elastic stress intensity factor (SIF) of a crack is modified by giving it an effective length of $(a+a_o)$

$$\Delta K = \Delta \sigma \sqrt{\pi(a+a_o)} \quad (2-4-1)$$

where $\Delta \sigma$ is the applied nominal stress range, and a_o is a constant for a given material and heat treatment. Actually it was Smith [1977] who first introduced the concept of the parameter a_o and named it as intrinsic crack length. The threshold stress at a very short crack length will approach the fatigue limit of the material ($\Delta \sigma_o$), based on small smooth specimens, and from Eq. (2-4-1) the threshold stress intensity ΔK_{th} can be obtained as

$$\Delta K_{th} = \Delta \sigma_o \sqrt{\pi a_o} \quad (2-4-2)$$

or

$$a_o = \left(\frac{\Delta K_{th}}{\Delta \sigma_o} \right)^2 \frac{1}{\pi} \quad (2-4-3)$$

These equations assume a geometry factor, F , equal to unity. Following this model, for any crack of length a , the threshold stress $\Delta \sigma_{th}$ is then obtained as:

$$\Delta \sigma_{th} = \frac{\Delta K_{th}}{\sqrt{\pi(a+a_o)}} \quad (2-4-4)$$

This relationship was tested with a series of experiments on steel and aluminium alloys by the authors. Short cracks were initiated at notches in these experiments and then they machined away the notches and determined the threshold stress levels for the cracks. Because cracks frequently start from notches, brittle materials that often break due to crack growth were sometimes referred to as notch sensitive. As stated in their papers, agreement of the

prediction of the model (Eq. (2-4-4)) and the test data were very good. Taylor and O'Donnell [1994] also tested this theory and found it to apply to a wide range of materials.

For many materials such as mild steels, alloy steels and other alloys, the values of a_o are very small [Ting and Lawrence, 1993] and can be neglected compared with notch depth. For example, A533B Steel, $a_o=0.0762$ mm; AISI4340 Steel, $a_o=0.0508$ mm; AL2024-T351 Alloy [DuQuesnay *et al*, 1986], $a_o =0.1016$ mm. Therefore, when $K_t > K_t^*$, the sharp notched specimens are 'crack-like', and Smith and Miller's model is quite efficient for predicting the fatigue failure. However, the correlation with experimental data was found to be very poor when Smith and Miller's model was used to test for the data of some other materials, like cast iron. Taylor and colleagues [Taylor *et al*, 1996] solved this problem by introducing a material constant, a_c . The notch depth is augmented by it, thus modelling the notch as a crack of length $(D+ a_c)$. It was shown that the value of a_c is similar to the short crack parameter a_o .

In ElHaddad's model the physical meaning of a_o is unclear. However it is a reasonable approximation. And the addition of the geometry factor, F , which contains a_o , to Eq. (2-2-8), may be better for getting a material constant, a_o . Combinations of Smith's model and ElHaddad's model could be used for prediction of fatigue failure in notched specimens or components.

Chapter 3 Further Study of the Crack Modelling Method

3.1 Introduction

The research in this thesis started from the crack modelling method (CMM). The previous work made by Taylor and his colleagues [Taylor and Lawless, 1996] had showed its success in 2-D problems and potential advantages in application on engineering components. Further work needed to be carried out in order to make the technique more suitable for a wide range of applications for both scientific and engineering usage. This work included the study of the path distance effect, the mesh density effect, and the path orientation effect. In this chapter, all these effects will be examined.

3.2 The Focus Path

The prerequisite for the application of CMM is that the geometric feature of a specimen or component has some features of a real crack, such as a $1/\sqrt{r}$ singularity. The method examines the stress field in the region of this feature. Furthermore only one path on which a stress-distance ($\sigma-r$) curve is determined in this region is needed for evaluating the stress intensity from the FEA, ΔK_{FE} . This specific path is defined as the “focus path”. Although previous work had shown some characteristics of the focus path, it is still worth discussing how to choose this path, in order to develop a systematic way of choosing this path which will be used throughout this work.

3.2.1 Path orientation, the rule of lowest ΔK_{FE}

The path for CMM is a straight line which radiates from the stress concentration point. Assuming that a fatigue crack is loaded in Mode I, where the crack's sides move perpendicularly apart, the opening stress, i.e. the maximum principal stress (MPS), will drive the crack to grow. So the path direction should represent the direction on which the crack will grow in general. Previous work has confirmed that this is a correct way to determine the path

direction [Taylor *et al*, 1997]. In that case, the direction of crack growth could be understood by examining a failed component. The prediction agreed well with the experimental data using the path direction. Also if the MPS direction is perpendicular to the crack front, the path direction should be normal to the MPS direction. It is true that the MPS direction will change during the crack propagation. Keeping the path normal to the MPS direction from the beginning to the end will be very difficult, and in doing so the path will be a curve instead of a straight line. However, we will not make the path like this. We concentrate on the total life of a component or specimen, in which crack initiation and early growth takes the most part. We assume that the MPS is the main driving force for fatigue failure. So the MPS direction here only refers to the MPS direction at or near to the stress concentration place.

Experimental testing was carried out on a single-edge notched specimen, which was subjected to pull-push loads; the notch depth was 3 mm; the material of the specimen was a cast Al-alloy, LM25; the fatigue limit of plain specimens $\Delta\sigma_0$ was 77.48MPa; the threshold ΔK_{th} was 5.97 MPa m^{1/2} [Wang *et al*, 1999]. The stress field was analysed using the finite element method. Fig. 3.2.2 shows MPS contour plot of the specimen. In this case, β , which is defined in Fig. 3.2.1, is equal to zero. Examining a failed specimen, a crack surface was at a symmetrical plane $\alpha = 0$, as shown in Fig.3.2.1. So the path should be at $\alpha = 0$. A series of lines are drawn with variable α values for comparison. Fig. 3.2.3 shows the $\Delta\sigma$ -r curves at variable α values. Fig.3.2.4 shows the effect of the path orientation on value of ΔK_{FE} , using applied load equal to the experimental fatigue limit.

At $\alpha = 0$, the prediction error is only 7.03%. It is evident that our assumption is right. Moreover, the value of α varied from 0° to 60° without any large change in ΔK_{FE} , and even at 60° the change in ΔK_{FE} was only 15%. This illustrates that the CMM is not sensitive to the path direction. This character is very good for applications.

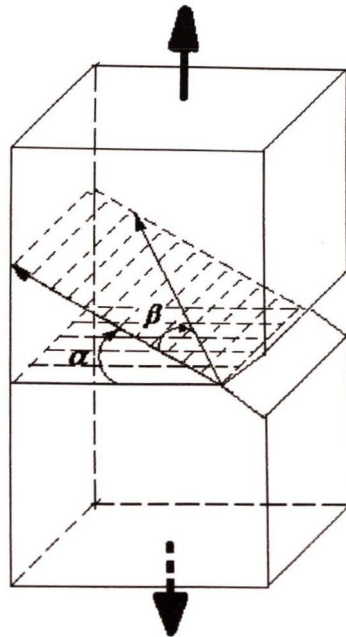


Fig. 3.2.1 Path choice on a 3D model of a single-edge notched specimen

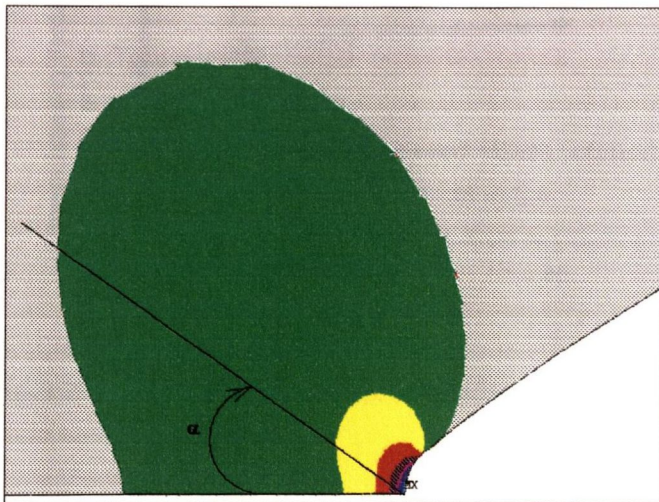


Fig.3.2.2 MPS contour plot of a single notched specimen and angle definition in 2D model

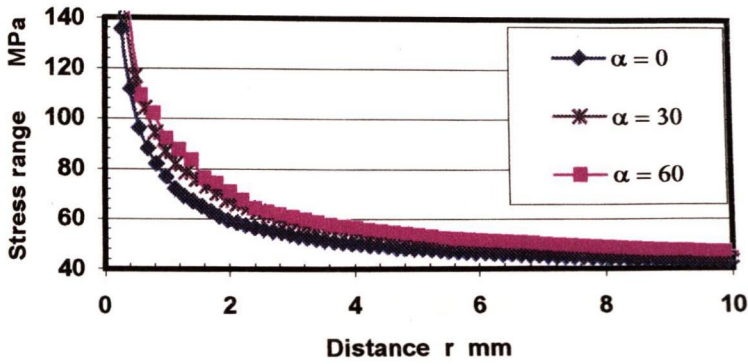


Fig. 3.2.3 $\Delta\sigma$ - r curves of the single notched specimen

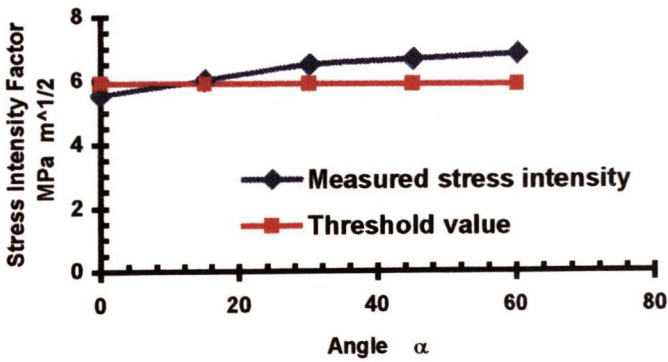


Fig.3.2.4 Path direction effect on predicted result using CMM

Considering the question that a crack path is unknown in a body, how do we choose the path orientation on a MPS contour plot? There should be a unique path for a given case

theoretically; if the value of ΔK_{FE} from the path is more than the threshold value, failure will occur. For the above example, the path is at $\alpha = 0$, which is normal to the MPS direction. How does this path differ from the others?

2D Stress Fields

The $\Delta\sigma-r$ curves in Fig.3.2.3 illustrate important information. For clarity only three curves, $\alpha = 0^\circ$, 30° and 60° , are shown. A distinguishable difference can be seen. Starting from an identical point, the hot spot, each curve has the same maximum stress value; ending at points where stress field tends to be uniform, the curves tend to be overlapped after a distance. The difference among each line is that the rates of the stress reduction with increasing r value are different. Increasing α reduces the rate of reduction; the highest rate is at $\alpha = 0$. All these result in variable ΔK_{FE} values when using CMM. The variation in a certain region is monotonic; a curve with a higher rate brings a lower ΔK_{FE} value. On the path $\alpha = 0$, the stress in the $\Delta\sigma - r$ curve decreases faster than from a path drawn at any other angle, as shown in the figure. This results in the lowest value of ΔK_{FE} from any other path. We call this phenomenon the “Rule of lowest ΔK_{FE} ”.

For a component with a complex geometry, a set of stress/distance curves would be drawn from the stress concentration point and the CMM could give a ΔK_{FE} value on each curve. However, only one from the path that is normal to the MPS direction is the right answer. The rule of lowest ΔK_{FE} can be used to identify the MPS direction and give the solution at the same time.

3D Stress Fields

In order to test the rule being available in a 3D stress field, two examples are shown below. The first example is a 3D model of the single-edge notched bar shown in Fig. 3.2.1. The size of the bar is 12x18x140 mm. A tensile stress of 60 MPa is applied to the end of the bar. The stress concentration place is located at the point F which can be seen if the figure, actually on both sides. From this point, a series of lines with variable α and β are drawn on the MPS

contour plot. Fig.3.2.5 shows the evaluation of ΔK_{FE} values using CMM on variable lines. The path of $\alpha = 0$ and $\beta = 0$ produces the lowest ΔK_{FE} as expected. It proves that the Rule of lowest ΔK_{FE} is right in this case. Also the results show that the difference on each path is small.

In a general 3D case where the crack path is not known, the path choice can be divided into two steps; the first step is drawing a plane which is normal to the MPS direction; the second step is drawing a series of lines in this plane, radiating from the hot-spot, and then selecting the line on which the ΔK_{FE} value is found to be lowest. Fig. 3.2.6 shows the detail of the path choice. The body is subjected to a load P; the hot spot is at F; $\mathbf{n}-\mathbf{n}'$ is the plane normal to the MPS direction.

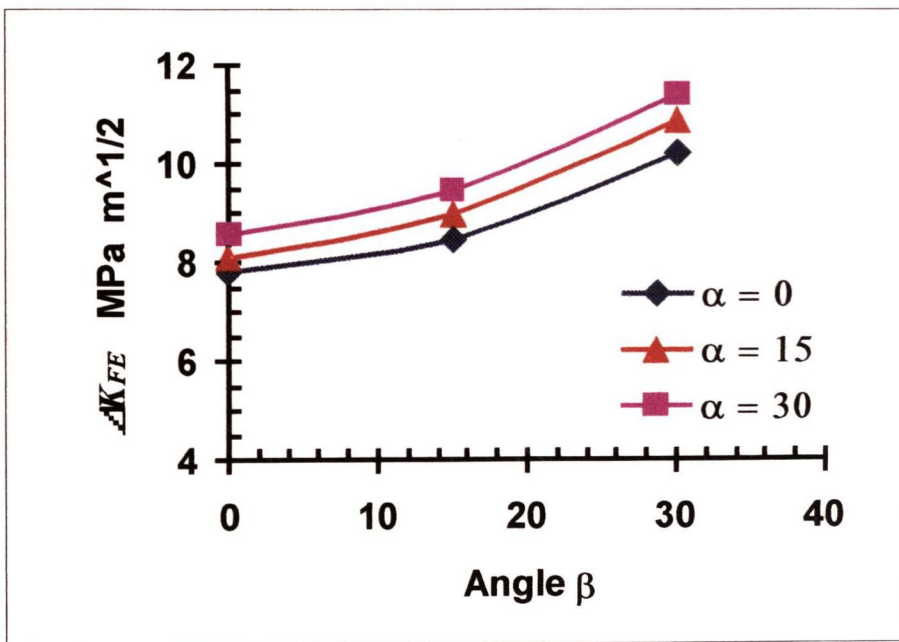


Fig. 3.2.5 Evaluation of ΔK_{FE} on the 3D model

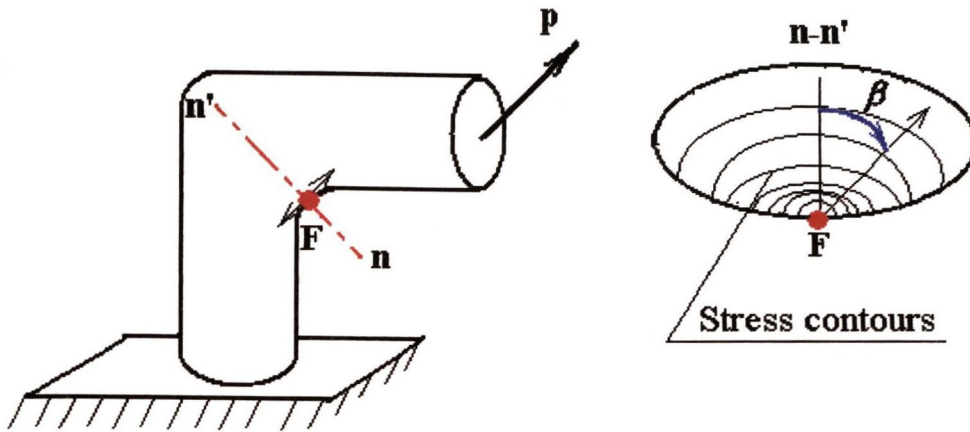


Fig. 3.2.6 Schematic illustration of choosing the path

The second example is a notched bar subjected to a torsion load (actually an automotive camshaft). The details of the fatigue test and the finite element analysis will be shown in Section 7.3. Fig. 3.2.7 shows the schematic illustration of the path choice in this situation. Considering a brittle material bar, such as a cast iron, subjected to torsion, \mathbf{M} , the crack plane, $\mathbf{n}-\mathbf{n}$, is 45° from an axis of the bar. This plane is normal to the MPS direction according to stress analysis. Assuming the fatigue failure starts from a point F , the stress condition at the point is illustrated in the figure; a series of lines are drawn radiating from this point; then the ΔK_{FE} values are evaluated using CMM. It is expected that the path of $\beta = 0^\circ$ will give the lowest ΔK_{FE} value. On the camshaft, the same process was carried out. The evaluating ΔK_{FE} values on each line are shown in Fig. 3.2.8. Because a notch existed, the path which gives the lower ΔK_{FE} value is not at $\beta = 0^\circ$; it is about at $\beta = 15^\circ$. However the difference in ΔK_{FE} between the two lines is very small, only 3.7%. Even at $\beta = 45^\circ$, the difference is still only 9.1%. This proves again that CMM is not sensitive to the path orientation. The threshold ΔK_{th} is $15.96 \text{ MPa m}^{1/2}$ so the prediction is very good in this case.

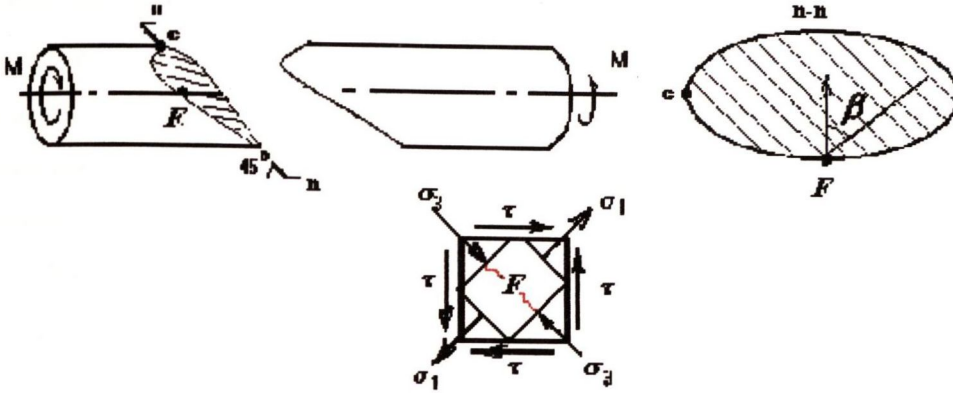


Fig. 3.2.7 Schematic illustration of the path choice in a bar subjected a torsion load, assuming a stress concentration at F .

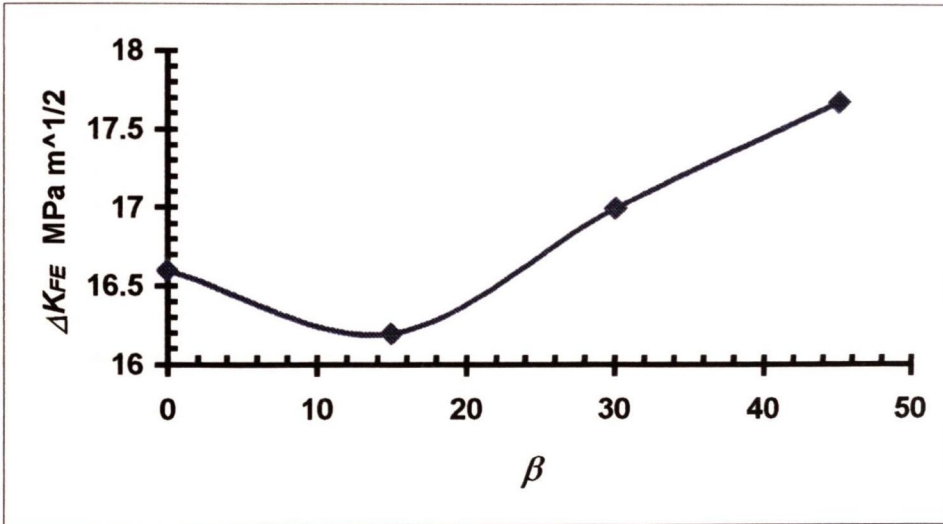


Fig. 3.2.8 Evaluating ΔK_{FE} values on variable lines for the camshaft

3.2.2 Minimum distance

For any $\Delta\sigma-r$ curve, the focus path is that part of the curve to be examined, which will be limited by the minimum distance r_{min} and maximum distance r_{max} , shown in Fig. 3.2.9. r_{min} can not be zero for the following reason. CMM produces a best fit between a curve from the

Westergaard equation and a $\Delta\sigma$ - r curve from the path mentioned above. The fit error, defined as the percentage difference between the area under the crack curve and the area under the $\Delta\sigma$ - r curve, is minimised. Eq. (2-2-6) gives a stress value of infinity at $r = 0$, whereas the FE data gives a finite stress at this point. If r_{min} were zero, the fit error would be infinite. This implies that the comparison of curves must begin at some value, r_{min} , shown in Fig. 3.2.9. Theoretically, r_{min} should be as small as possible, but avoid being zero. Numerically, it is impossible due to the limit of the FE mesh density. Three examples will now be highlighted, which show the effect of r_{min} on different materials, geometry and loads.

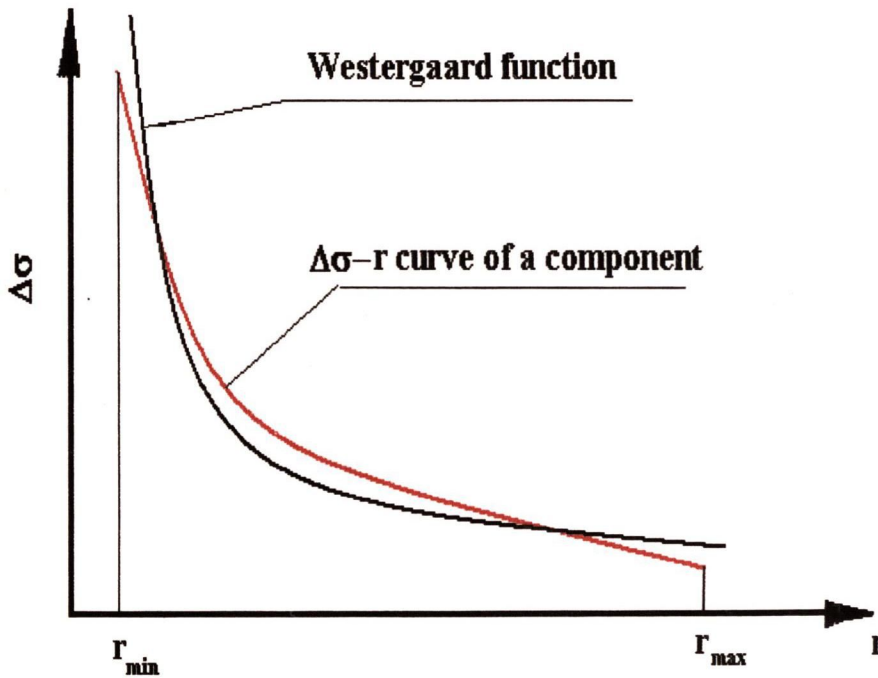


Fig. 3.2.9 Definition of the minimum distance and maximum distance

The first example is a single-edge notched specimen, as shown in the last section. The previous work suggested using $r_{min} = a_0$ [Taylor, 1996]. The underlying logic of this was that short fatigue cracks would initiate from the notch at an early stage. These cracks would typically grow to a length a_0 and would disrupt the stress field over this distance. In this case, a_0 is 1.89 mm and the error of the prediction is only 3%, as shown in Fig. 3.2.10. This result supports the suggestion. However, in a range of 0.14 mm to 4 mm, the variable r_{min} does not

bring much difference on the prediction for a constant r_{max} of 17 mm. Compared with ΔK_{th} , the biggest difference is less than 17%. It implies that CMM is not sensitive to the choice of r_{min} , at least in this case.

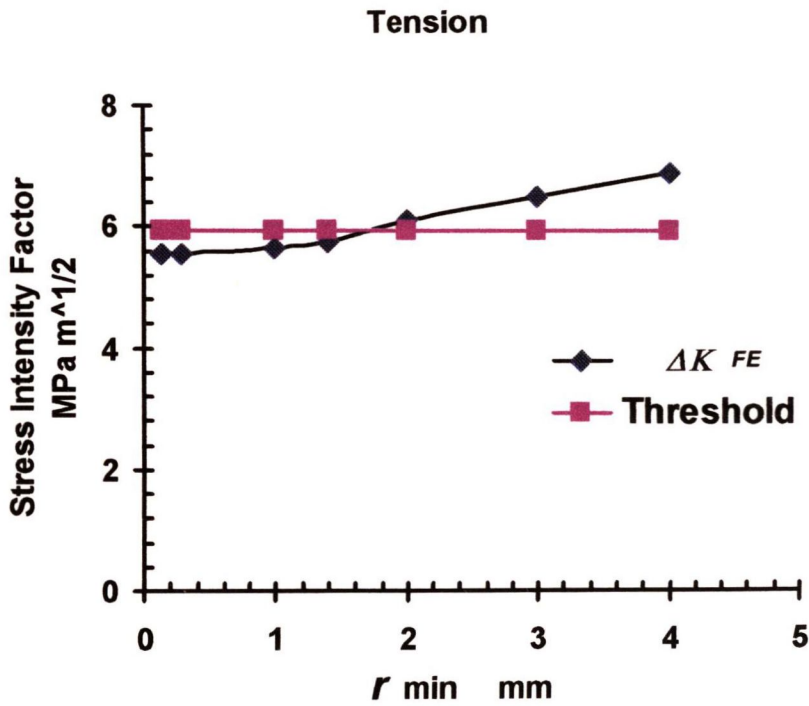


Fig. 3.2.10 Effect of r_{min} on the prediction of LM25 specimen subjected to tension load,

$$r_{max} = 17 \text{ mm}$$

The second example is a mild steel bar subjected to rotating bending [Frost, 1974; Smith and Miller, 1978]. The specimens were machined into a 12.7 mm outside diameter containing a circumferential vee-notch 1.3 mm deep and 0.1 mm root radius; $R = -1$; $\Delta K_{th} = 6.5 \text{ MPa m}^{1/2}$;

$a_o = 0.05$ mm. Fig. 3.2.11 shows the r_{min} effect on the evaluation of ΔK_{FE} , with a constant r_{max} of 5.05 mm. This data will be used in a later chapter.

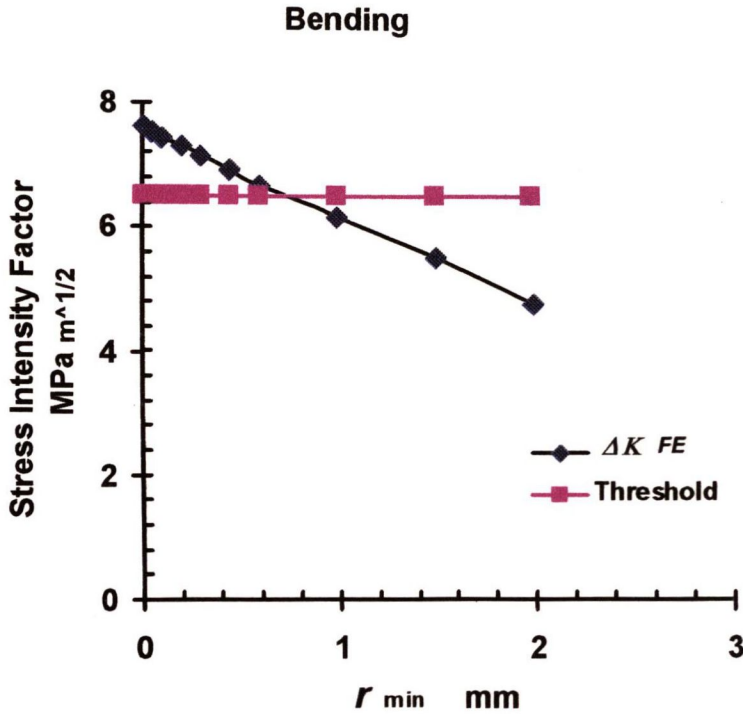


Fig. 3.2.11 Effect of r_{min} on the prediction of a mild steel specimen subjected to bending, $r_{max} = 5.05$ mm

The third example is the camshaft subjected to torsion loads, as mentioned in the last section. The material constant a_o of this cast iron is 2.24 mm. Fig. 3.2.12 shows the variation of ΔK_{FE} when increasing r_{min} . The r_{max} value is kept as a constant, 11.25 mm. Again a good prediction is obtained when $r_{min} = a_o$. Starting at 0.093 mm, the valid region for r_{min} extends to approx 3.5 mm. In this region the error from any r_{min} is less than 20%.

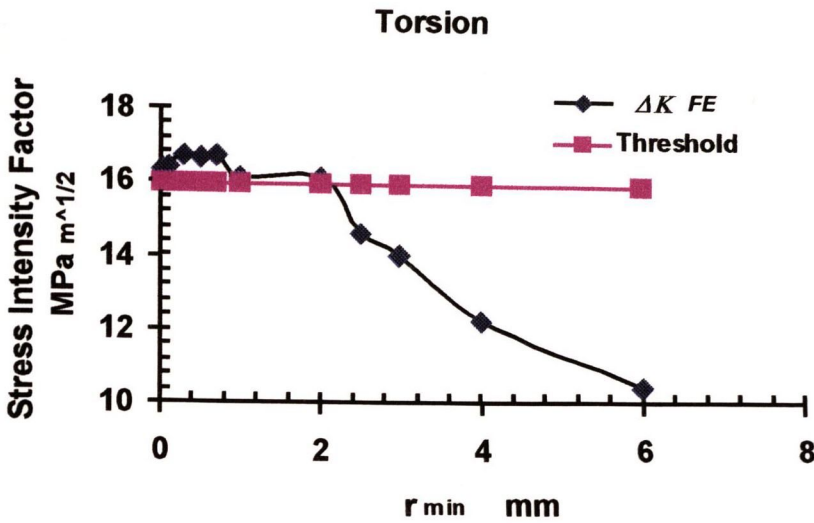


Fig. 3.2.12 Effect of r_{min} on the prediction of a camshaft subjected to torsion load,
 $r_{max} = 11.25$ mm

In general, these three examples include three kinds of materials, three kinds of geometries and three kinds of load conditions. They cover a wide range of applications. The conclusions from the previous examples, all indicate a common trend, i.e. CMM is not sensitive to the choice of r_{min} . The conclusion supports Taylor's suggestion. Furthermore, any selection of $0 < r_{min} \leq a_o$ is valid in all these situations.

3.2.2 Maximum distance

The choice of r_{max} also requires some discussion. It is expected that the focus path should include all information about the stress concentration, i.e. the part over which the geometrical feature raises stresses above their nominal values. However, in the general case of complex component geometry, it may not be clear what these nominal stress values are. With this in mind, a series of r_{max} values was analysed on a σ - r curve in order to find a general rule.

Fig. 3.2.13 shows three typical $\Delta\sigma$ - r curves; (a) is a common curve from a stress concentration in a tensile stress field, such as a single notch plate subjected to tensile stress; (b) represents a curve from more than two stress concentrations in a body; (c) behaves as a body subjected to bending; the stress goes negative beyond a neutral axis.

According to the analysis above and the previous work, it was decided to use the entire tensile stress distribution for (a) and (c). For (b), it is necessary to examine the curve; the focus part should be in the region where the σ - r curve is consistently decreasing; several values should be tested if possible; the final r_{max} value should give the lowest K value. The three examples are still used to verify the decision above. We did not have an example for (b) at this stage, so this was not considered.

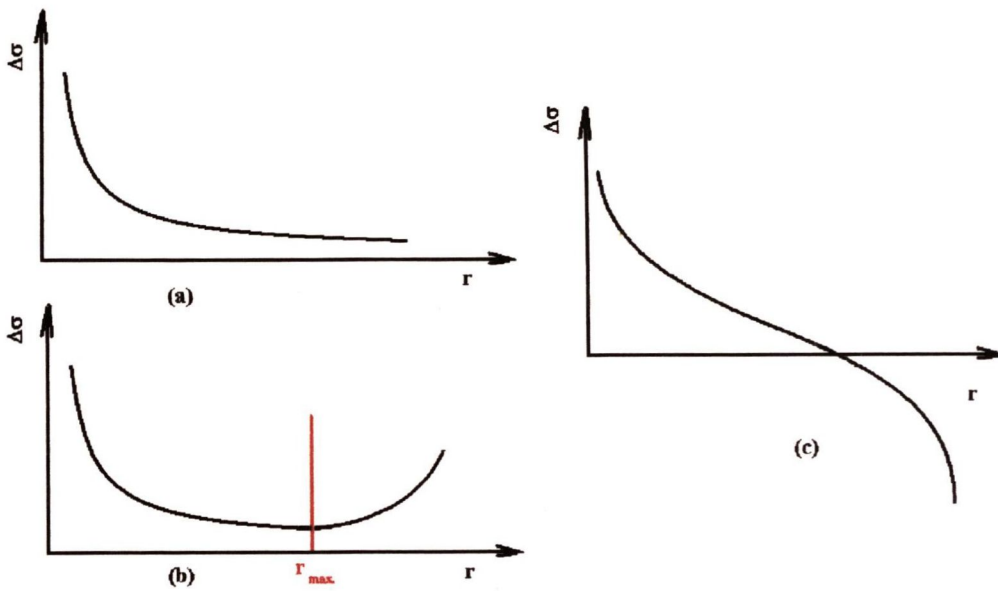


Fig. 3.2.13 Typical $\Delta\sigma$ - r curves from stress concentrations

Fig. 3.2.14 shows the predicted ΔK_{FE} values of the first example, the LM25 single-edge notched specimen. ΔK_{FE} almost remains a constant on variable r_{max} from 1 mm to 17 mm; the fit error also keeps about the same level, between 7 and 11 %; the biggest prediction error comparing with the test data is less than 15%. This means that the choice of r_{max} does not have much effect in this case.

The second example is used to verify the type (c) $\Delta\sigma$ - r curve, which is from a body subjected to bending load. Due to the existence of bending loads, the remote stress in the notched mild

steel bar did not tend to some unique value, but continued to decrease, passing through zero at the neutral axis and becoming negative. In this case the neutral axis was 5.05 mm away from the notch root. Fig. 3.2.15 shows the $\Delta\sigma$ - r curve and the best-fit curve at $r_{max} = 6$ mm; the former goes negative whereas the latter still keeps positive; the fit error is 40%. This implies that CMM treats negative as zero. Fig. 3.2.16 shows the ΔK_{FE} changing with variable r_{max} . The prediction error in a range of r_{max} from 1 mm to 6 mm is less than 20%. This proves that CMM is not sensitive to the r_{max} choice in the bending condition.

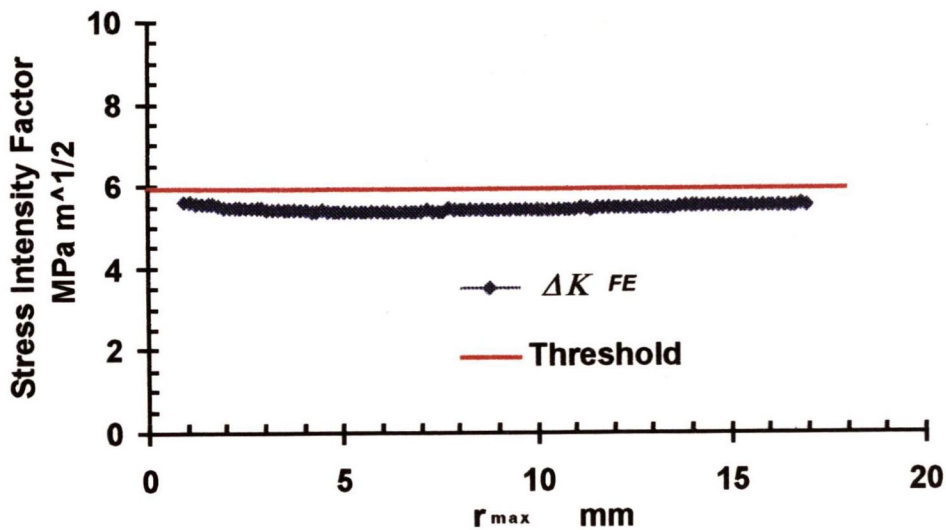


Fig. 3.2.14 Predicted ΔK_{FE} values on variable r_{max} for the single-edge notched specimen

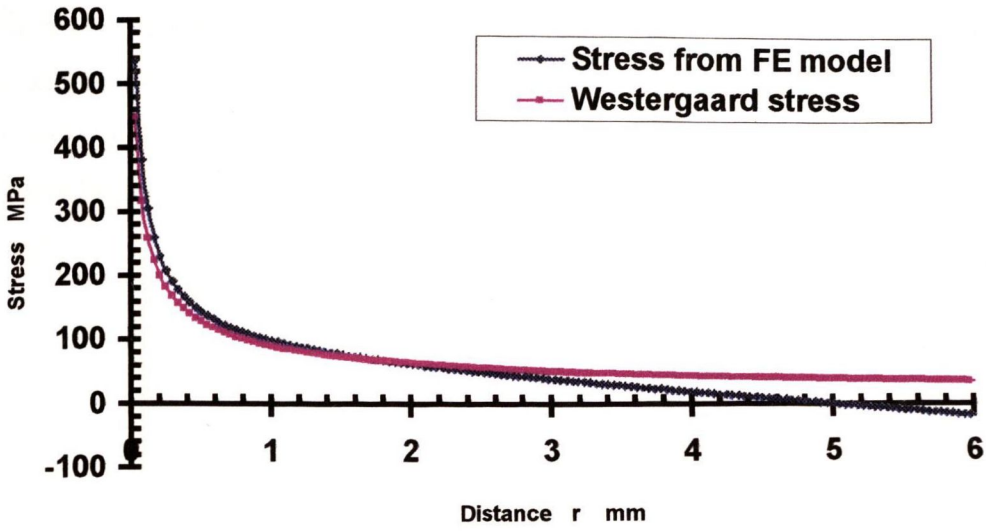


Fig. 3.2.15 $\Delta\sigma - r$ curve and its best-fit curve on the notched mild steel bar

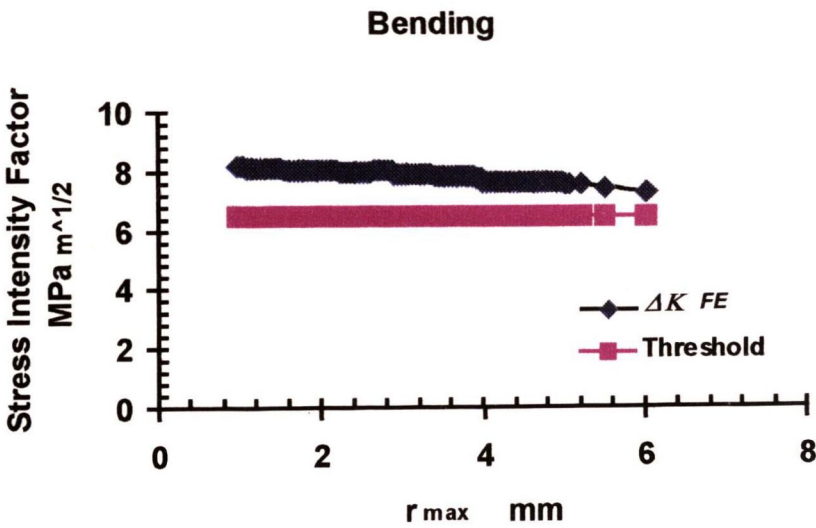


Fig. 3.2.16 Predicted ΔK_{FE} values on variable r_{max} for the notch mild steel specimens subjected to rotating bending, $r_{min} = 0.01\text{mm}$

The third example, the camshaft subjected to torsion, is a blunt notch sample; the notch root radius is 1.5mm with a 1mm depth. In a range of r_{max} from 1mm to 11.5 mm, the change in ΔK_{FE} was small, as shown in Fig. 3.2.17. On a constant value of $r_{min} = 0.3\text{mm}$, the prediction error on each selected point is less than 13.5%. This means that r_{max} effect is very small and can be neglected in this case.

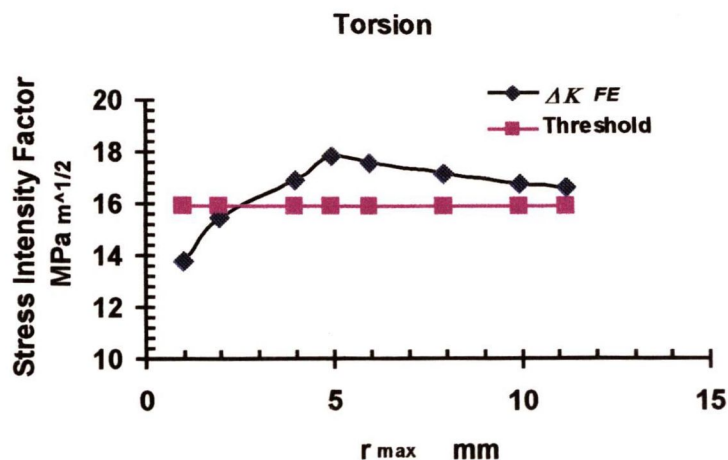


Fig. 3.2.17 Prediction error on variable r_{max} values for a camshaft under torsion, $r_{min} = 0.3 \text{ mm}$

In general, the results from all the examples, including different materials, load conditions and geometry, illustrate that r_{max} does not affect much the fatigue failure prediction when using CMM. The results support the suggestion for the types (a) and (c) made earlier in the section. The suggestion for the type (b), which will not be met in this thesis, still needs to be verified.

3.3 The Effects of Mesh Density

In this thesis most stress analyses were done using finite element modelling (FEM). The prediction accuracy will thus be affected by the element mesh density. Previous work showed that CMM was not sensitive to mesh refinement. In one case an increase in mesh density which raised the value of the hot spot stress by 32% had a negligible effect on the prediction [Taylor *et al*, 1999].

The concept of a general mesh density in a 2D model includes densities in two directions; around the root of the notch, i.e. the peripheral direction and the radial direction from the hot spot. The latter is directly related to the σ - r curve to be examined. Since the basic material parameter is the short crack constant a_0 , the definition of the radial density might be a function of a_0 . The element size in the vicinity of the hot spot should be smaller than r_{min} . The radial density is defined as

$$d_r = \frac{a_0}{l_r} \quad (3-3-1)$$

where l_r is the average element length along the radial direction. The peripheral density d_p is defined as a function of the root radius ρ , which could be evaluated by

$$d_p = \frac{S}{l_p} \quad \text{and} \quad S = \frac{\pi\rho}{2}, \quad (3-3-2)$$

where S is a quarter of the circle of radius ρ . l_p is the average element length around the root.

These definitions are easy to use. Taking the single-edge notched specimen as an example again, if there are five elements around the notch root, so the peripheral density d_p is equal to 5; fifteen elements around the root, then $d_p = 15$, as shown in Fig. 3.3.1. The root radius is 0.1 mm. If d_p is less than one, this means that the element length around the notch is larger than S and the root arc will be modelled as a straight line as shown in Fig.3.3.1 (a).

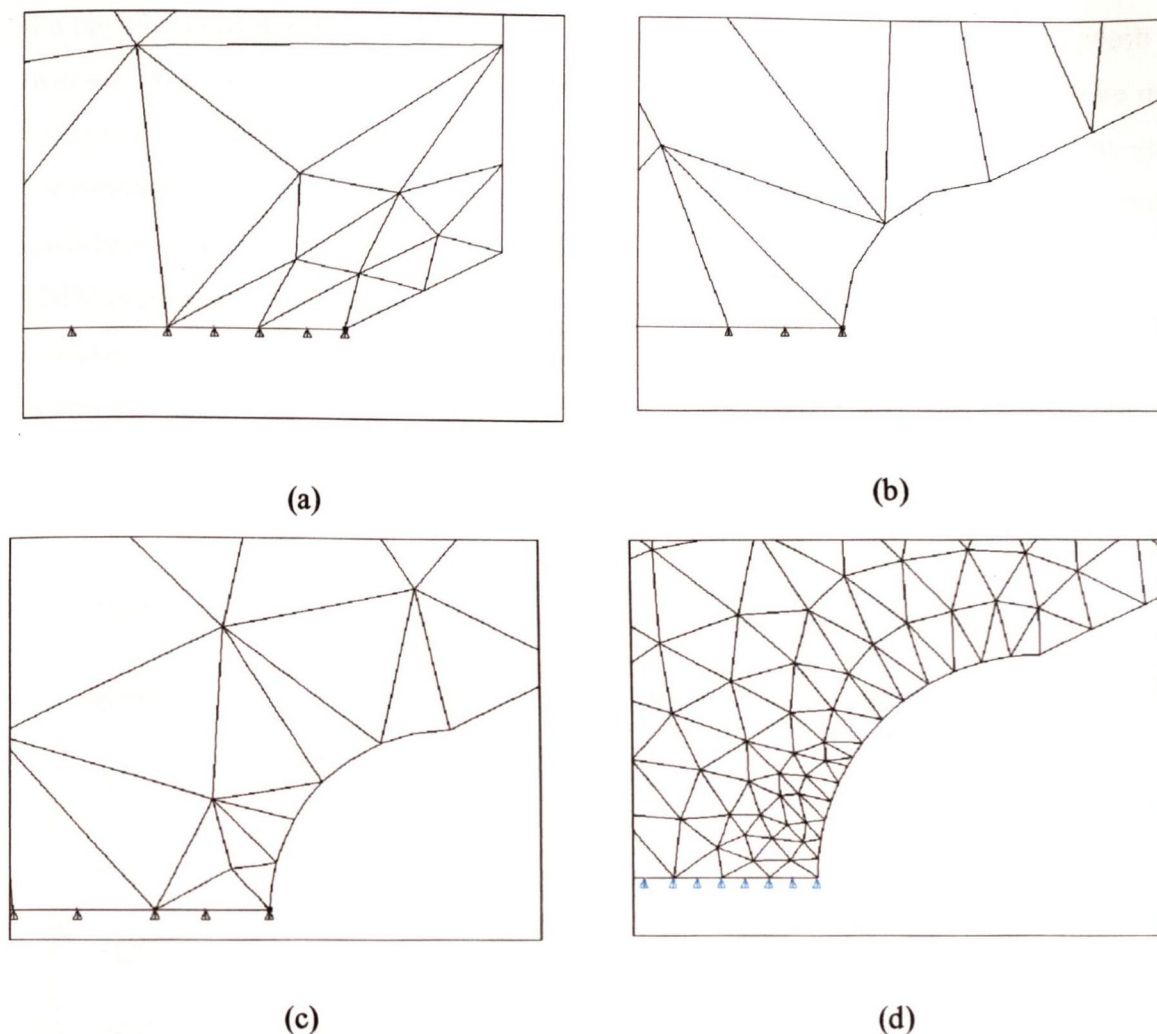


Fig. 3.3.1 Mesh density on the notch root of the single-edge notched specimen, some examples: (a) $d_p = 0.11$, $d_r = 1.125$; (b) $d_p = 2$, $d_r = 4.1$; (c) $d_p = 5$, $d_r = 10$; (d) $d_p = 15$, $d_r = 25$.

Six different mesh densities were modelled using FEM; from Mesh 1 of $d_p = 0.05$ and $d_r = 0.54$ to Mesh 6 of $d_p = 15$ and $d_r = 25$. The $\Delta\sigma-r$ curves from each density are shown in Fig. 3.3.2. It can be seen that a fine mesh gave a high accuracy of the stress field, particularly in the vicinity of the hot spot; the MPS value increased from Mesh 1 of 106.3 MPa to Mesh 6 of 647.1 MPa. There is not much difference between Mesh 5 and 6; the maximum value of Mesh 5 is 637.1 MPa, which means that the stresses from the two densities converge. However, the stress goes down very quickly at higher mesh density; in a very short distance,

the big stress difference from variable density vanishes; even though the stress in Mesh 6 is over six times that in Mesh 1, it goes down to about the same value from the coarse mesh when $r = 0.5$ mm. This reflects the character of the stress field in the vicinity of the stress concentration place; the stress comes up to the maximum at the hot spot and attenuates quickly away from the spot. Because of the character, the choice of r_{min} definitely affects the CMM prediction. In the present case, a_o is 1.89 mm and if we use the suggestion of $r_{min} = a_o$, one cannot see the effect from the mesh density. In order to investigate the effect, we use r_{min} as small as possible.

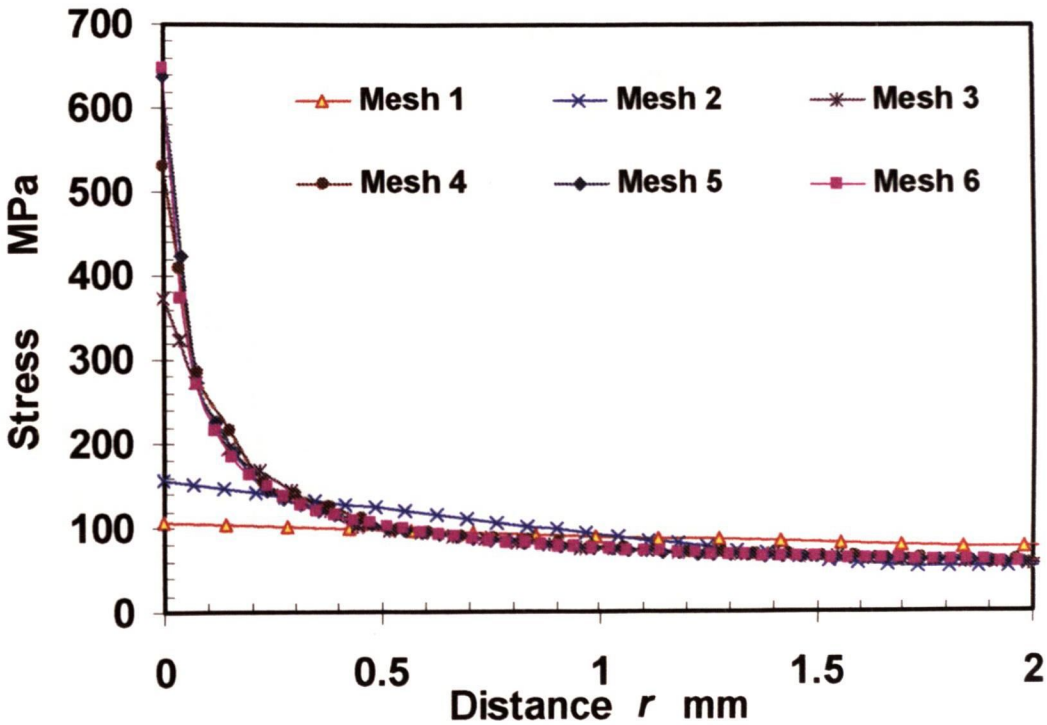


Fig. 3.3.2 $\Delta\sigma$ - r curves of the LM25 specimen with variable mesh density

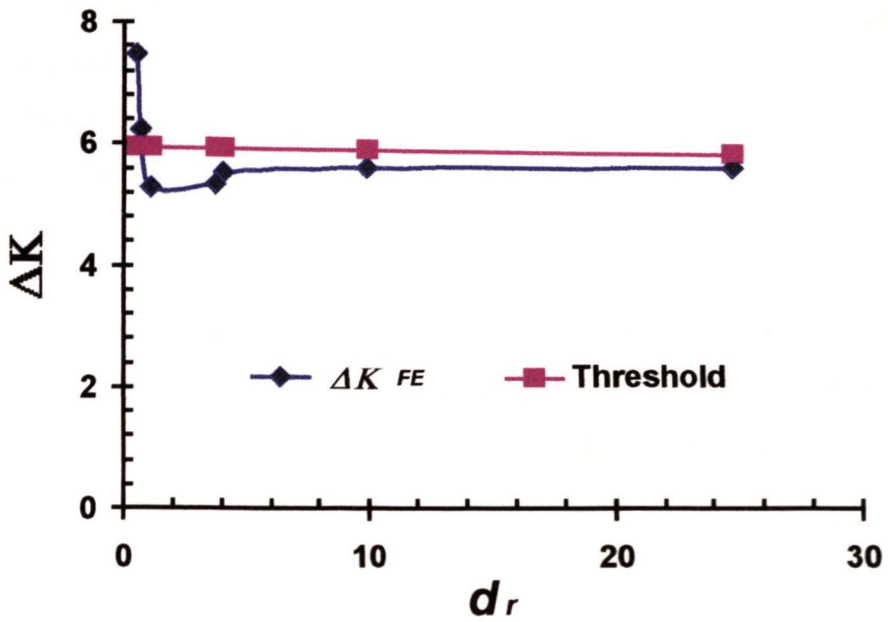
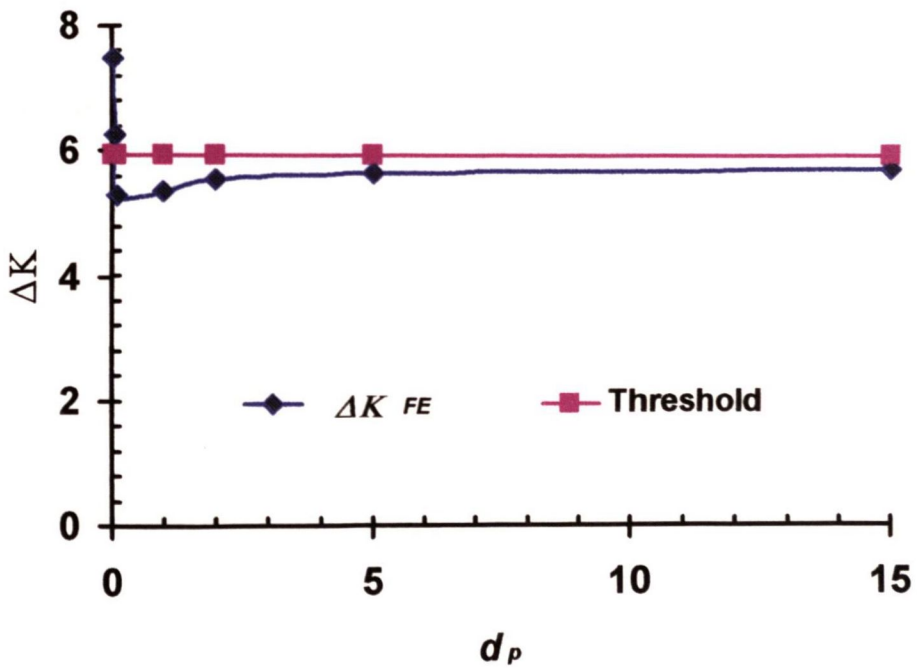
Fig. 3.3.3 Predicted ΔK_{FE} with variable d_r Fig. 3.3.4 Predicted ΔK_{FE} with variable d_p

Fig. 3.3.3 and 4 show the prediction results with variable d_r and d_p respectively. ΔK_{FE} converges quickly with d_p or d_r increasing; there is not much difference between the data from Mesh 2 and Mesh 6. This implies that it is not necessary to model the details of the notch root when it is small; at least in the present case, the accuracy of the prediction can be accepted without modelling the root radius. The reason why CMM is not sensitive to the mesh density can be explained as follows: the method counts the stress from the entire curve, not a local part. The change of the stress in variable mesh density is only limited to a small part relatively. So this change, only in the immediate vicinity of the hot spot, does not affect the evaluation of ΔK_{FE} significantly, which depends on the entire $\Delta\sigma-r$ curve. Finding a critical value of d_r or d_p needs much more work and it depends on the geometry. However in applications, it is not necessary to have a critical value. For a sharp notch, if the notch root is modelled by its radius, a reliable value of ΔK_{FE} is possible. For a blunt notch where the stress lever is not so high, any reasonable mesh density will make ΔK_{FE} reliable. This has been proved by the previous work. In practice one can decrease mesh density until convergence occurs: this analysis suggests that this will happen if d_p and d_r are less than 1.0.

3.4 Conclusions

1. CMM is not sensitive to the path orientation. The path for CMM should be normal to the MPS direction and the rule of lowest ΔK_{FE} can be used to find the path in a complex situation.
2. CMM is not sensitive to the minimum distance. A range of $0 < r_{min} \leq a_0$ is valid in all cases concerned in this thesis and it is suggested to limit r_{min} as small as possible.
3. CMM is not sensitive to the maximum distance. For specimens subjected to tensile or bending loads, it is suggested to use the entire tensile stress distribution. For a component with more one notch it is suggested to use r_{max} on which the $\Delta\sigma-r$ curve is monotonic function.
4. CMM is not sensitive to FE mesh density because it concerns the entire $\Delta\sigma-r$ curve. Any reasonable mesh density will make a reliable ΔK_{FE} possible.

Chapter 4 Modification of CMM for the Short Crack Problem

4.1 Introduction

For a sharply notched sample, the Crack Modelling Method (CMM) is equal to LEFM because the sharp notch can be modelled as a crack using Smith and Miller's model. However, problems were encountered in the present work when the method was applied to physically small notches that, like short cracks, display anomalous behaviour that cannot simply be predicted from material data obtained from larger features. The questions are:

- ◆ Can the CMM be used for short cracks?

If the answer to this question is yes, the second question is

- ◆ How can we apply the method to notches or to components which have the short crack effect?

In this chapter, several attempts are made to modify CMM for use in these situations. Various methods are examined critically and recommendations are made.

For any given crack, we can simply measure the crack length, and compare it to a standard (e.g. the material constant a_0) to find out whether the crack is a short crack or not. This can be done for sharp notches (using the notch depth, D). However, a notch with a big root radius may not have short crack effect even if the notch depth D is very small. Also a stress concentration on a component may not have a well-defined D value. The point is that we should find out an equivalent crack length first and then compare it with a_0 . We use $\Delta\sigma_{\text{PRED}}$ to represent the predicted stress in range.

4.2 Method 1 – Comparing with $\Delta\sigma_0$

Considering a cracked sample under cyclic loads, the fatigue limit, $\Delta\sigma_{oc}$, can be described using the ElHaddad method as shown in Fig. 4.2.1. An initial approach can be made by using LEFM or CMM, which gives an approximate value $\Delta\sigma_{PRED}$. In this case both methods are identical. If the value $\Delta\sigma_{PRED}$ is larger than the fatigue limit of a plain specimen, i.e. $\Delta\sigma_{PRED} > \Delta\sigma_o$ (or if it is smaller by only a small amount), then one has a short crack problem. For example, if $\Delta\sigma_{PRED} = \Delta\sigma_o$, i.e. two lines cross at the point A, then the crack length, $a = a_o$, and the true value of $\Delta\sigma_{oc}$ will be lower by a factor of $\sqrt{2}$, at the point B in the figure. For any crack length a at the point C in the figure, the true value at the point D will be lower by the factor of $\sqrt{(a + a_o)/a}$. If the crack length a is much longer than a_o , the factor will tend to be 1, and $\Delta\sigma_{oc} = \Delta\sigma_{PRED}$.

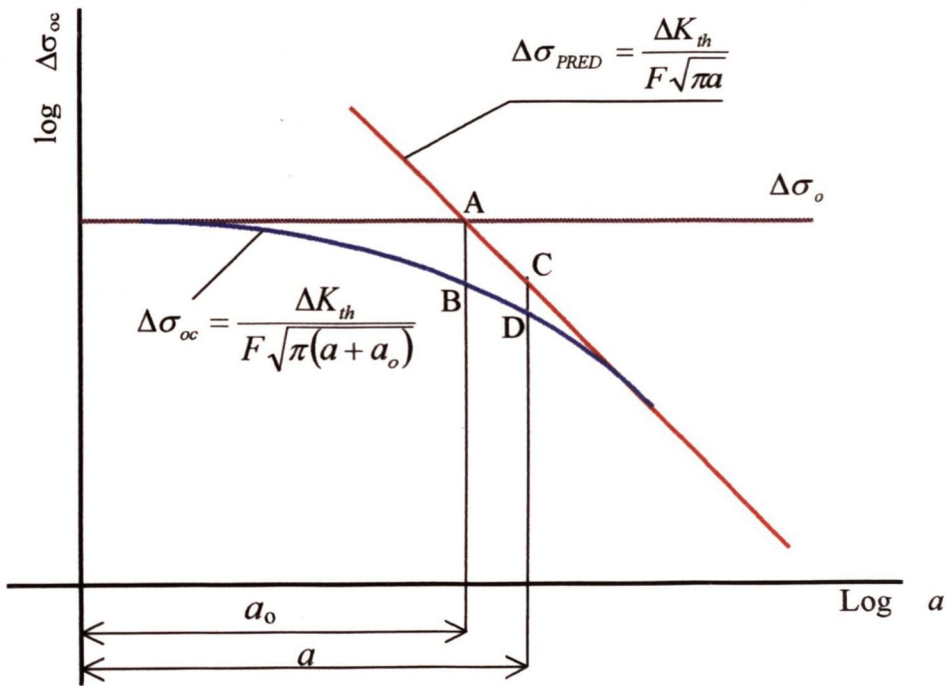


Fig. 4.2.1 Schematic illustration of the method 1

For a notched specimen, the notch depth D can be used to replace the crack length a for evaluating $\Delta\sigma_{PRED}$. An equivalent crack length a_{eq} can be found:

$$a_{eq} = \left(\frac{\Delta K_{th}}{F \Delta\sigma_{PRED}} \right)^2 \frac{1}{\pi} \tag{4-2-1}$$

The fatigue limit of the notched specimen $\Delta\sigma_{on}$ can be predicted using

$$\Delta\sigma_{on} = \frac{\Delta\sigma_{PRED}}{\sqrt{(a_{eq} + a_o) / a_{eq}}} \quad (4-2-2)$$

However, this needs to be checked against experimental data. The set of data points chosen for testing was from the literature [DuQuesnay *et al*, 1986]. The specimens were machined with a central circular hole, with variable radius, in a flat plate. The thickness of the plate was 2.5 mm and the width was 44.6 mm. The material was aluminium alloy Al2024-T351, with the material properties of $\Delta K_{th} = 5 \text{ MPa m}^{1/2}$, $\Delta\sigma_o = 248 \text{ MPa}$ and so $a_o = 0.13 \text{ mm}$. These are also used later, in Chapter 6.

Table 4.2.1 Corrected predictions on Al 2024-T351 specimens

Depth D mm	Exp. data $\Delta\sigma_{on}$ MPa	CMM $\Delta\sigma_{PRED}$ MPa	LEFM $\Delta\sigma_{PRED}$ MPa	$\Delta\sigma_{PRED} / \Delta\sigma_o$ (CMM)	a_{eq} mm	Corrected prediction MPa
0.12	159.14	250.22	257.52	1.01	0.13	175.91
0.25	122.61	168.88	178.41	0.68	0.28	139.49
0.5	121.22	115.67	126.16	0.47	0.59	104.78
1.5	83.95	63.89	72.84	0.26	1.95	61.86

Table 4.2.1 shows the initial predictions from CMM and LEFM; the values a_{eq} were evaluated from Eq. (4-2-1). The correction was made using Eq. (4-2-2). It was clear that the notch of $D = 0.12 \text{ mm}$ was a short notch because $\Delta\sigma_{PRED}$ was very close to $\Delta\sigma_o$. So the correct value should be lower by a factor of $\sqrt{2}$, which was proved to be right by the experimental data. For $D = 0.5 \text{ mm}$, the equivalent crack length was more than four times of the a_o value, so the short crack effect was small. The prediction error was 13.5% with correction and 4.5 % without correction. This implied that this point was very close to a_2 in Fig. 2.3.1 and both methods were valid. The last point in the table was out of the question: neither a long crack nor a short crack; when using the notch method (see Section 2.2.1) the prediction error was only -2.3% , so this is classified as a blunt notch.

The predicted $\Delta\sigma_{PRED}$ from LEFM, in which the notch depth D was used as the crack length, is also listed. There was a consistent difference: CMM showed lower values than LEFM on each data point. The reason was that the values of a_{eq} from CMM were larger than the corresponding notch depth D . Since CMM models notches as cracks and works out a_{eq} instead of using notch depths as crack lengths, using CMM on notched samples is more reasonable than using LEFM theoretically. However, the difference was not big, so LEFM was still useful in this type of specimens. A comparison between the two methods to predict results on some other specimens will be shown in Chapter 6.

Another example was from the same literature; the geometry and load condition were the same as in the previous example: the material was Steel SAE 1045, with material properties of $\Delta K_{th} = 13.9 \text{ MPa m}^{1/2}$, $\Delta\sigma_o = 608 \text{ MPa}$ giving $a_o = 0.17 \text{ mm}$. These will also be used later, in Chapter 6. The results are shown in Fig. 4.2.1. The prediction was significantly improved on each point, except the one with $D = 1.5 \text{ mm}$ which was a blunt notch.

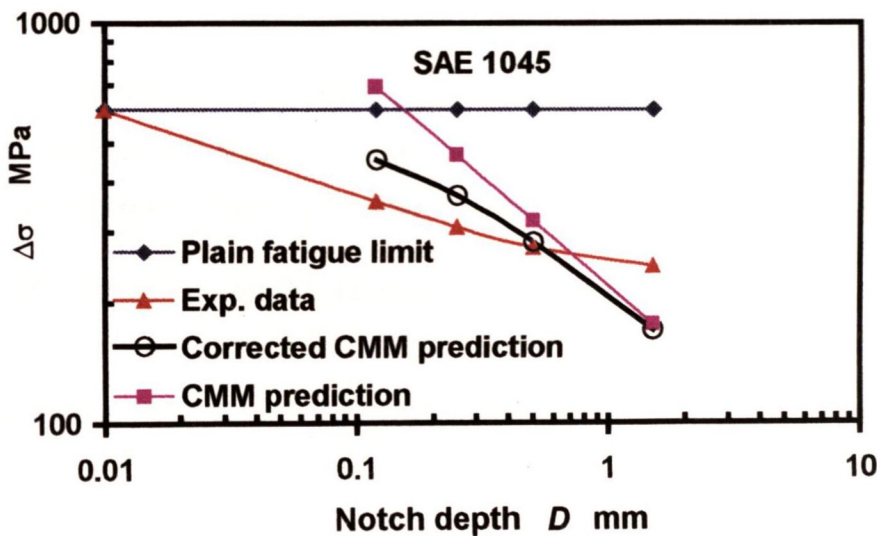


Fig. 4.2.1 Prediction results on SAE 1045 specimens using CMM and the correction

If a given notch behaves as a long crack, i.e. a_{eq} is much bigger than a_o , $\Delta\sigma_{on}$ will be close to $\Delta\sigma_{PRED}$ and $\sqrt{(a_{eq} + a_o)/a_{eq}}$ will tend to 1. Therefore, the method can be used for both short and long crack problems and can be employed to judge whether a given notch behaves a

short crack or not. The following example proved this deduction, as shown in Table 4.2.2. This group of data was from the same literature as in Section 3.3.2. The specimens were mild steel bars with 1.3 mm notch, subjected to rotating bending loads. The ratios $\Delta\sigma_{PRED} / \Delta\sigma_o$ were very small, so the values of a_{eq} were close to the notch depth and notches behaved as long cracks. The difference between the original value and the corrected value was very small. This example also illustrates that the method could be used in a body subjected to a bending load.

Table 4.2.2 Corrected predictions on mild steel bars subjected to rotating bending loads

Depth D mm	Exp. data $\Delta\sigma_{on}$ MPa	CMM $\Delta\sigma_{PRED}$ MPa	$\Delta\sigma_{PRED} / \Delta\sigma_o$	a_{eq} mm	Corrected Prediction MPa	Error %
0.005	90.54	78.47	0.15	1.29	77.00	-14.95
0.05	90.54	78.47	0.15	1.29	77.00	-14.95
0.1	90.54	77.43	0.15	1.33	76.02	-16.03
0.2	96.10	78.47	0.15	1.29	77.00	-19.88

A major limitation of the method is that the nominal stress must be known, so it is applicable for notched samples and for some components with simple geometries, but not for any problem in which nominal stress is hard to estimate.

4.3 Method 2 –Using a_w as the equivalent crack length

For a given problem, CMM produces two parameters, σ_w and a_w which represent the stress and half crack length in the Westergaard model (see Eq. (2-2-4)). Can we use a_w as a_{eq} ? If we can, we will know whether the problem is short crack or not. It is necessary to test the idea on notched specimens. Table 4.3.1 lists a set of predicted results which show that a_w can be used as a_{eq} on specimens with a central circular hole in a flat plate subjected to tensile stress. This condition is similar to the Westergaard condition, a central through crack in an infinite plate subjected to tensile stress.

In the table, predicted stress intensity factor, ΔK_{FE} , and predicted fatigue limit, ΔP_o , are listed. η is a correcting factor which is equal to $\sqrt{(a_w + a_0)/a_w}$. CMMscr represents the revised CMM including the short crack correction. Comparing with Table 4.2.1, the values of a_w here are almost the same as the values of a_{eq} and the corrected results are almost the same as well. Since there is no need to compare with $\Delta\sigma_o$, it is not necessary to know the nominal stress. This is a big advantage over Method 1, implying that the method could be used for complex geometry. However, it needs to be tested.

Table 4.3.1 Crack Modelling Method prediction for Al 2024-T351 specimens

Notch depth mm	CMM ΔK_{FE} MPa m ^{1/2}	Predicted ΔP_o using CMM kN	Error %	a_w mm	η	CMMscr ΔK_{FE} MPa m ^{1/2}	Predicted ΔP_o using CMMscr kN	Error %
0.12	3.18	27.88	57.10	0.13	1.41	4.50	19.71	11.08
0.25	3.63	18.84	37.78	0.28	1.21	4.39	15.57	13.86
0.50	5.24	12.90	-4.58	0.60	1.10	5.78	11.69	-13.49
1.50	6.57	7.13	-23.86	2.00	1.03	6.78	6.91	-26.22

For comparison, Table 4.3.2 lists the predictions using LEFM and the ElHaddad method on the same data as used above, using the notch depth D . A comparison between LEFM and CMM on these data confirms that there is not a significant difference between the two. In addition, no significant difference is seen between the ElHaddad method and CMMscr. Relatively, predictions from CMM and CMMscr are slightly more conservative than those from their LEFM equivalents.

The second group of data chosen for testing the method was from the literature [Ting, 1993; Lukas, 1986], also discussed later in Chapter 6. The specimens were machined into notched cylindrical bars with a diameter of 5 mm, which were very different in shape from the Westergaard case. The notches were semi-circular. The fatigue limit of plain specimens, $\Delta\sigma_o$, was 440 MPa and the threshold of the material (Steel 15313 (2.25Cr-1Mo)), ΔK_{th} , was 12

MPa m^{1/2} giving $a_o = 0.237$ mm. Fatigue tests were carried out under push-pull load, i.e. R was -1.

Table 4.3.2 Prediction for the fatigue failure in Al2024-T351 specimens

Notch depth D mm	LEFM Method			ElHaddad Method		
	ΔK_{FE} MPa m ^{1/2}	ΔP_o kN	Error %	ΔK_{FE} MPa m ^{1/2}	ΔP_o kN	Error %
0.12	3.09	28.71	61.82	4.46	19.89	12.11
0.25	3.48	19.67	43.88	4.28	15.95	16.70
0.50	4.91	13.75	1.74	5.52	12.25	-9.36
1.50	6.18	7.58	-19.07	6.44	7.27	-22.36

Table 4.3.3 shows the prediction from CMM and CMMscr. Almost every notch geometry was a short crack; the correction significantly improved the predictions. This confirmed that a_w could be used as the equivalent crack length a_{eq} and the method was applicable on these types of specimens which were subjected to tensile stress.

Table 4.3.3 Prediction using CMM and CMMscr on Steel 15313 CNB samples

Notch depth D	CMM Predicted $\Delta\sigma_{PRED}$	Error (CMM) %	a_w	η	CMMscr Predicted $\Delta\sigma_{PRED}$	Error (CMMscr) %
0.03	1163.44	170.9	0.034	2.8	412.10	-4.1
0.05	802.72	99.0	0.06	2.2	360.80	-10.6
0.07	708.59	120.6	0.092	1.9	374.71	16.6
0.2	386.93	63.3	0.306	1.3	290.46	22.6
0.4	243.33	16.5	0.77	1.1	212.78	1.9
0.76	153.86	-0.7	1.2	1.1	140.60	-9.3

The experimental data is listed in Table 4.3.4 with the prediction using LEFM and the ElHaddad method. For small D , the equivalent crack length a_w is close to the corresponding notch depth D . When D is over 0.4 mm, the difference between the two is significant; D

could not be used as a_{eq} anymore and CMMscr showed better estimates on the last two data points than the ElHaddad method. CMM also predicted well on these two data. This implies that the value of a_2 in the Kitagawa-Takahashi curve (see Section 2.4.1) may be between 0.77 and 1.2 mm for this kind of material; both CMM and CMMscr could be used in this overlap region. It needs to be tested.

However there was no significant improvement when applying CMMscr to the specimen under bending. Taking a mild steel bar subject to rotating bending (see Section 3.3.2) as an example a_w was 3.2 m for this 1.3 mm notched sample, which could not be used as a_{eq} . When a_w tends to infinity, σ_w tends zero. The reason is that the CMM program tries to obtain the best fit of the $\Delta\sigma$ - r curve with the Westergaard stress function. In this situation, both parameters, a_w and σ_w , are meaningless. The Westergaard stress may not be suitable for obtaining a_{eq} in the stress field caused by bending. One may make a_w equal to a_{eq} by using bending stress function instead of the Westergaard stress function in the CMM, but this has not been tested here.

Table 4.3.4 Prediction using LEFM and ElHaddad method on Steel 15313 CNB samples

Notch depth D	Experimenta l Data $\Delta\sigma_{gross}$	LEFM Predicted $\Delta\sigma_{PRED}$	Error %	ElHaddad Predicted $\Delta\sigma_{PRED}$	Error %
0.03	429.5*	1103.64	157.0	369.94	-13.9
0.05	403.4	854.88	111.9	356.82	-11.5
0.07	321.2	722.50	124.9	345.00	7.4
0.2	237.0	427.44	80.4	289.17	22.0
0.4	208.9	302.24	44.7	239.51	14.7
0.76	155.0	219.27	41.5	191.44	23.5

* The experimental data in the literature were given in terms of net-section threshold stress range. The author changed them into the gross-section threshold stress range because the nominal stress refers to the gross-section stress. In fact the stress on the net-section is not uniform, so there is no physical meaning for the net-section threshold stress and the expression can cause confusion.

In general CMMscr has a much bigger range of application potentially because it can be used on the body with irregular geometry under uniaxial tensile loads and no nominal stress is needed. This needs to be proved. However it will not detect the short crack problem in components subjected to bending loads. More verification of this method is reported in Chapter 6.

4.4 Method 3 – Adding a_0 or extrapolating the stress/distance curve

We can judge whether a given crack is short or not by using Eq. (2-2-1) in Chapter 2, $K = F\sigma\sqrt{\pi a}$. Adding a small amount a_0 to the crack length, if the crack is short, will greatly increase ΔK ; if the crack is long ΔK will be unaffected. We can imagine doing this to notches and components (Fig. 4.4.1).

Since CMM is not sensitive to mesh density, no special elements are needed for modelling a crack. A real short crack problem was used for verifying the method. The sample with a radius of 0.25 mm (Table 4.2.1) was used, adding a_0 at the stress concentration place in the FE model. Before adding a_0 , $\Delta K_{FE} = 3.67 \text{ MPa m}^{1/2}$ when loaded at the fatigue limit; after adding a_0 in the FE model, ΔK_{FE} was $4.15 \text{ MPa m}^{1/2}$. The threshold ΔK_{th} was $5 \text{ MPa m}^{1/2}$, so the method improved the prediction significantly.

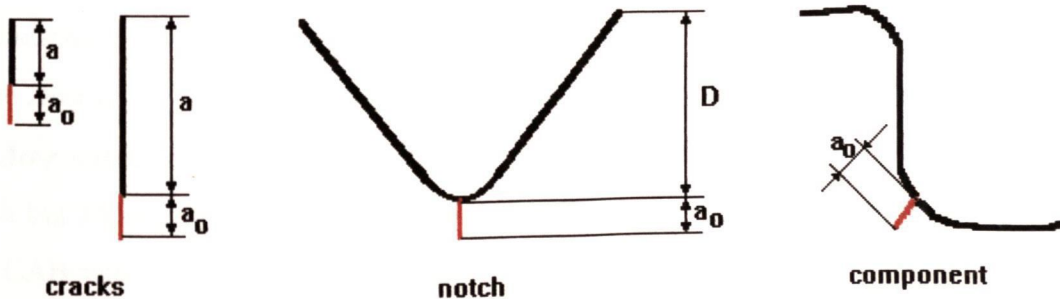


Fig. 4.4.1 Adding a_0 in different situations

Another example was from Table 4.3.4. The prediction results from adding a_o and not adding a_o are listed in Table 4.4.1. The prediction of each data point, except $D = 0.76$, was much improved by adding a_o in the FE models.

Table 4.4.1 Prediction comparison between before and after adding a_o on Steel 15313 CNB samples

Notch depth D	Experimental	CMM	Error	CMM	Error
	Data $\Delta\sigma_{\text{gross}}$	not adding a_o $\Delta\sigma_{\text{PRED}}$	not adding a_o %	adding a_o $\Delta\sigma_{\text{PRED}}$	adding a_o %
0.03	429.5	1163.4	170.88	391.6	-8.81
0.05	403.4	802.7	99.00	372.3	-7.69
0.07	321.2	708.6	120.59	363.7	13.21
0.2	237.0	386.9	63.27	288.7	21.83
0.4	208.9	243.3	16.50	212.4	1.69
0.76	155.0	153.9	-0.74	140.7	-9.23

A disadvantage of the method is that a huge FE model will be needed for the analysis, when applying the method to engineering components, especially if a_o is small. This will greatly limit the application to engineering components. Therefore it was necessary to develop a simple way of using the idea of the method without adding a crack of length a_o in the FE model.

Considering a stress-distance ($\Delta\sigma-r$) diagram, a similar result can be realised by adding a part of the $\Delta\sigma-r$ curve in front of the notch tip ($r = 0$). As illustrated in Fig. 4.4.2, the curve AB is the $\Delta\sigma-r$ curve from the notch root before adding a_o ; the curve C'A'B' is from the same notch but adding a_o . Assuming that AB and A'B' are identical, CA is extrapolated from AB and CAB will replace C'A'B' as the input $\Delta\sigma-r$ curve of CMM. This is an approximate method: AB is not exactly identical to A'B' and the extrapolated curve CA is not as same as C'A'. We found that the difference between AB and A'B' was limited at small distances and the effect of the difference between CA and C'A' was also limited. Therefore the error caused by CAB replacing C'A'B' was small.

To test this method we took An Al 2024-T351 specimen with $D = 0.25$ mm as example, shown in Fig. 4.4.3. In order to add the a_o value, we moved the original $\Delta\sigma$ - r curve a distance of a_o to the right and made the trend line using polynomial format, $y = 1228.1x^4 - 4210x^3 + 5138.5x^2 - 2636.1x + 609.64$; we extrapolated the curve and used the data as an input file for CMM. The prediction results are listed in Table 4.4.2.

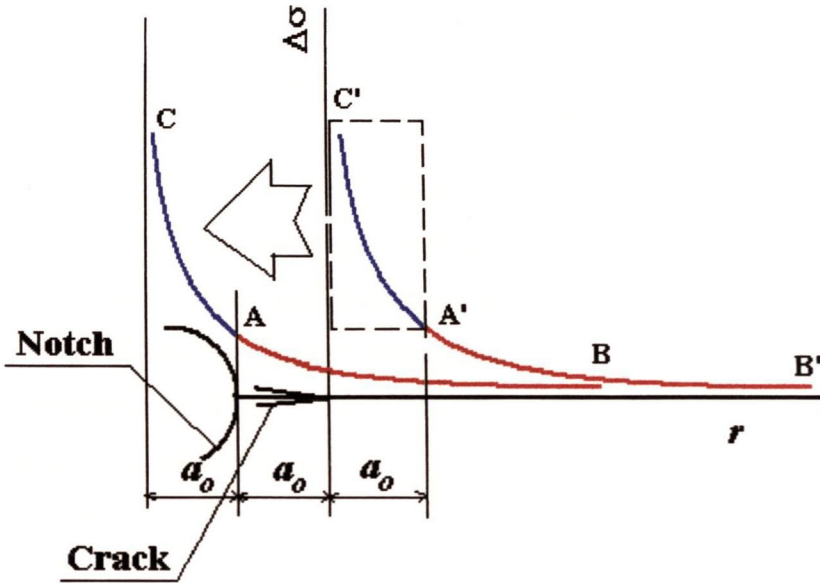


Fig. 4.4.2 Illustration of the extrapolation method

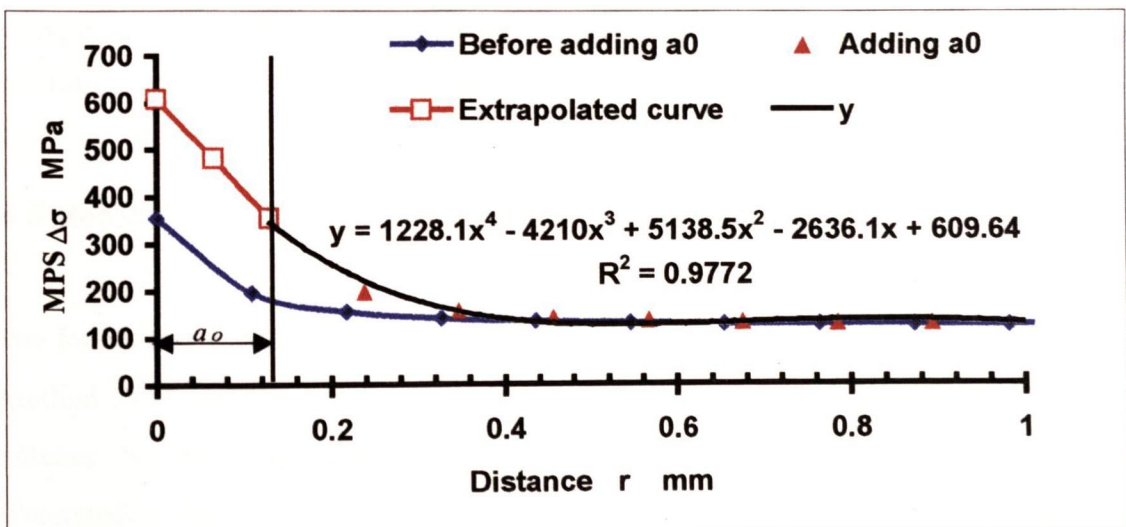


Fig. 4.4.3 Extrapolating a curve from a notch model.

Table 4.4.2 Extrapolating method for 2024-T351 specimens with varies of notch radiuses

Notch depth D mm	Experimental data. $\Delta\sigma_{on}$ MPa	Predicted $\Delta\sigma_{PRED}$ MPa	$\Delta\sigma_w$ MPa	a_w mm	Error %
0.12	159.1	184.76	159	0.24	15.47
0.25	122.61	125	122	0.53	0.81
0.5	121.22	84.94	116	1.25	-31.51
1.5	83.95	51.14	76	4.2	-43.18

At the points of notch radii 0.12 and 0.25 mm, the prediction agreed well with the experimental data, even better than previously. For the large notches, which were actually blunt notches, the method showed an overestimate, which was expected. The key point of the method is to choose a good function format for extrapolating the data. At this stage we used a polynomial format, which seemed not very good because the prediction on the notch of $D = 0.5$ mm was not as good as expected. An exponential format may be a better function for describing the stress gradient in the vicinity of a crack.

In general the method of adding a crack length of a_o at the stress concentration point can be used for the short crack problem, but the method needs a big FE model when applied to engineering components. This greatly limits its utility. Its equivalent method, the extrapolating method, may solve the problem. The initial work has shown promising results but further work is needed to be done in the future.

4.5 Method 4 – Average of NM & CMM

We found that CMM overestimated $\Delta\sigma_{on}$ due to the short crack effect, while the Notch Method (NM, see Section 2.2.1) underestimated $\Delta\sigma_{on}$ due to the stress gradient of small notches. So the solution must lie somewhere between the two. A typical example is illustrated in Fig. 4.5.1; $\Delta\sigma_{oc}$ is the fatigue limit of a flat plate specimen with variable centre crack length; $\Delta\sigma_{on}$ is the fatigue limit of a flat plate specimen with a centre hole (CNP). The line labelled CMM in the figure represents the prediction results $\Delta\sigma_{PRED}$ for both notched and

cracked specimens; the line NM in the figure represents the prediction results for notched specimens. In this situation, notched samples and cracked samples variable behave differently; the former tends to the NM line with increasing the radius of holes; the latter tends to the CMM line when the crack length is over a_2 .

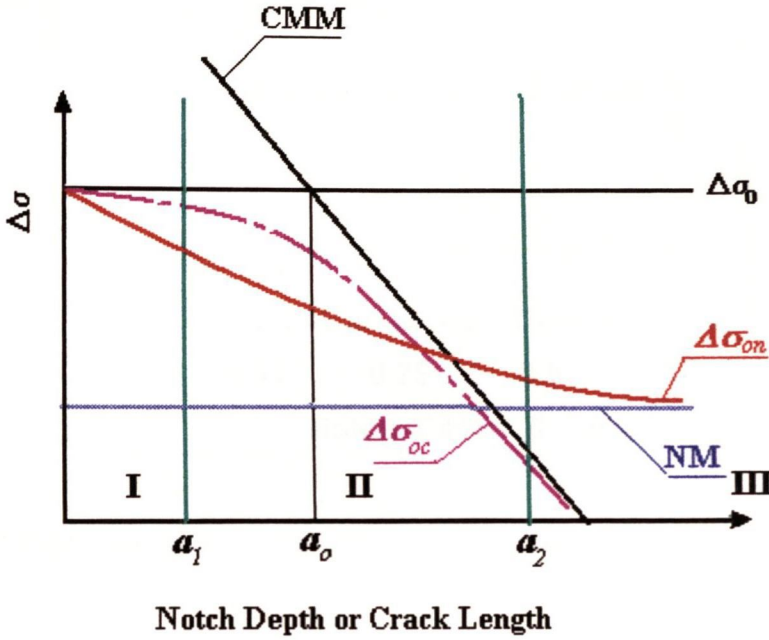


Fig. 4.5.1 Comparison of NM and CMM on the prediction of notched specimens

Considering $\Delta\sigma_{on}$ curve, normally an assessment of whether a given notch is short or not can be made by comparing the prediction results from the two methods. If NM's result is lower than CMM's one, this must be a short crack problem. In the short notch area, Region II ($a_1 < D < a_2$), a simple way to approach the test data is to average the results from both methods; this was named as the Average Method (Ave.). The application on Al 2024-T351 CNP samples is shown in Fig. 4.5.2. The method gave a very good prediction. More verification will be shown in the Chapter 6. The method may be suitable in Region I as well but as $a \rightarrow 0$, the CMM prediction will tend to infinity, so the Ave. prediction will become too large. For Region III, it depends on the detail of the geometry, for example, the notch depth and notch radius.

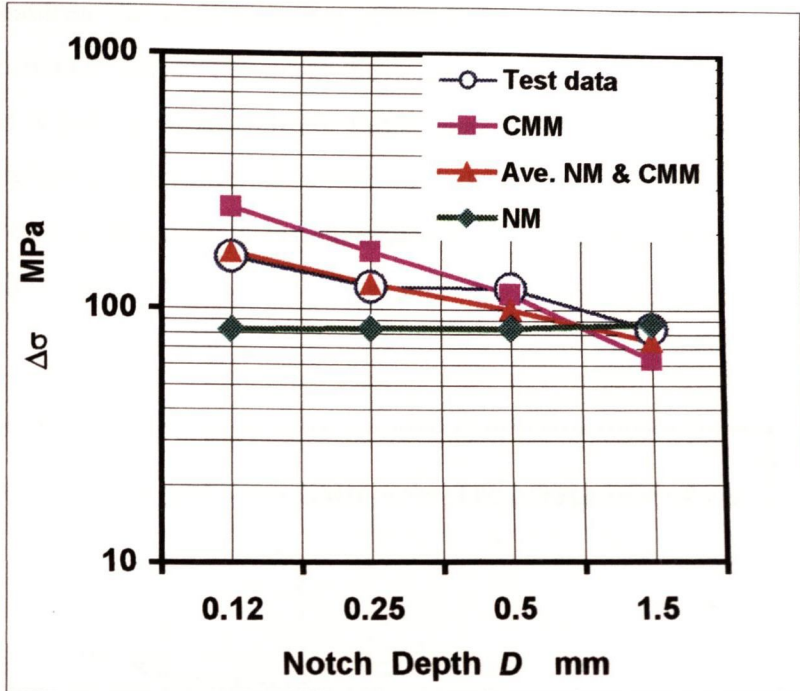


Fig. 4.5.2 Prediction on Al 2024-T351 CNP samples using the Average Method

Fig. 4.5.3 shows another example of the short crack problem. Again, the prediction was very good using the method. The details of these specimens will be described in the Chapter 6.

Ave. was specially designed for short crack problems. The method does not need nominal stress and is not limited by the load type. Also it is easy to use. Nor requiring a notch depth, the method can be applied to components. For a given notch or fillet which is not sharp, comparing predictions from NM and CMM, one can assess whether it is a short crack problem or not. For a short crack problem, CMM will produce an overestimate while NM will give an underestimate. If the notch or fillet is sharp, a crack like, using CMM is the best choice. Theoretically, the three methods, NM, CMM and Ave., nearly cover all regions in Fig.4.5.1, except if D is very small in Region I, where $\Delta\sigma_{on}$ is close to $\Delta\sigma_o$.

Further improvement of this method is needed for more accurate prediction. Taking Fig. 4.5.3 as an example, the test data curve was not just in the middle between the other lines, it was closer to NM curve. So instead of taking the average value, putting a weight on one side could be helpful for a closer estimate. The weight should be a function of material properties

and geometry features. An understanding of the mechanism of crack growth in the early stages of fatigue is essential to construct the weight function. From this point of view, the Average Method is just an initial, simple and approximate approach. However, the testing results were promising. Considering errors caused by many factors, such as a scatter in material properties, numerical analysis, manufacturing tolerance etc., it may be acceptable for engineering applications.

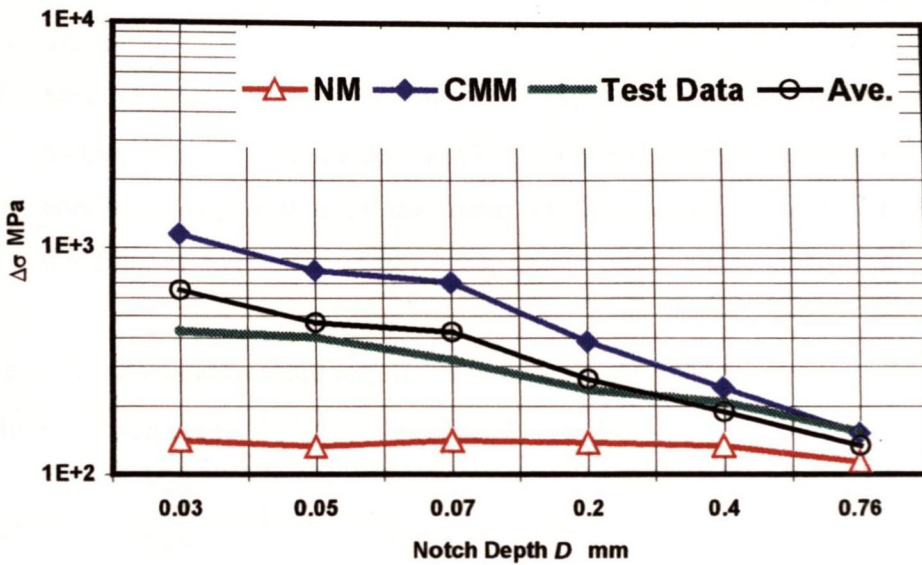


Fig. 4.5.3 Another short crack problem example, Steel 15313 (2.25Cr-1Mo) CNB under Push-pull load [Lukas *et al*, 1986]

4.6 Conclusions

1. CMM can be used for the short crack/notch problem after revision. Several modifications make the method available for different situations, such as different geometry and loads. Revised methods show a good agreement with several sets of experimental data.
2. Method 1 can be used to judge whether a given notch is small or not and predict the fatigue failure on specimens and components subjected to tensile stress or bending load, but the method requires the nominal stress to be known.

3. Method 2 is valid for notched specimens and components subjected to uniaxial fatigue load. No nominal stress is required for the utility of the method. The method can predict fatigue loads. It cannot be used for bending loads.
4. Method 3 can be used for both judging and predicting the short crack/notch problem. The method is not constrained by any kind of geometry and load conditions. The method may need a big FE model for engineering components. Using the extrapolating method, in which an imaginary crack length is added in the stress/distance plot, may solve the problem; the initial approach has shown promising results.
5. Method 4 is applicable on notched specimens or engineering components. The method does not require special FE models and material constant a_0 . Any type of load conditions will not limit the utility of the method. It may be limited to certain notch/crack size.

Table 4.6.1 Limitations and requirement of revised CMM for short crack/notch problems

Method	Long crack	Short crack/notch	Tension	Bending	K_t needed
1	Yes	Yes	Yes	Yes	Yes
2	Yes	Yes	Yes	No	No
3	Yes	Yes	Yes	Yes	No
4	No	Yes	Yes	Yes	No

Table 4.6.1 lists the limitations and requirement of each revised method. At this stage, although any more general method has not been found yet, one could find a suitable method among the four for a given short crack/notch problem. It is necessary to verify the methods on more experimental data before applying them to engineering components. The verification should include the main effects of fatigue failure, such as material, load type, load ratio, geometry, size effect etc. At the moment, judging correctly whether a given fatigue problem was a short crack problem or not was still a vital question needing to be solved for practical application of these four methods. This will be discussed further in Chapter 8, where a general methodology for the selection of the appropriate method will be discussed.

Chapter 5 A New Method of Prediction

5.1 Introduction

Although the Crack Modelling Method (CMM) was successfully modified for the short fatigue crack prediction on notched samples (see Chapter 4), some potential problems have been identified when applied to engineering components. For example, it is hard to define a nominal stress when a component has a complex geometry; it is difficult to distinguish that a given component with the geometry feature belongs to the short crack or long crack categories. Also, a crack in a stressed body can propagate in a combination of the three opening modes, mode I, II or III. The current Crack Modelling method concentrates on a crack growing under an opening or *mode I* mechanism and examines the First Principal Stress. However, many service failures occur from cracks subjected to mixed mode loading [Qian and Fatemi, 1996 and Brown and Miller, 1989].

Due to the inconvenience of the Crack Modelling Method for short crack problems, a new theory is presented in this chapter which approaches the problem in a different way. The new theory is still based on a consideration of the stress field of the component but now attention is focussed on a small region close to the stress concentration. We begin with a theory known as the critical distance theory; modify the theory using fracture mechanics; incorporate short cracks and then extend the approach to notched specimens or components. We will build a “bridge” linking behaviours between uncracked bodies and cracked bodies. The aim is to develop a general solution, applicable to cracks, notches, other geometry features and plain specimens, which takes account of size effects in an intrinsic fashion.

5.2 Background of the Theoretical Model

The present methodology is based on the critical distance theories. These theories have been used in the analysis of notches and plain specimens for over 40 years, since the work of Peterson [1959], Neuber [1958], Siebel and Stieler [1955] and others. The basic idea in the theories is to examine the stresses not only at the notch tip but also within a certain volume of

material surrounding the notch. It is assumed that fatigue failure will occur if the average cyclic stress within this volume exceeds some given value.

This methodology had been realised in various different ways that are all essentially the same. For example, Siebel and Stieler [1955] expressed their predictions in terms of the normalised stress gradient at the notch. Peterson [1959] used the notch root radius as the determining parameter. Usually the stress field is approximated in some way so as to simplify the calculations. For example, Peterson assumed a linear stress-distance variation (i.e. a constant stress gradient) so that the average stress over a certain distance could be approximated by the stress at a given point.

In practice, the correct distance (i.e. the one that gives the best predictions) varies considerably from one material to another. It tends to be larger (over 1 mm) in low strength materials, and much smaller (less than 0.1 mm) in high-strength materials. Up to now the appropriate distance has been found from experimental data. After analysing a large amount of the experimental data, Peterson developed an empirical relation between this distance and the UTS in steels. His results are widely used in industry.

The major weak point of all of these critical-distance approaches is the choice of the distance parameter. The accurate determination of this parameter is a major problem because small variations in the distance chosen can lead to large errors, especially for sharp notches. Additional errors arise from other simplifying assumptions, such as the assumption of constant stress gradient and the reliance on root radius as the only relevant geometric parameter.

5.3 New Approach to Find the Critical Distance

We begin by making a hypothesis that the fatigue limit of cracked bodies and of uncracked bodies can be predicted using the same theory. The hypothesis follows the premise of fatigue life prediction for bodies under high-cycle fatigue loading. Mechanistically, this amounts to saying that the processes of crack initiation and short-crack growth which are necessary precursors to the failure of uncracked bodies, are not fundamentally different from the

process of crack extension which is necessary for the failure of a body containing a long crack. Historically, cracked and uncracked bodies have been considered using different theories, based on ΔK for the former and $\Delta\sigma$ (or $\Delta\varepsilon$) for the later. If the present hypothesis is correct, then methods of analysis which work for plain and notched bodies, such as the critical-distance approach, will also work for cracked bodies.

Irwin [1957] found the analytical solutions for the stress and displacement fields in the vicinity of crack tips subjected to the three modes of deformation. For *mode I*, the stress field is given by

$$\begin{Bmatrix} \sigma_{xx} \\ \sigma_{yy} \\ \sigma_{xy} \end{Bmatrix} = \frac{K_I}{\sqrt{2\pi r}} \cos \frac{\theta}{2} \begin{Bmatrix} 1 - \sin \frac{\theta}{2} \sin \frac{3\theta}{2} \\ 1 + \sin \frac{\theta}{2} \sin \frac{3\theta}{2} \\ \sin \frac{\theta}{2} \cos \frac{3\theta}{2} \end{Bmatrix} \quad (5-3-1)$$

where the stress components and the co-ordinates r and θ are shown in Fig. 5.3.1. Eq. (5-3-1) represents the case of plane strain and neglects higher-order terms in r . Because higher-order terms in r are neglected, the equations are exact in the limit as r approaches zero and are a good approximation in the region where r is small compared with other x - y planar dimensions. We will use this solution for determining the critical distance in this section.

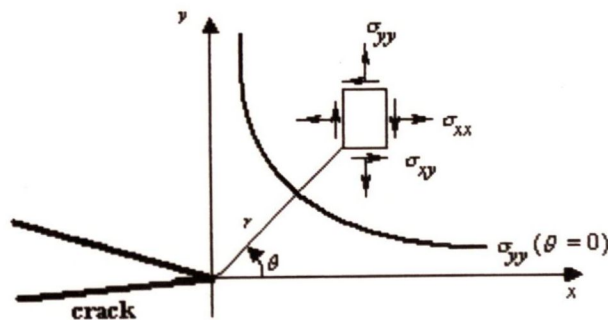


Fig. 5.3.1 The elastic stress field near a crack tip

Three possible ways are presented for obtaining the stress value. They will be referred to as the *point*, *line* and *area* methods. These methods are named depending on whether the stress at a fixed point is used, or whether the stress is found by averaging over a given line or area. In each case, the region concerned will commence at the stress concentration and end at some fixed distance from it.

5.3.1 Point Method

The point method is the application of a simple critical-distance approach to a long crack. Considering Eq. (5-3-1), the stress causing crack opening can be written as

$$\sigma_{yy} = \frac{K_I}{\sqrt{2\pi r}} \quad (5-3-2)$$

where σ_{yy} is the stress at a distance r ahead of a crack at an angle of $\theta = 0$. K_I is the stress intensity factor. This equation can be used to find the critical distance, d_c , for which an applied stress range $\Delta\sigma$ gives rise to the fatigue limit of plain specimens, $\Delta\sigma_o$ and the stress intensity factor in range, ΔK_I , gives rise to the material threshold, ΔK_{th} . The result is

$$d_c = \left(\frac{\Delta K_{th}}{\Delta\sigma_o} \right)^2 \left(\frac{1}{2\pi} \right). \quad (5-3-3)$$

d_c is thus a material constant related to the fatigue properties of the material. It is also related to the load ratio R . The distance d_c has its own direction which is at the angle of $\theta = 0$. This direction is the same as we defined for the path in the Crack Modelling Method, which is normal to the direction of the maximum principal stress. In the method we assume that if the stress at the distance d_c is equal to or larger than the fatigue limit $\Delta\sigma_o$, the crack will grow and fatigue failure will occur.

The length d_c can be compared to the a_o parameter defined by ElHaddad *et al* [1980] as described in Chapter 2:

$$a_o = \left(\frac{\Delta K_{th}}{\Delta \sigma_o} \right)^2 \left(\frac{1}{\pi} \right). \quad (5-3-4)$$

Substituting this into Eq. (5-3-3), the value of d_o is equal to $a_o/2$. ElHaddad's equation was purely empirical, and the parameter a_o was not given any physical significance. The above analysis implies that: (a) the critical-distance approach can be used to predict the fatigue limit of a cracked body, and (b) the physical significance of the a_o parameter is that it is directly related to this critical distance.

5.3.2 Line Method

Instead of considering a point, the line method is an average method considering the stress distribution on a line. Considering the Eq. (5-3-1) again, if the stress is integrated over a distance d , assuming unit thickness, a force that drives the crack to open can be expressed as

$$\int_0^d \sigma dr = \int_0^d \frac{K_I}{\sqrt{2\pi r}} dr. \quad (5-3-5)$$

Since K_I is independent of the distance, r , above equation can also be expressed as

$$K_I = \sqrt{\frac{\pi}{2d}} \int_0^d \sigma dr. \quad (5-3-6)$$

For any value of d , K_I is a constant; so Eq. (5-3-6) can be used to evaluate the K_I value if one knows the stress field in vicinity of a crack tip. In Fracture Mechanics, the principle of superposition is often used to calculate K_I as a function of crack length; the details of the principle can be seen in the literature [e.g. Bueckner, 1970].

By definition, at the fatigue limit of this cracked body, $\Delta K = \Delta K_{th}$ and $d = d_{cl}$. Substituting Eq. (5-3-4) into Eq. (5-3-6), the applied stress range of $\Delta \sigma$, which is a function of distance, r , can be displayed as a function of the fatigue limit stress range, $\Delta \sigma_o$, in integration form:

$$\left(\frac{1}{d_{cl}} \int_0^{d_{cl}} \Delta \sigma dr \right) \sqrt{\frac{\pi d_{cl}}{2}} = \Delta \sigma_o \sqrt{\pi a_o} . \quad (5-3-7)$$

Comparing both sides of the above equation, it is found that the average stress over some distance, d_{cl} , is equal to the fatigue limit and this distance is equal to $2a_o$. That is

$$\frac{1}{2a_o} \int_0^{2a_o} \Delta \sigma dr = \Delta \sigma_o . \quad (5-3-8)$$

In this case the critical distance, d_o , is found analytically as the function of the material's threshold and plain-specimen fatigue limit. Eq. (5-3-8) can also be shown in another way, as the function of material threshold, e.g.

$$\sqrt{\frac{\pi}{4a_o}} \int_0^{2a_o} \Delta \sigma dr = \Delta K_{th} . \quad (5-3-9)$$

The method is called the Line Method because of its line integral. The rule for choosing the analysis path, which is used in the Point Method and Line Method, is the same as in the Crack Modelling Method.

5.3.3 Area Method

There is a similar identity related to the area method. If the average stress is evaluated over a semicircular area ahead of the crack tip, of radius d , then the stress intensity factor K_I is characterised by an average stress, thus using Eq. (5-3-1):

$$\sigma_{ave}|_{r=d} = \frac{4}{\pi d^2} \int_0^{\frac{\pi}{2}} \int_0^d \frac{K_I}{\sqrt{2\pi r}} \cos \frac{\theta}{2} \left(1 + \sin \frac{\theta}{2} \sin \frac{3\theta}{2} \right) r dr d\theta \quad (5-3-10)$$

Another expression can be written as

$$K_I = 1.61\sqrt{d}\sigma_{ave}|_{r=d} \quad (5-3-11)$$

K_I is a constant for any value of d , so Eq. (5-3-11) can be used to evaluate the K_I value if one knows the stress field in vicinity of a crack tip. If the stress intensity factor in range, ΔK_I , gives rise to the material threshold, ΔK_{th} , substituting Eq. (5-3-4) into Eq. (5-3-11), we can find that the average stress in range $\Delta\sigma_{ave}$ is related to the fatigue limit of plain specimens $\Delta\sigma_o$; if $d = a_o$, then the threshold for crack propagation is characterised by an average stress, which is slightly larger than $\Delta\sigma_o$.

$$\Delta\sigma_{ave}|_{(Area, r=a_o)} = 1.1\Delta\sigma_o. \quad (5-3-12)$$

All of the methods imply that the critical-distance concept can be used in conjunction with the elastic stress distribution ahead of a crack, to predict whether or not the crack will propagate. In this case the relevant distance is related to a_o . For the point and line methods the correspondence is exact. For the area method, using a distance of a_o , the resulting prediction of the fatigue limit based on $\Delta\sigma_o$ (omitting the factor 1.1) is a slightly conservative estimate.

Now we have three methods which can predict the fatigue failure of a long crack. The point method examines the stress at the distance of $a_o/2$; the line method examines the average stress on the distance from 0 to $2a_o$; the area method examines the average stress over a semicircular area with a radius of a_o . Fig. 5.3.2 shows the geometrical definition of the point, line and area on a crack. We will extend the methods to short cracks and notches. In those cases, the geometrical definition of the methods is identical.

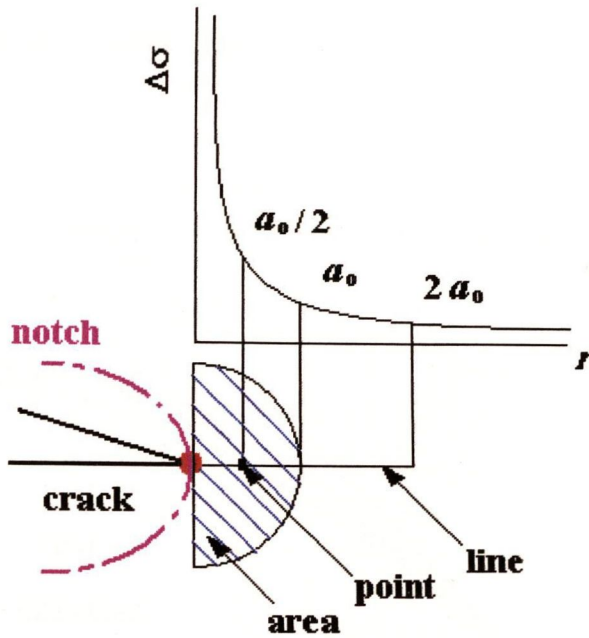


Fig. 5.3.2 The geometric definition of the point, line and area on a crack or notch

5.4 Application of the Model to Short Cracks

We extend this concept to consider the effect of crack size in this section. In order to do this, we use the Westergaard [1939] stress function, which is the exact result for the stress distribution to allow consideration of cases where the crack length is comparable in size to a_0 and the stress values at all positions are required. For a through crack in an infinite plate loaded by a uniform tensile stress σ , applied normal to the crack, Westergaard has shown that the elastic stress as function of distance from the crack tip, $\sigma(r)$ is:

$$\sigma(r) = \sigma \sqrt{1 - \left(\frac{a}{a+r}\right)^2} \quad (5-4-1)$$

This is the stress which acts in the same direction as the applied stress, i.e. in the crack opening direction. Fig. 5.4.1 shows predictions for the fatigue limit ($\Delta\sigma_{oc}$) as a function of crack length using the new point, line and area methods. The material constants chosen are those for a typical medium-carbon steel, tested by DuQuesnay et al [1986] at $R = -1$. Using the stress distribution of Eq. (5-3-2) results in the prediction labelled LEFM which is valid

only for long cracks. Use of Eq. (5-4-1) causes a reduction in fatigue limit which is more pronounced as a decreases, tending to $\Delta\sigma_o$ at zero crack length. The figure also shows the ElHaddad method.

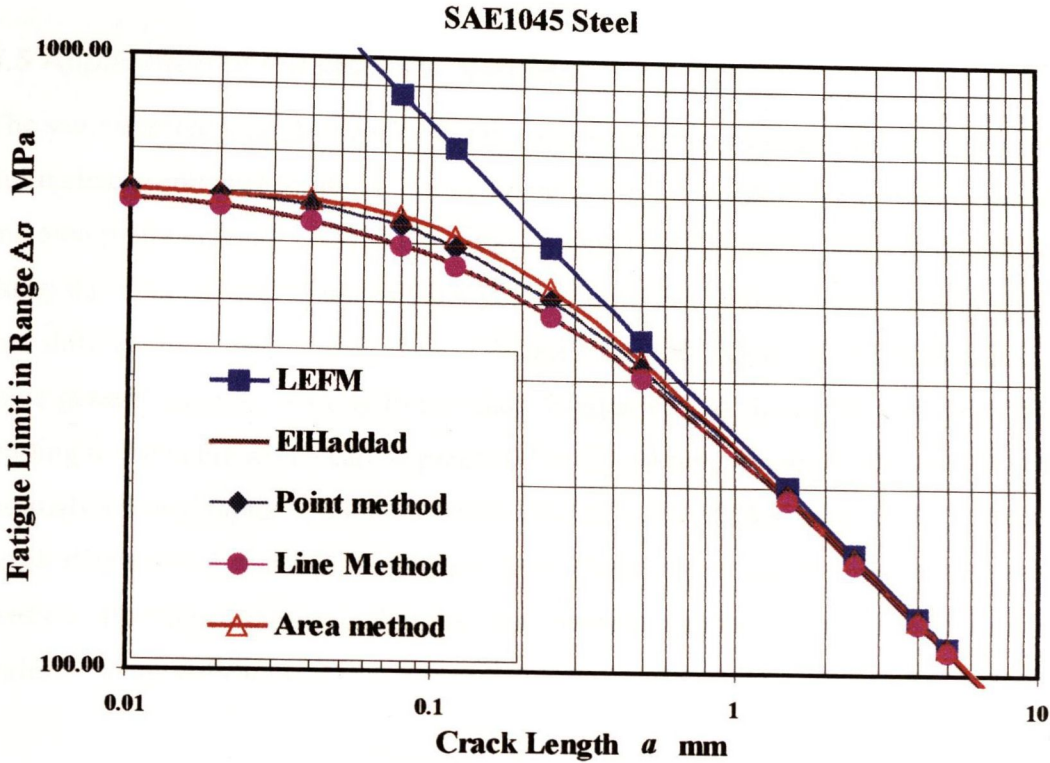


Fig.5.4.1 Prediction of the fatigue limit using the point, line and area method

All three methods (point, line and area) follow the general form of the ElHaddad line, indicating that they would give reasonable approximations to the experimental data. In fact the line method gives exactly the same result as the ElHaddad method, as can be shown mathematically as follows. The average stress over the distance from zero to $2a_o$ using Eq. (5-4-1) is:

$$\begin{aligned} \Delta\sigma_{ave} \Big|_{r=0-2a_o} &= \frac{1}{2a_o} \int_0^{2a_o} \Delta\sigma \sqrt{\frac{1}{1 - \left(\frac{a}{a+r}\right)^2}} dr \\ &= \Delta\sigma \sqrt{\frac{a+a_o}{a_o}} \end{aligned} \quad (5-4-2)$$

If this average stress is set equal to $\Delta\sigma_o$, then the applied stress $\Delta\sigma$ in Eq. (5-4-2) is equal to $\Delta\sigma_o$ (see Eqs. (5-3-4)). This is an important result because it provides a rational explanation for the empirical law of ElHaddad and thus gives a physical significance to the length parameter a_o .

5.5 Application of the Model to Notches

The same approach can be applied to the consideration of notches. We used the linear elastic finite element method to obtain the stress field. Fig.5.5.1 shows the results of the point, line and area predictions for circular holes in the same medium carbon steel as mentioned above, using the same critical distance values. The figure also shows some experimental data for four different hole diameters at $R = -1$ [DuQuesnay *et al*, 1986]. All prediction lines show the same general features, tending to the plain fatigue limit as the notch size tends to zero, and tending to the value which can be predicted using the notch method when notch size is large. As analysed in Chapter 4, some of circular holes behaved like short cracks and the one with notch depth of 1.5 mm behaved like a blunt notch which can be predicted using the notch method. The figure shows us that the new methods can overcome these types of problems without any modification.

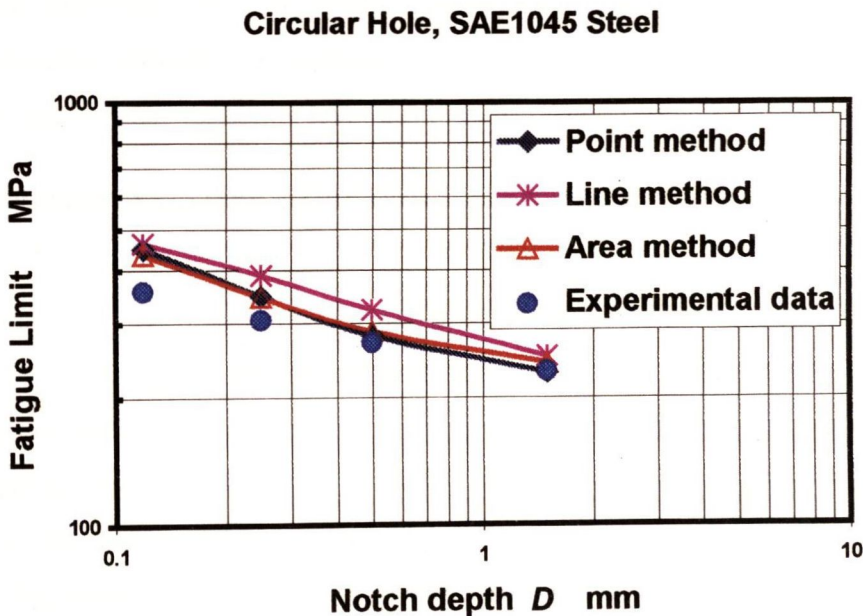


Fig. 5.5.1 Prediction the fatigue limit of circular holes using the point, line and area methods, compared with experimental data.

5.6 Discussion

5.6.1 Input parameters needed

It has been shown that a single theory can predict the fatigue limits of both cracks and notches and can also account for the variation of fatigue limit with size in both of these features. This is a useful result because it brings together two areas of the subject which have traditionally been treated quite separately.

The present approach also has the advantage that it removes the empiricism which was inherent in earlier treatments of the size effect. This has been done by identifying the length constant as a_o which is a quantity that can be calculated knowing two other experimental quantities: the plain-specimen fatigue limit ($\Delta\sigma_o$) and crack propagation threshold (ΔK_{th}).

The threshold value is relatively difficult to measure since it involves monitoring the growth of a crack at various applied stress intensity values. A simpler approach is to deduce ΔK_{th} from the fatigue limit of specimens containing sharp notches. In principle it is possible to find all three quantities ($\Delta\sigma_o$, ΔK_{th} and a_o) from fatigue limit data measured from any two different geometric features, e.g. notches of two different shapes or cracks of different sizes. This is very useful because fatigue testing is expensive and time-consuming.

5.6.2 Comparison of the new methods with previous approaches

Next we discuss two previous approaches to this problem. The first is the work of Klesnil and Lucas [1980] who predicted the fatigue limit for a notch by assuming that the critical stage in the process was the growth of a crack of length l_c , a length which is almost the same as a_o . This method has the advantage that it models the known physical process of fatigue: the growth of a crack. Disadvantages are the simplifying assumptions that must be made concerning the stress intensity of this crack/notch combination in the elastic/plastic stress field and, more importantly, uncertainty about the growth rate of the small crack, which will be subject to the size effect discussed above. Also it is difficult to imagine how this method could be applied to cracks.

Another approach of interest is that of Pluvinage and co-workers [Boukharouba *et al*, 1995; Pluvinage, 1997] who extended their concept of a notch stress intensity factor to include the idea of a critical distance, X_e . Their approach is similar to the point method used in the present work, except that X_e is not a material constant; it is primarily related to the notch stress distribution, being an estimate of the distance over which the stress remains relatively high compared to the hot spot stress. They define this as the region over which their notch stress intensity factor is unable to predict the stress level. Material properties are introduced because the stress distribution is modified in an elastic-plastic analysis which takes account of the material's cyclic stress-strain behaviour. Grain size is also used, though it is not clear how this is taken into account. Overall the model is similar to the present one but the definition of the critical distance is complex and liable to extrapolation errors. It requires specialised material information, the cyclic stress-strain curve, which is relatively difficult to obtain. The method does not seem to be able to predict the size effect, or the behaviour of cracks.

5.6.3 Extension to other loading modes

Based on the linear elastic stress analysis, the new theory developed in this chapter gives the possibility of using any stress components, such as the maximum principal stress (MPS), Von-Mises stress etc. The rule of choosing the stress components depends on material type and the type of loading mode. In this thesis attention is focused on the opening crack mode, which is caused by MPS.

However, many service failures occur from cracks subjected to mixed mode loading. For example, the fatigue failure of a mild steel bar under torsional loads may be caused by the maximum shear stress [Brown and Miller, 1989]. It is necessary to develop a methodology to satisfy these engineering requirements. In fact, the new theory developed in this chapter can be extended to any other crack modes and also to mixed modes. In the following paragraphs, we will take the Line Method as an example to show how to apply the new methods to the other two modes.

From fracture mechanics, the resulting asymptotic solutions for mode II, in plane sliding, are

$$\begin{Bmatrix} \sigma_{xx} \\ \sigma_{yy} \\ \sigma_{xy} \end{Bmatrix} = \frac{K_{II}}{\sqrt{2\pi r}} \begin{Bmatrix} -\sin \frac{\theta}{2} \left(2 + \cos \frac{\theta}{2} \cos \frac{3\theta}{2} \right) \\ \sin \frac{\theta}{2} \cos \frac{\theta}{2} \sin \frac{3\theta}{2} \\ \cos \frac{\theta}{2} \left(1 - \sin \frac{\theta}{2} \sin \frac{3\theta}{2} \right) \end{Bmatrix}. \quad (5-6-1)$$

And mode III, anti-plane shear, it can be shown that

$$\begin{Bmatrix} \sigma_{xz} \\ \sigma_{yz} \end{Bmatrix} = \frac{K_{III}}{\sqrt{2\pi r}} \begin{Bmatrix} -\sin \frac{\theta}{2} \\ \cos \frac{\theta}{2} \end{Bmatrix}. \quad (5-6-2)$$

When θ is equal to 0, only one non-zero stress component exists in each mode. They are

$$\begin{aligned} \sigma_{xy} &= \frac{K_{II}}{\sqrt{2\pi r}}, & \text{for mode II;} \\ \sigma_{yz} &= \frac{K_{III}}{\sqrt{2\pi r}}, & \text{for mode III.} \end{aligned} \quad (5-6-3)$$

In the same way as in developing the Line Method, the stress intensity factor for each mode can be obtained and they are

$$\begin{aligned} \Delta K_{II} &= \sqrt{\frac{\pi}{4a_o}} \int_0^{2a_o} \Delta \sigma_{xy} dr, & \text{for mode II;} \\ \Delta K_{III} &= \sqrt{\frac{\pi}{4a_o}} \int_0^{2a_o} \Delta \sigma_{yz} dr, & \text{for mode III.} \end{aligned} \quad (5-6-4)$$

In fracture mechanics, criteria of fatigue failure under mixed model loading are related with ΔK_{II} and ΔK_{III} . For different models various criteria should be used for fatigue crack prediction. This is beyond the study in this thesis.

5.6.4 Further work

An interesting finding of the present work is that there appears not to be a fundamental difference between the behaviour of cracks, the behaviour of blunt stress concentrations such as holes or indeed the behaviour of plain, unnotched specimens. The fatigue limit of all three categories of geometrical feature can be predicted using the same general law. Now it is recognised that fatigue failure involves two quite different processes: the initiation of a crack and its subsequent propagation through the body. But the present work suggests that, at least as far as the fatigue limit is concerned, these processes are indistinguishable, so that the presence of a pre-existing crack does not alter the mechanism by which fatigue proceeds to failure. So further research is needed to understand the mechanism of fatigue failure.

Three different methods have been mentioned here: the point, line and area methods. It has been shown formally that they can all give solutions that are exact for a long crack. For short cracks, the solutions differ from the ElHaddad law and from each other by less than 10%. For the case of circular holes the differences were larger, 20%, but care should be exercised here because the type of experimental data used has an uncertainty of at least 10%, so a large amount of data would have to be analysed in order to distinguish between the various methods. So far only circular holes are analysed; more applications to specimens and components will be reported in the following chapters.

5.7 Conclusions

1. Critical-distance analyses, which are normally used to predict the fatigue limits of notched bodies, can also be applied to bodies containing long, sharp cracks. In this case the critical distances can be found analytically, as functions of the material's threshold and plain-specimen fatigue limit. The distance parameters are related to a_0 which is the ElHaddad constant used in short-crack analysis.
2. Short crack effects can be predicted using the critical-distance analyses. The variation of fatigue limit with crack length is found to be similar to that in ElHaddad's equation. Experimental data can be predicted with reasonable accuracy in this way.
3. The same methods can also be used to predict the behaviour of notches: analysis of data on circular holes in two different materials gave good predictions of the fatigue limits as a function of hole size.

Chapter 6 Notched Specimen Verification

6.1 Introduction

In this chapter, experimental data reported in the literature and in-house results are used to assess the validity of the new theories developed in the previous chapters. The effect of notch depth, of notch acuity, of notch and specimen type, of load ratio, and of material properties on the threshold stresses are considered. Particular attention is paid to the inclusion of very small notches in order to test prediction of the size effect. As a comparison, some traditional methods are tested using these data as well.

A total of ten methods were applied on the notched specimens. They are:

1. LEFM – the standard crack prediction following Smith and Miller, using the following equation

$$\Delta\sigma_{on} = \Delta K_{th} / F\sqrt{\pi D}. \quad (6-1-1)$$

The fatigue limit $\Delta\sigma_o$ here is the nominal (gross section) stress applied to the notched specimen. The constant F is determined by the geometry of the equivalent crack.

2. ElHaddad – the LEFM prediction modified using ElHaddad's correction for the stress intensity, using Eq. (2-4-1).
3. CMM – the crack modelling method.
4. NM – the notch method as used by Smith and Miller (using Eq. (2-2-3)).
5. CMMscr – the crack modelling method modified by the ElHaddad correction using a_o . For notched specimens with regular geometry, the Methods 1 and 2 in Chapter 4 are identical.
6. AVE. CMM&NM – Method 4 in Chapter 4 in which a prediction is made by averaging the fatigue limit found from the CMM and NM methods. The method was developed for analysing small notches.
7. PM – the point method using stresses at a point $a_o/2$ from the hot spot.
8. LM – the line method, averaging stresses over a line of length $2a_o$.

9. AM – the area method, averaging stresses over a semi-circle of radius a_o .
10. K&L – the Klensnil & Lucas method (Eq. (2-1-5)), taken to typify previous critical distance methods.

6.2 Experimental Details

A total of ten different sets of experimental data were chosen for verification; they are listed in Table 6.2.1. The materials included two aluminium alloys, two cast irons, three carbon steels, and two special alloy steels. The notch types of specimens included a circumferential notch cylindrical bar (CNB), a centre notch in a flat plate (CNP), a double edge notch in flat plate (DENP), and a single edge notch in flat plate (SENP). The values of load ratio R were from -1 to 0.7 . The load types included tension and bend. The fatigue limit was defined at 10^7 cycles.

6.2.1 Steel samples

- Mild Steel (0.15%C)

Two sets of data were chosen for axial loading. The geometries of these two group samples were different. One of them was machined in 43 mm outside diameter bar containing a circumferential vee-notch 5.08 mm deep and of root radii varying from 0.05 mm to 5.08 mm. The other was machined in 64 mm width flat plate with 5.08 mm double edge notches and root radii varying from 0.1 mm to 7.62 mm. Both of them were tested in push-pull [Frost, 1974 and Harkegard, 1981].

Another set of data was used for assessing rotating bending. The samples were made of the same material but with different heating treatment. The specimens were machined in 12.7 mm outside diameter bar containing a circumferential vee-notch 1.3 mm deep and of root radii varying from 0.005 mm to 2.3 mm. All specimens were stress-relieved for one hour at $650\text{ }^\circ\text{C}$ *in vacuo* after final machining and were tested in rotating bending [Frost, 1974]. Because of the heat treatment the threshold stress intensity factor was lower than usual (ΔK_{th}

= 6.5 MPa m^{1/2}). The same kind of specimens with different sizes and geometry were also tested in reversed direct stress. Smith and Miller [1978] treated these notches, of which the stress concentration factor was larger than a certain value ($K_t = 3$), as cracks and got predictions which compared well with the experimental results.

- SAE 1045

DuQuesnay *et al* [1986] tested this material for the investigation of the short crack effect. Flat plate specimens were machined from rolled plates such that the loading axis was parallel to the final direction of rolling. Circular notches were then drilled at the centre of the plate specimens. Notch diameters of 3 mm, 1 mm, 0.5 mm, and 0.24 mm were used. The surface of each specimen was hand polished to remove any sharp edges surrounding the notch. The geometry and dimensions of each notch were then checked by means of a travelling microscope with a resolution of 0.025 mm. The specimens were tested in uniaxial, fully reversed stressing ($R = -1$) until fracture. For this simple notch geometry the stress field was given by Airy's equation,

$$\sigma(\chi) = \frac{\sigma}{2} \left(2 + \left(\frac{a_n}{\chi} \right)^2 + 3 \left(\frac{a_n}{\chi} \right)^4 \right) \quad (6-2-1)$$

where a_n is the size of the notch (i.e. the hole radius) and χ is the distance measured from the centre of the hole.

- Steel 15315 (2.25Cr-1Mo).

This is a pressure vessel steel. Lukas *et al* [1986] performed fatigue tests for investigating non-damaging notches. They used specimens with a cylindrical gauge section of 5 mm dia.. They machined circumferential semicircular notches with radii ranging from 10 to 800 μ m in the middle of the gauge length. After machining all specimens were subjected to a stress relief heat treatment and tested under symmetrical loading conditions ($R = -1$).

- SM41B

This is a structural low-carbon steel. The specimens were centre-notched plates whose width and thickness were 45 and 4 mm. The notch had a length of 6 mm and a tip-radius of 0.16 mm. After machining, the specimens were annealed at 1200 °C for 5 hours in vacuum and cooled in a furnace. A notch was made after the heat treatment with an electro-discharge machine and then the specimens were reheated at 650 °C for 90 min to relieve the residual stress. All specimens were electro-polished and then tested in uniaxial tension with varying load ratios [Tanaka and Nakai, 1983]. Another group of specimens were machined with varying tip radii and tested in push-pull.

6.2.2 Aluminium alloy samples

- Al 2024-T351

The details of the specimen and fatigue test are the same as the steel SAE 1045 [DuQuesnay *et al*, 1986].

- LM25

This is a cast aluminium alloy tested in house. Ingots were obtained from a local manufacturer. Specimens were machined in single edge notched tension bars. The width, thickness and length were 20 mm, 10 mm and 120 mm respectively. A through-thickness sharp notch was machined into the specimen. The notch depths were 3 mm and 5 mm. The notch tip radius was less than 0.1 mm and the angle of the vee-notch was 58°. This was expected to be a crack-like notch. Specimens were tested under uniaxial tension ($R = -1$) at room temperature. The fatigue tests were also carried out on material in the TF heat treatment form. In this form only 3 mm notched specimens were tested because of the limited number of samples.

6.2.3 Cast iron samples

- Grey cast iron

Taylor *et al* [1996] tested a grey cast iron (grade 17) to study the notch fatigue behaviour. The specimens were machined in 30 mm outside diameter bar containing a circumferential vee-notch 3.18 mm deep, of root radius 0.3 mm and vee-notch angle 90°. The fatigue testing was carried out in uniaxial tension to obtain the fatigue limit at four different R ratios: -1, 0.1, 0.5 and 0.7.

Table 6.2.1 Material properties used in the threshold stress predictions

Case	Material	R	$\Delta\sigma_o$	ΔK_{th}	a_o	σ_y	Geometry
1	Mild steel (0.15%C) [Frost, 1974 and Harkegard, 1981]	-1	420	12.8	0.296	340	CNB# $D = C, \rho = V$
2	Mild steel (0.15%C) [Frost, 1974 and Harkegard, 1981]	-1	420	12.8	0.296	340	DENP# $D = C, \rho = V$
3	Mild steel [Frost, 1974 and Smith & Miller, 1978]	-1	520	6.5	0.05		CNB* $D = C, \rho = V$
4	Steel SAE 1045 [DuQuesnay <i>et al</i> , 1986]	-1	608	13.9	0.166	472	CNP# $D = \rho = V$
5	Steel 15313 (2.25Cr-1Mo) [Lukas <i>et al</i> , 1986]	-1	440	12.0	0.237	380	CNB# $D = \rho = V$
6	Steel SM41B [Tanaka and Nakai, 1983]	-1	326	12.36	0.458	194	CNP#
		0.0	274	8.36	0.296	194	$D = C,$
		0.4	244	6.38	0.218	194	$\rho = C$
7	Steel SM41B [Tanaka and Nakai, 1983]	-1	326	12.36	0.458	194	CNP# $D = C, r = V$
8	Al-2024-T351	-1	248	5.0	0.129	357	CNP#

	DuQuesnay <i>et al</i> , 1986]						$D = \rho = V$
9	LM25	-1	77.5	5.94	1.87		SENP# $D = V, \rho = C$
10	Grey cast iron [Taylor <i>et al</i> , 1996]	-1	155	15.94	3.15		CNB# $D = C,$ $\rho = C$
		0.1	99	11.2	4.07		
		0.5	68	8.0	4.41		
		0.7	48	5.2	3.74		

Uniaxial tension test. * Rotating bending test.

Table 6.2.1 lists the material properties and test conditions of all specimens: (1) load ratio R , (2) fatigue limit range of plain specimens $\Delta\sigma_o$, (3) long-crack threshold stress intensity range ΔK_{th} , (4) yield stress σ_y , (5) geometry and (6) short crack constant a_o . ρ is notch tip radius and D is notch depth. C represents a constant value. V represents a variable value.

6.3 Stress Analysis

In each case an elastic finite element analysis was carried out using ANSYS software. The stress parameter used in all cases was the 1st principal stress, which is equal to the maximum principal stress in a tensile stress field.

6.3.1 Element type

For plate specimens, an 8-node element was used because it provides more accurate results than a 4-node element for mixed (quadrilateral-triangular) automatic meshes and can tolerate irregular shape without as much loss of accuracy. The elements have compatible displacement shapes and are well suited to model curved boundary shapes, especially at notch roots.

For circumferential-notch cylindrical bars, a harmonic element was used for 2-D modelling of axisymmetric structures with both axisymmetric and non-axisymmetric loading, such as uniaxial tension and bending. A quarter or half model was chosen for the sample with the symmetric structure. The boundary condition should be carefully applied at the symmetry

line. The use of an axisymmetric model greatly reduces the modelling and analysis time compared to that of an equivalent 3-D model.

6.3.2 Load condition

The stress at a point on the surface of a rotating bending specimen varies sinusoidally between numerically equal maximum tensile and compressive values once a revolution. In another words, assuming the specimens remain wholly elastic, $\Delta\sigma = 32 \Delta M / \pi \phi^3$, where $\Delta\sigma$ is the maximum surface stress in range, ΔM is the bending moment in range at the cross-section under consideration and ϕ is the specimen diameter. This non-axisymmetric load can be applied to the harmonic element.

In ANSYS the load is defined as a series of harmonic functions (Fourier series). For example, a load F is given by

$$F(\theta) = A_0 + A_1 \cos \theta + B_1 \sin \theta + A_2 \cos 2\theta + B_2 \sin 2\theta + \dots \quad (6-3-1)$$

Each term of the above series must be defined as a separate load step. A term is defined by the load coefficient (A_l or B_l), the number of harmonic waves (l), and the symmetry condition ($\cos l\theta$ or $\sin l\theta$). The number of harmonic waves, or the mode number, is input with the *mode* command. For rotating bending, the load is pure bending, we use $MODE = 1$ and $ISYM = \text{cosine}$ (as default). The applied moment (ΔM) due to an axial input force (ΔF_Y) for this case can be computed as follows

$$\Delta M = \int (\Delta F_Y (\cos \theta) / 2\pi\delta) (\delta \cos \theta) (\delta d\theta) = \Delta F_Y \delta / 2 \quad (6-3-2)$$

So the input force, ΔF_Y , can be determined by

$$\Delta F_Y = \frac{\Delta \sigma \phi^3}{16\delta} \quad (6-3-3)$$

where δ is the distance between the axis and the point where ΔF_Y is applied. Considering the effect of the concentration force, we apply ΔF_Y at a distance as far as 3 times the sample diameter away from the notch and the effect on the notch region, which is shown in the stress contour plot, is very small and can be neglected.

6.4 Definition of Prediction Error

In this thesis, the procedure of fatigue analysis can be divided into three general steps, as shown in Fig. 6.4.1. The first step is Stress Analysis. Stress analysis is carried out mostly using the finite element method. Sometimes analytical solutions may be used if the sample or component has a regular geometry.

The second step is Parameter Evaluation. There are several methods that are used or developed for fatigue failure prediction in this thesis. Each method involves different parameters. The parameters concerned with material behaviour are the threshold stress intensity factor ΔK_{th} and the fatigue limit of plain specimens $\Delta\sigma_o$. Corresponding parameters from the FEA are stress intensity factor range, ΔK_{FE} and stress range, $\Delta\sigma_{PRED}$, for applied loads ΔP_{FE} .

The third step is failure load prediction. The fatigue limit load range, ΔP_o , for a specimen or component can be found as shown in Fig. 6.4.1. In the equation, ΔP_{FE} represents a load applied to the FE model, which can be forces, displacements or temperature loads. Knowing the experimental fatigue limit test result, ΔP_T , the prediction error can be defined as shown in the equation (6-4-1):

$$Error = \frac{(\Delta P_o - \Delta P_T)}{\Delta P_T} * 100\% . \quad (6-4-1)$$

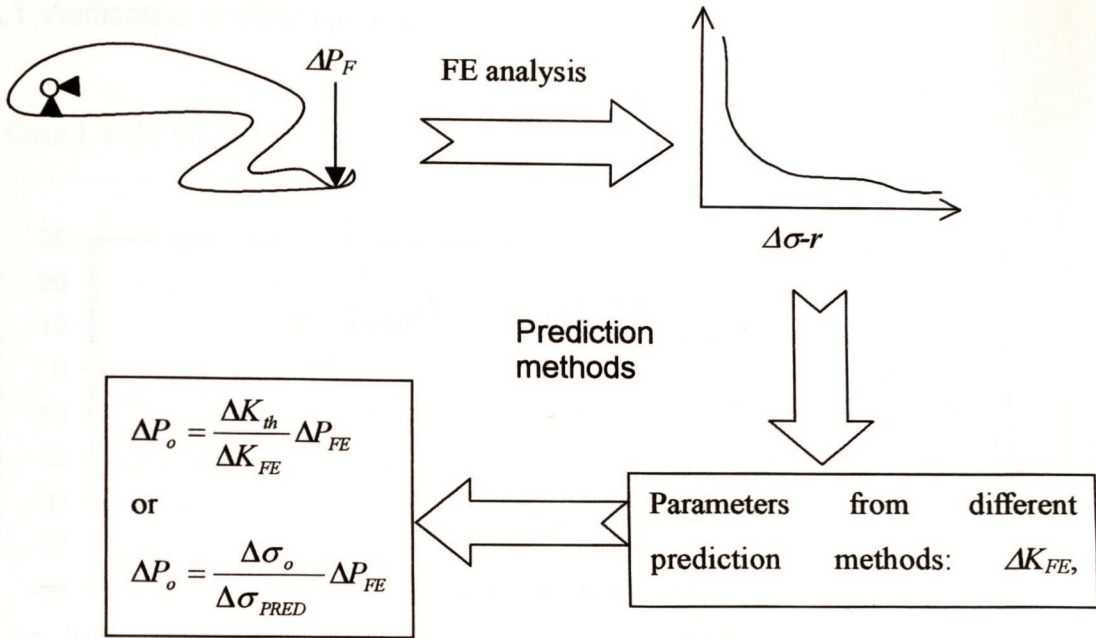


Fig. 6.4.1 Schematic present of the proceeding of prediction fatigue failure

If the error is positive, it means that the prediction is overrated, non-conservative. Otherwise the prediction is underrated, conservative. For engineering applications, an error between $\pm 20\%$ is acceptable, considering errors in experiments and numerical analysis.

6.5 Prediction Results

In this section, the prediction results are shown in the terms of the percentage difference between the predicted and experimental fatigue limits, with a negative value indicating a conservative prediction. Each case, is subdivided into three graphs for clarity; in each graph the following predictions are shown using variable method:

On graph (a) – LEFM, ElHaddad and CMM;

On graph (b) – NM, CMM, CMMscr and AVE.CMM&NM;

On graph (c) – PM, LM, AM, K&L.

In Case 9 only graphs (b) and (c) are shown because we use the ElHaddad method here to evaluate the threshold of the material (see in Chapter 7) instead of a prediction method.

6.5.1 Verification of steel samples

◆ Case 1 Mild Steel CNB

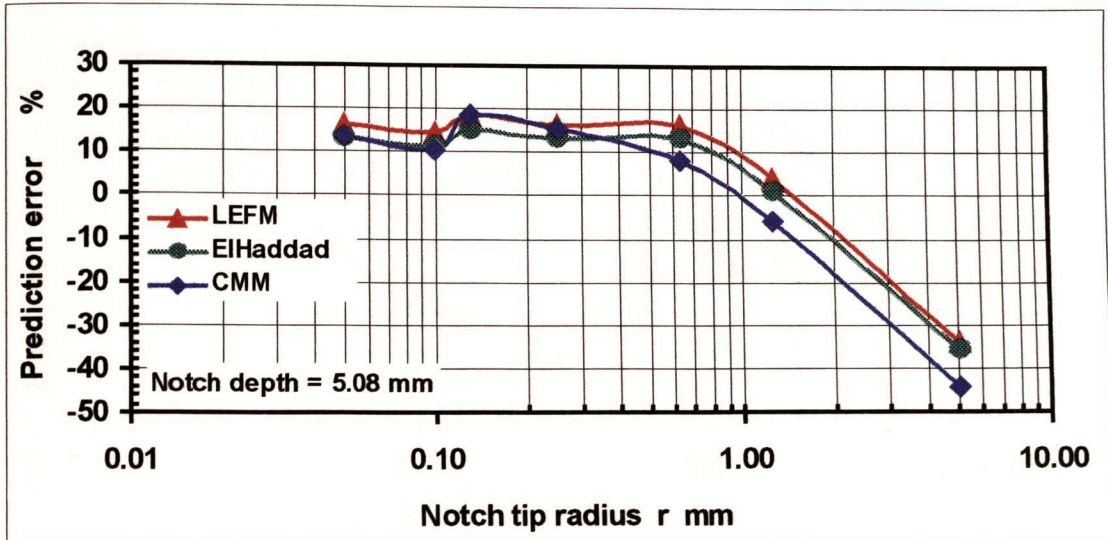


Fig. 6.5.1 (a) Prediction error on Mild Steel CNB samples

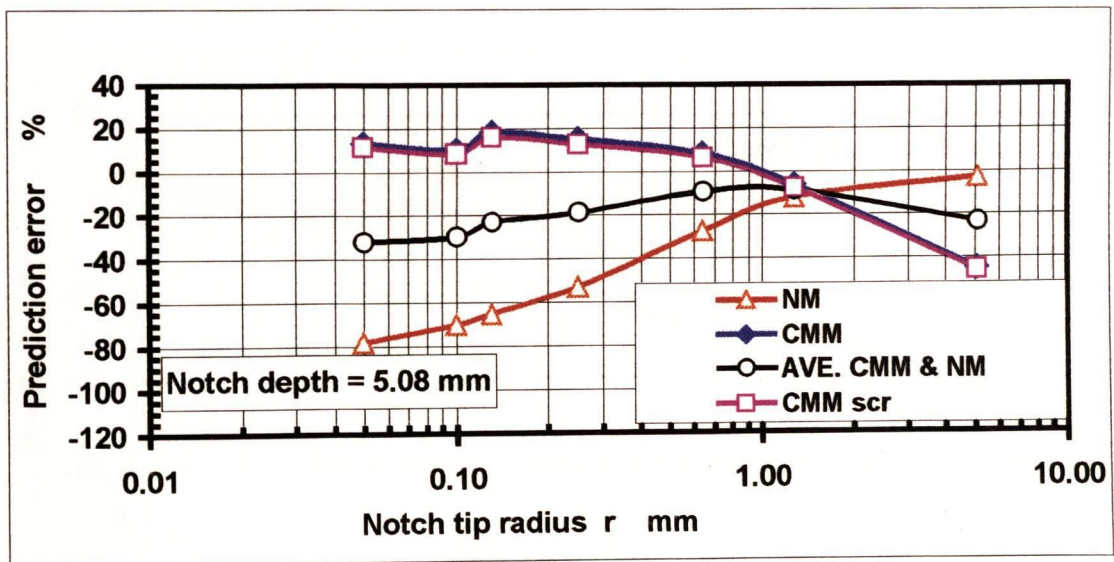


Fig. 6.5.1 (b) Prediction error on Mild Steel CNB samples

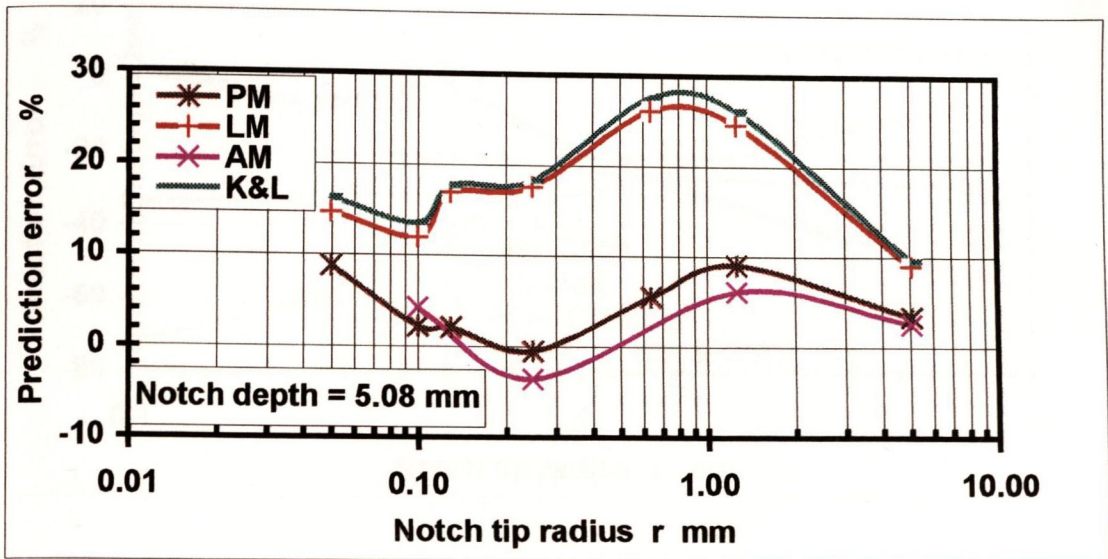


Fig. 6.5.1 (c) Prediction error on Mild Steel CNB samples

◆ Case 2 Mild Steel DENP

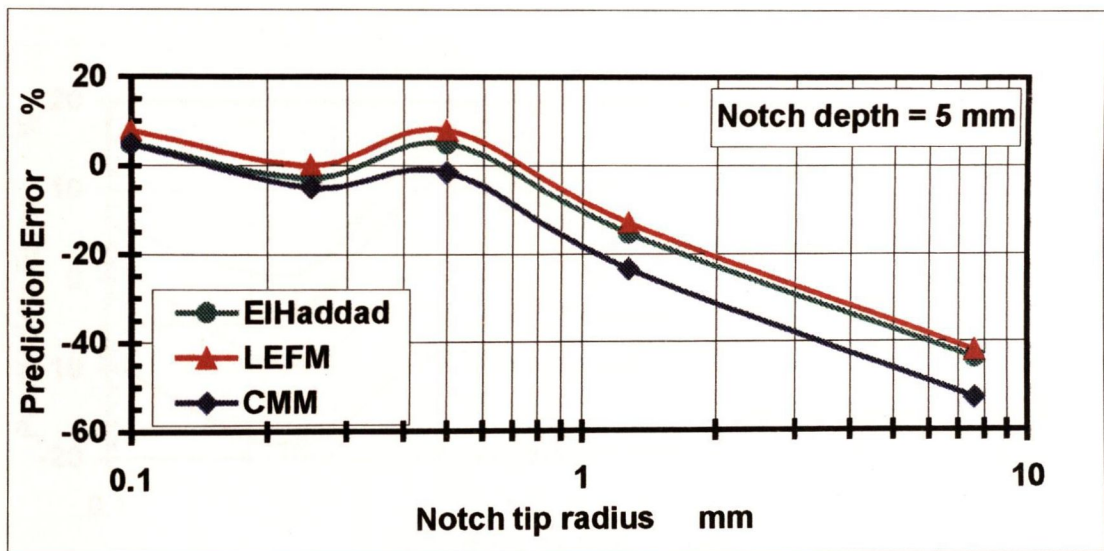


Fig. 6.5.2 (a) Prediction error on Mild Steel DENP samples

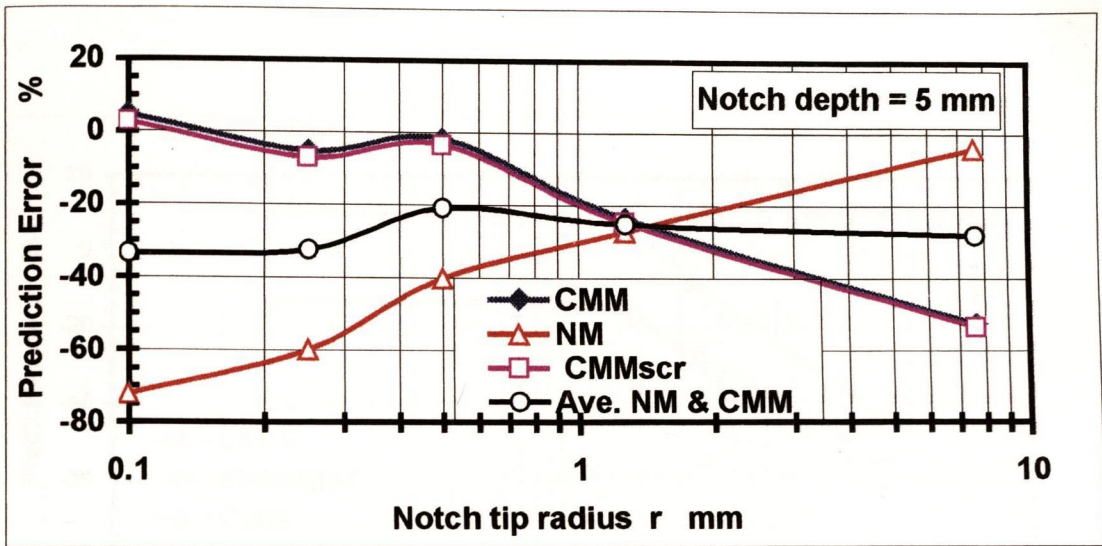


Fig. 6.5.2(b) Prediction error on Mild Steel DENP samples

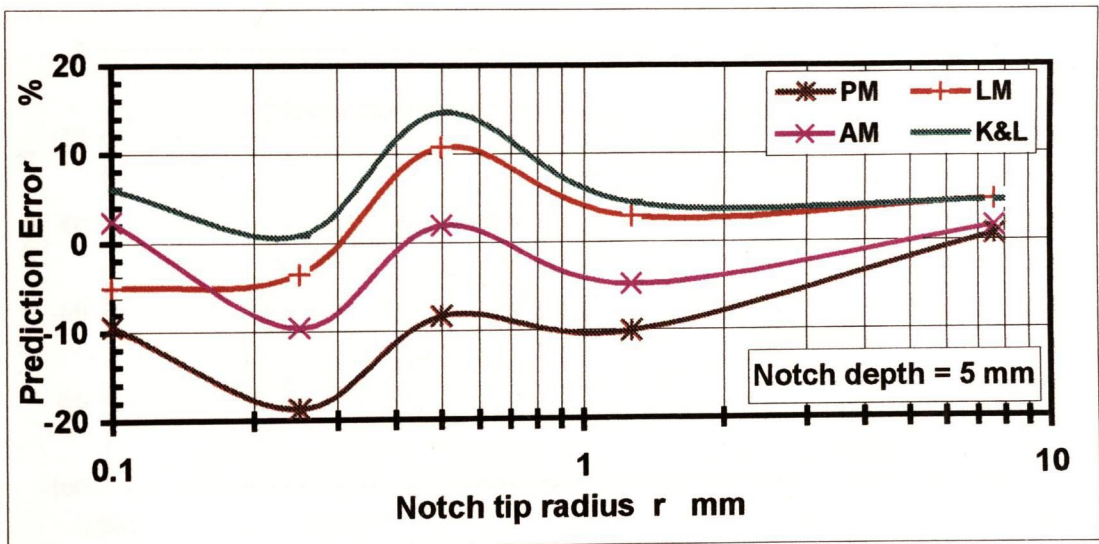


Fig. 6.5.2(c) Prediction error on Mild Steel DENP samples

◆ Case 3 Mild Steel CNB under rotating bending load

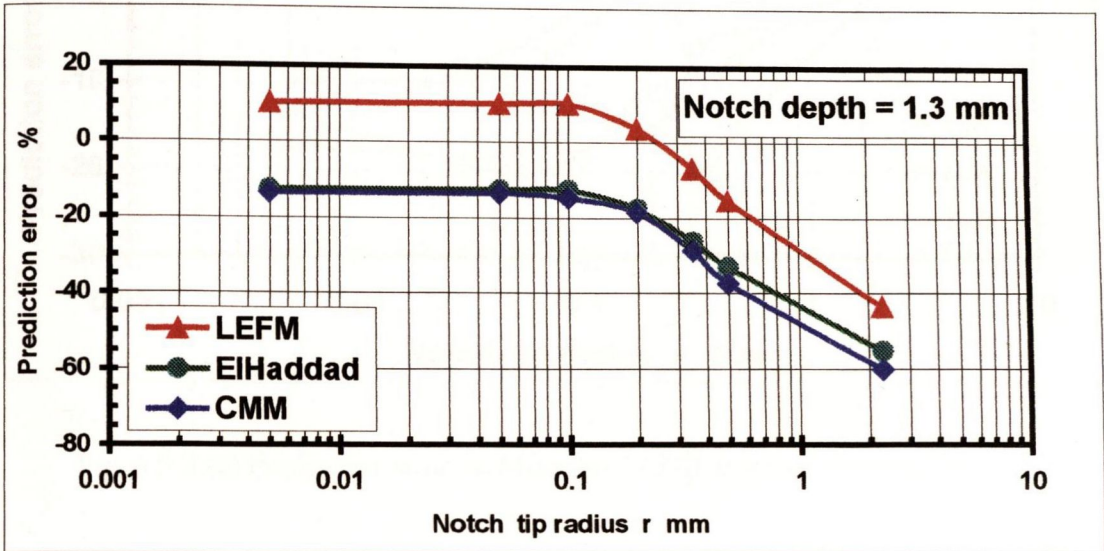


Fig. 6.5.3 (a) Prediction error on Mild Steel CNB samples, rotating bending.

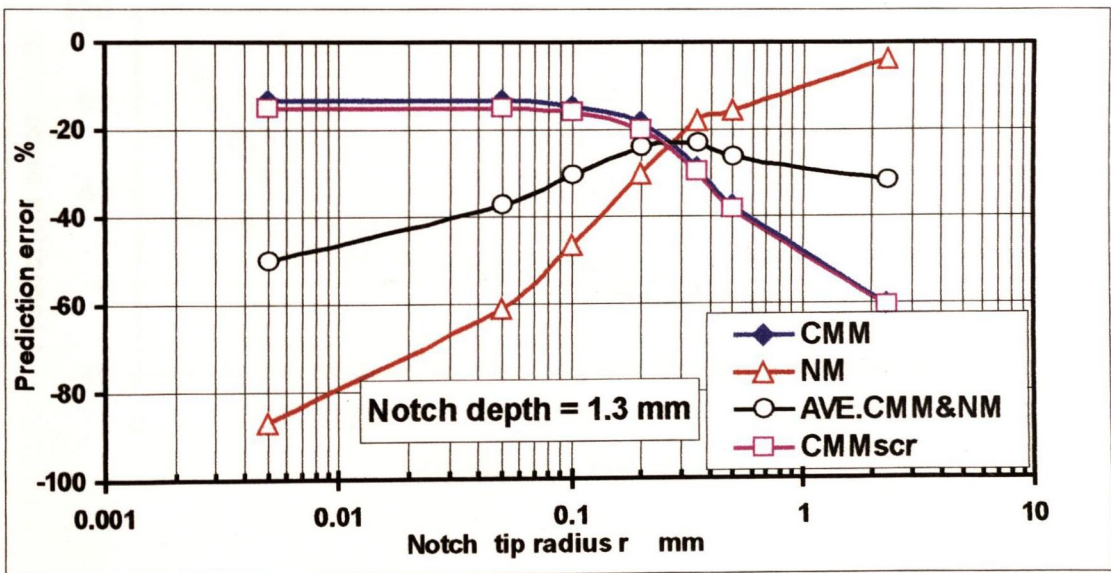


Fig. 6.5.3 (b) Prediction error on Mild Steel CNB samples, rotating bending.

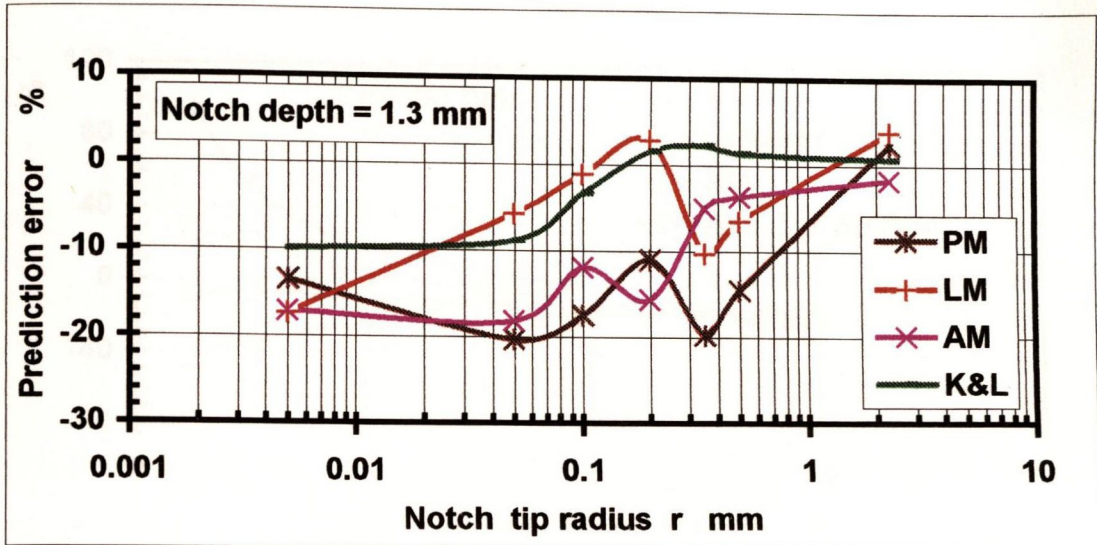


Fig. 6.5.3 (c) Prediction error on Mild Steel CNB samples, rotating bending.

◆ Case 4 SAE 1045 CNP

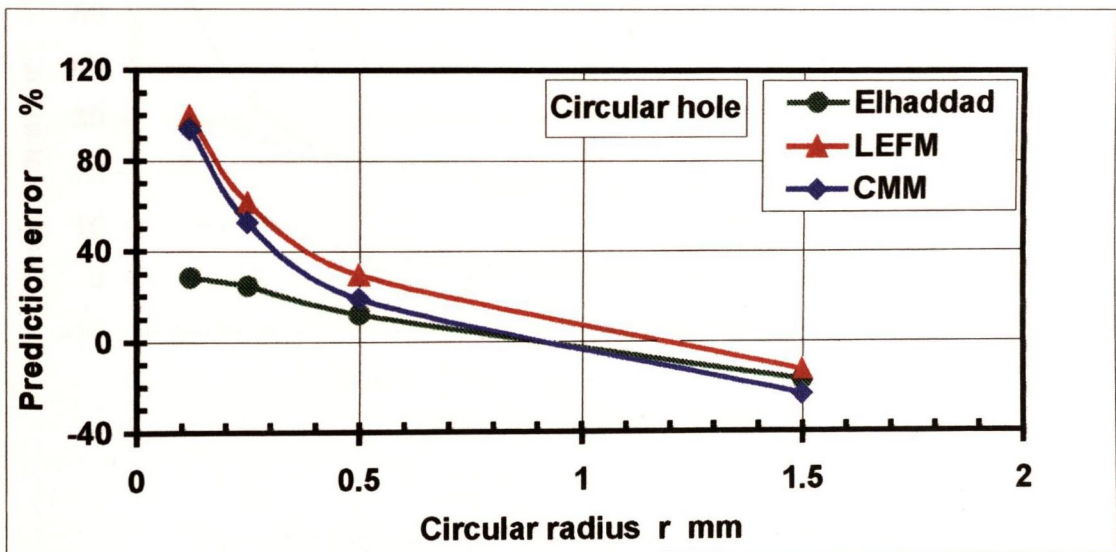


Fig. 6.5.4 (a) Prediction error on SAE 1045 CNP samples

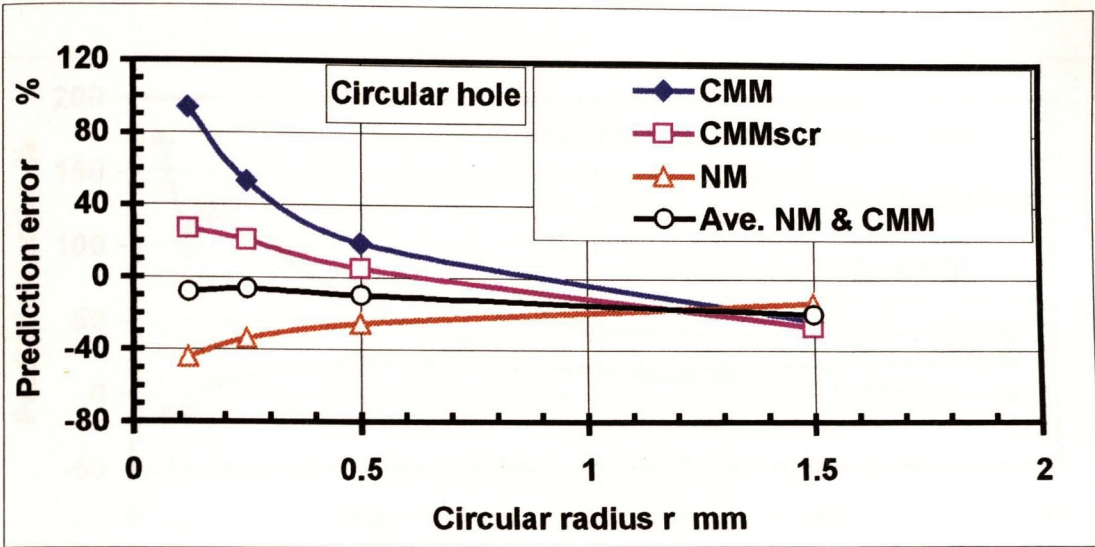


Fig. 6.5.4 (b) Prediction error on SAE 1045 CNP samples

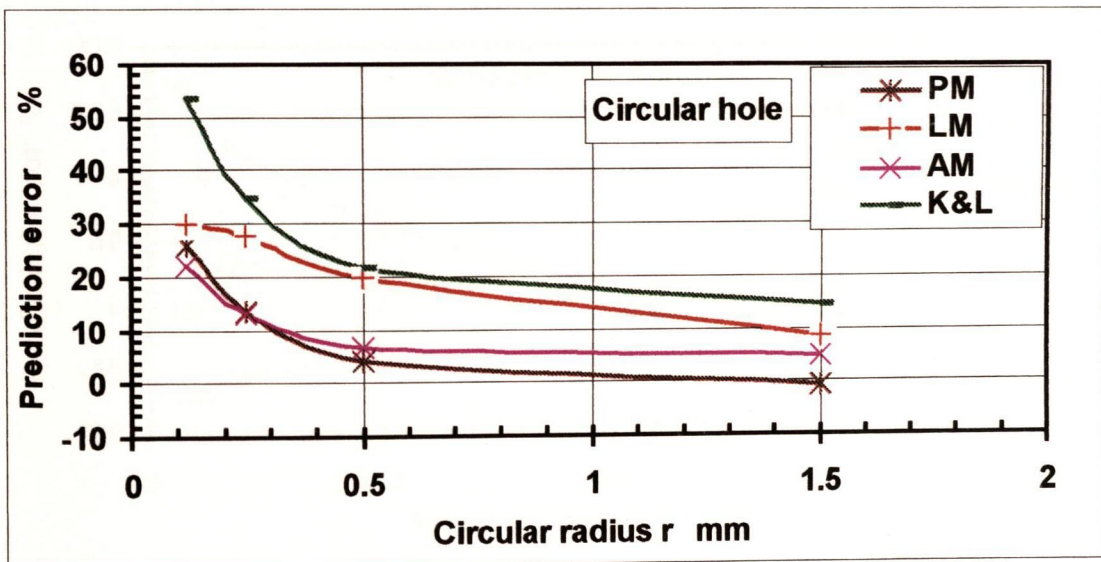


Fig. 6.5.4 (c) Prediction error on SAE 1045 CNP samples

◆ Case 5 Steel 15315 CNB

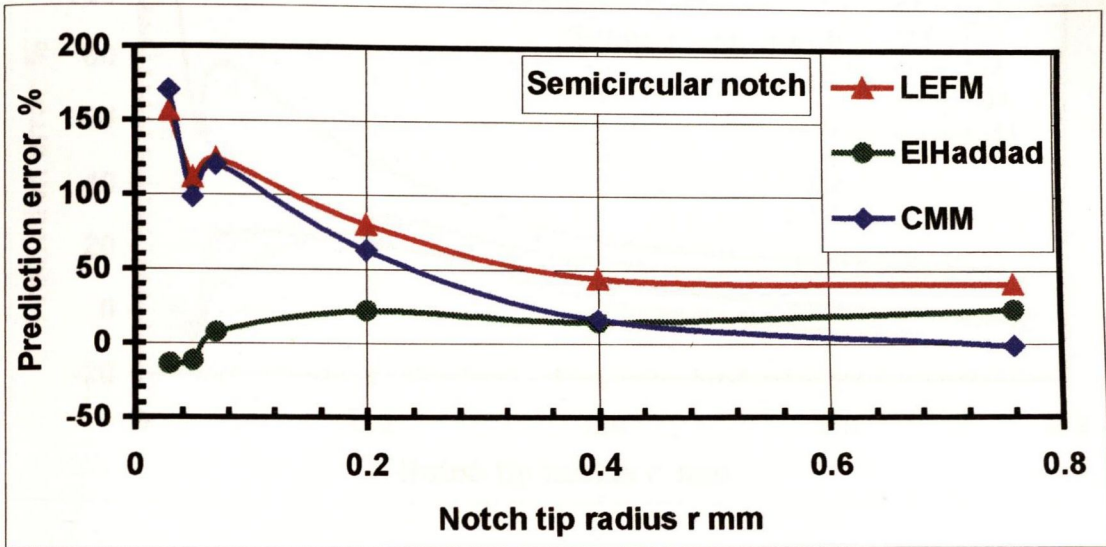


Fig. 6.5.5 (a) Prediction error on Steel 15315 CNB samples

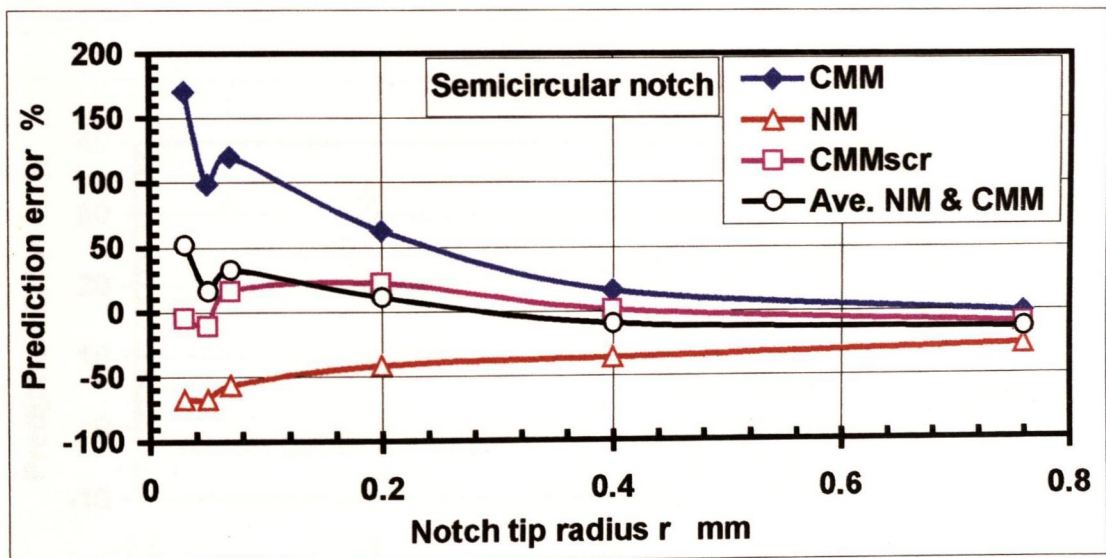


Fig. 6.5.5(b) Prediction error on Steel 15315 CNB samples

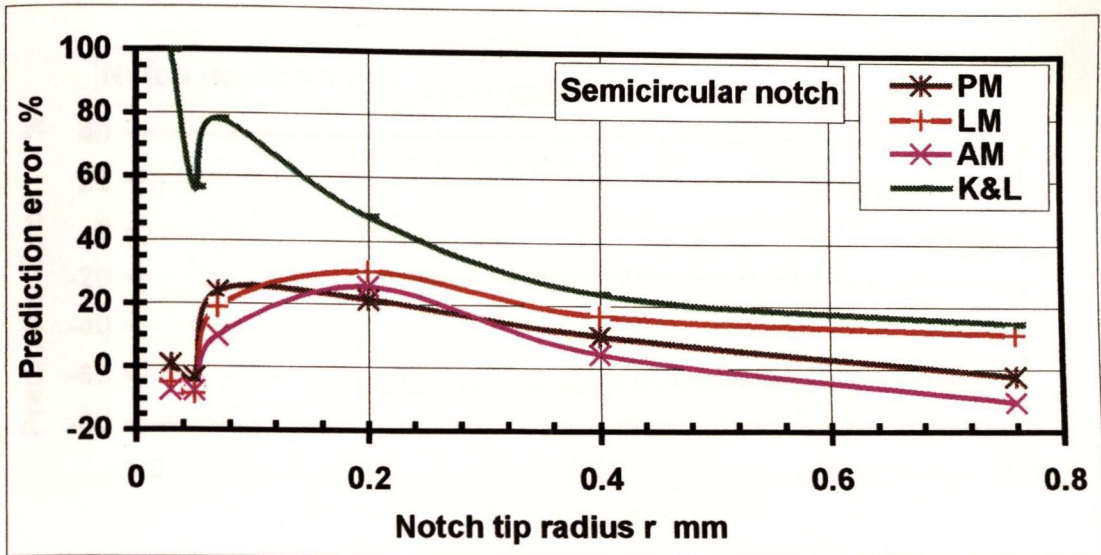


Fig. 6.5.5 (c) Prediction error on Steel 15315 CNB samples

◆ Case 6 SM41B CNP under variable load ratio

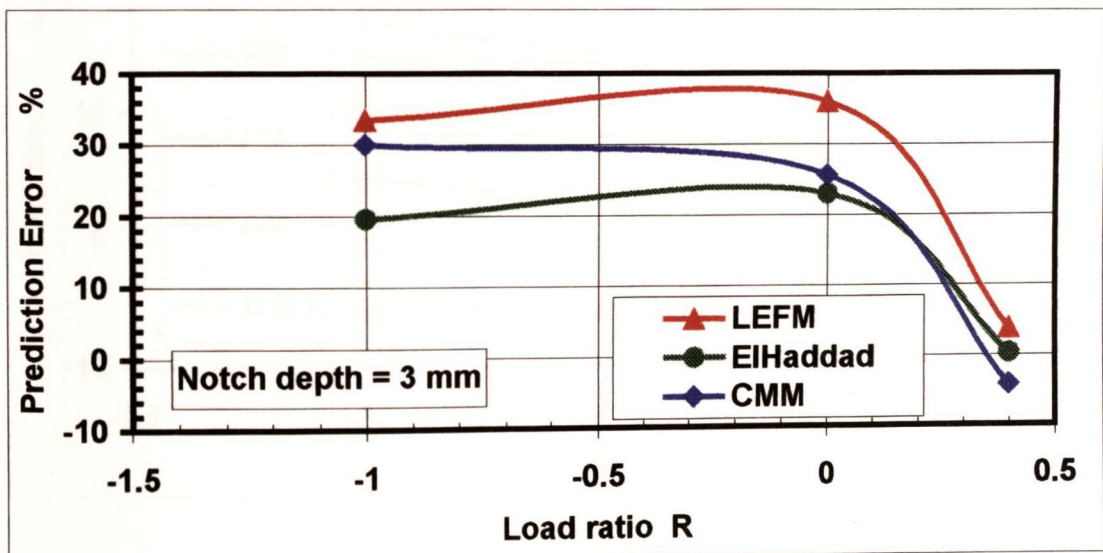


Fig. 6.5.6 (a) Prediction error on SM41B CNP samples

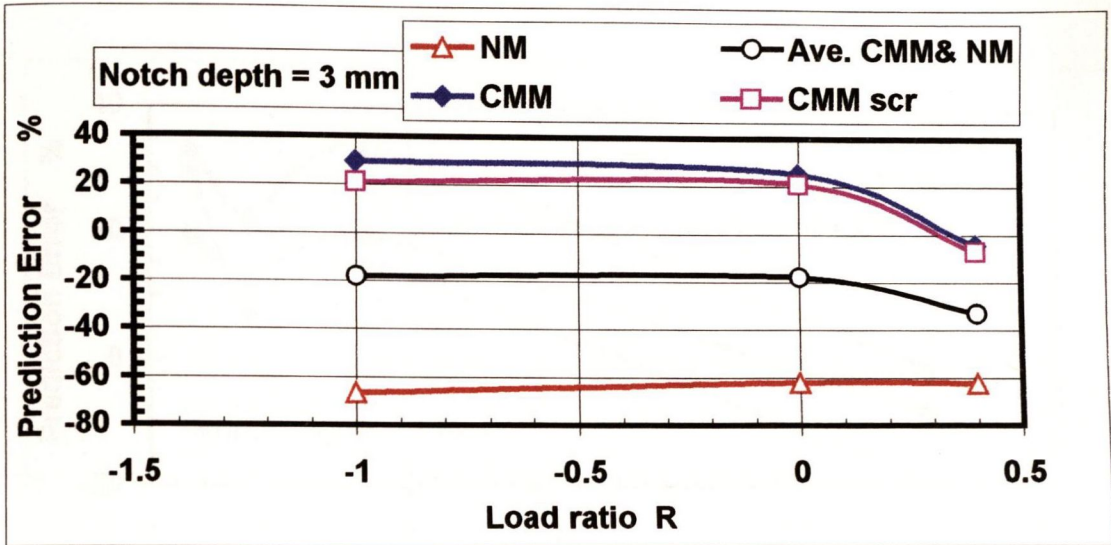


Fig. 6.5.6(b) Prediction error on SM41B CNP samples

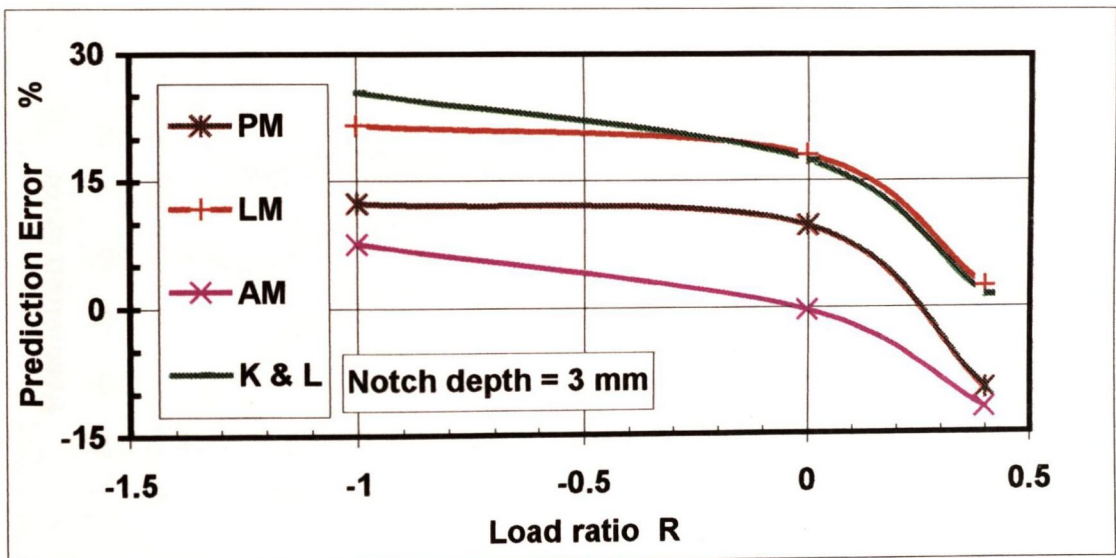


Fig. 6.5.6 (c) Prediction error on SM41B CNP samples

◆ Case 7 SM41B CNP

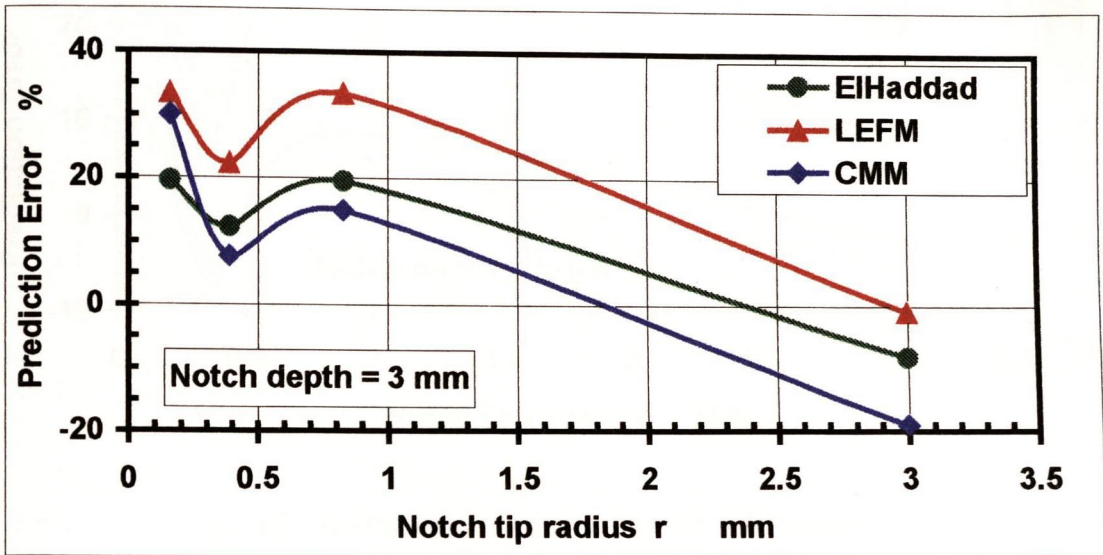


Fig. 6.5.7 (a) Prediction error on SM41B CNP samples

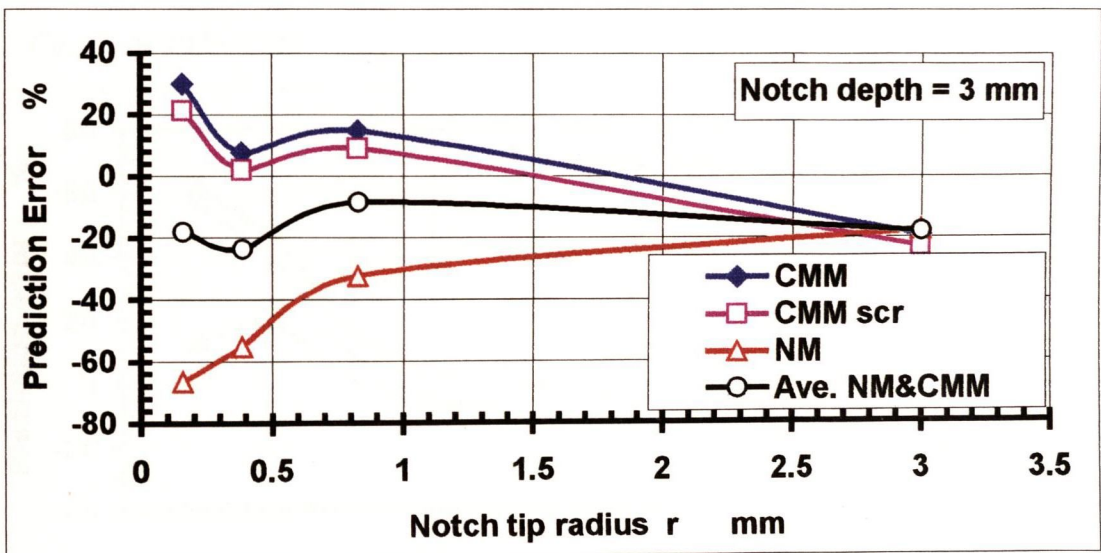


Fig. 6.5.7(b) Prediction error on SM41B CNP samples

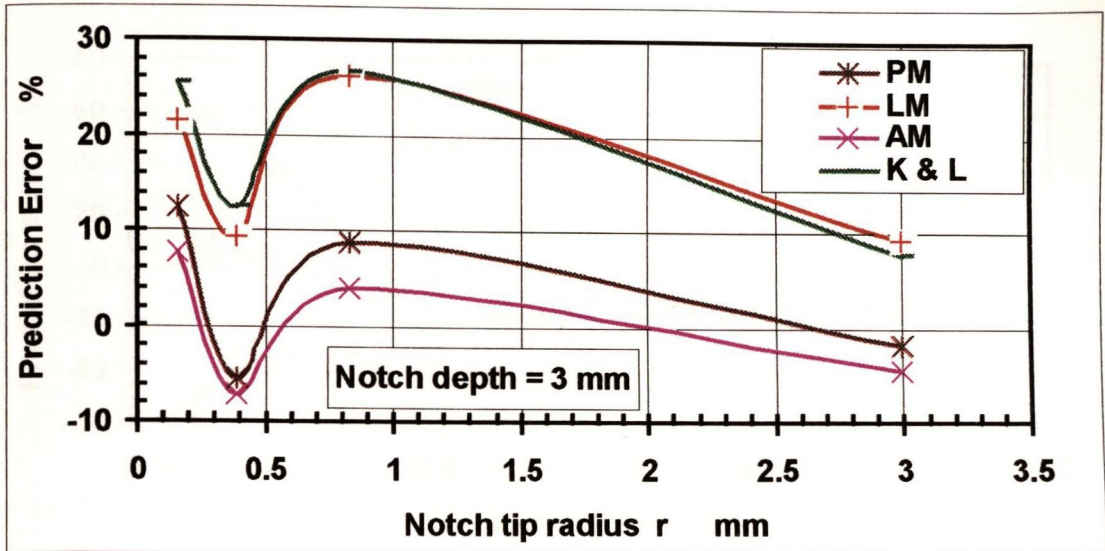


Fig. 6.5.7 (c) Prediction error on SM41B CNP samples

6.5.2 Verification of aluminium alloy samples

◆ Case 8 Al 2024-T351

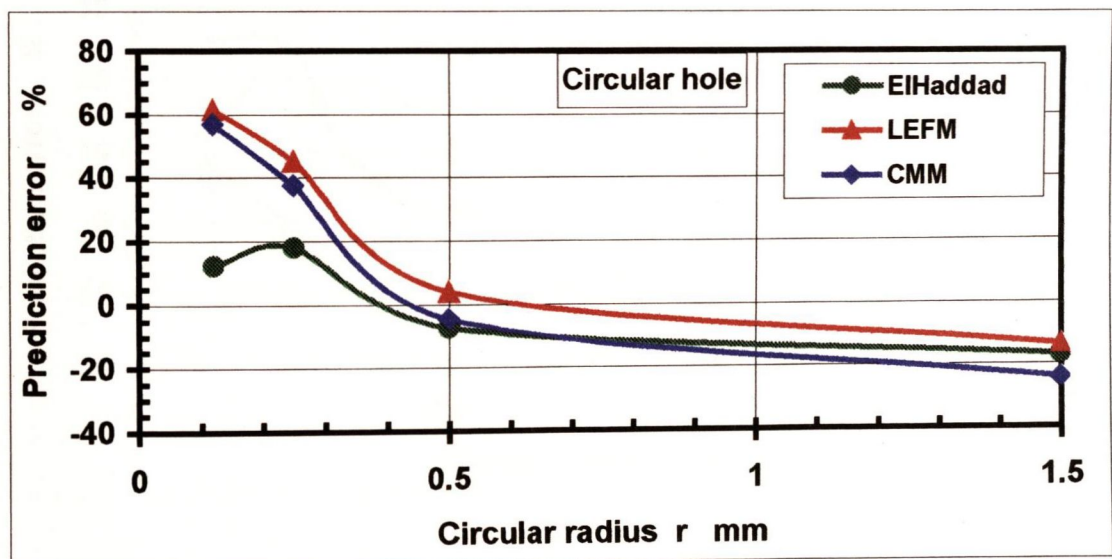


Fig. 6.5.8 (a) Prediction error on Al 2024 T351 CNP samples

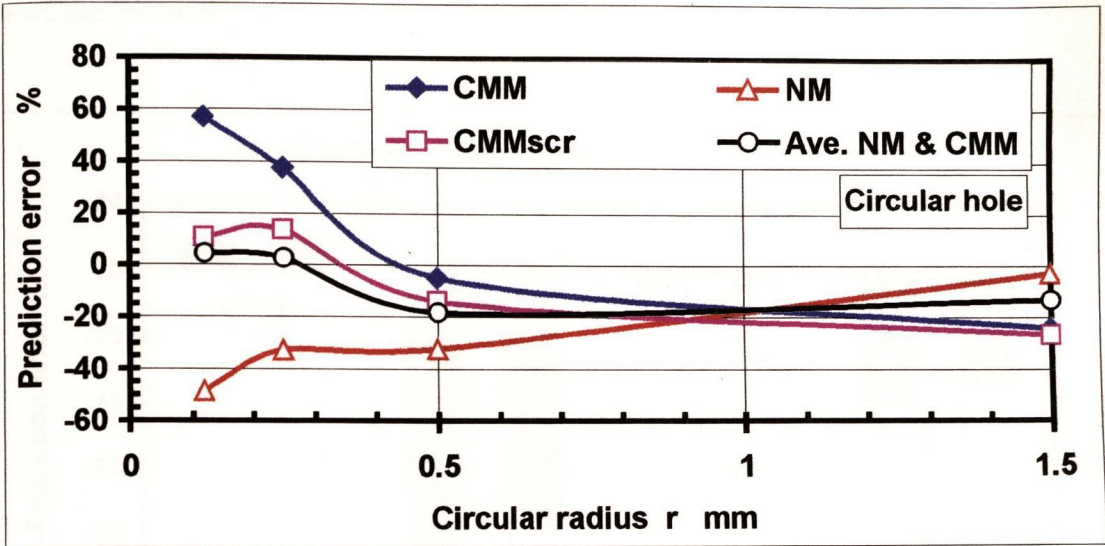


Fig. 6.5.8 (b) Prediction error on Al 2024 T351 CNP samples

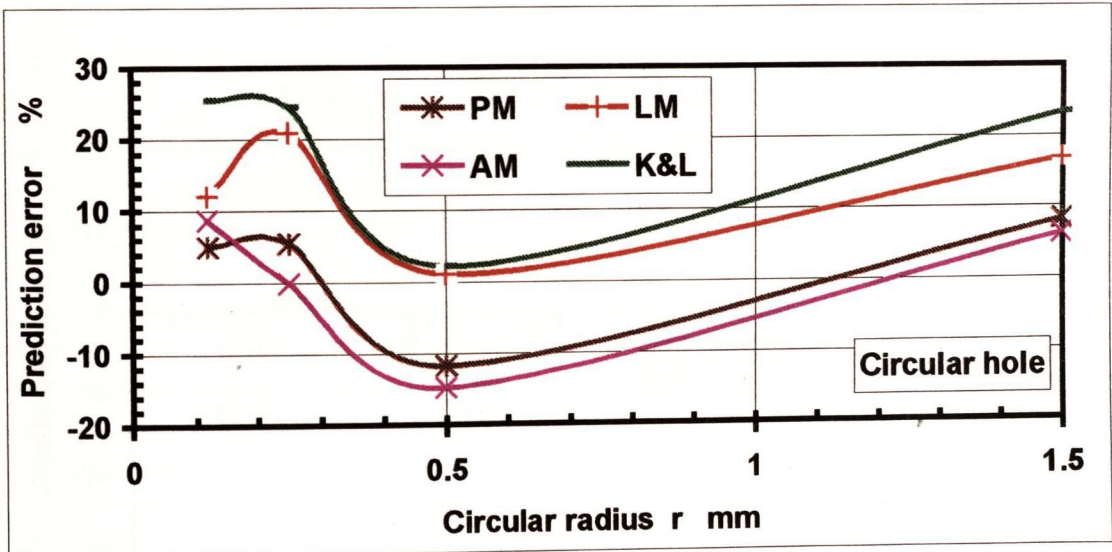


Fig. 6.5.8 (c) Prediction error on Al 2024T351 CNP samples

◆ Case 9 LM25

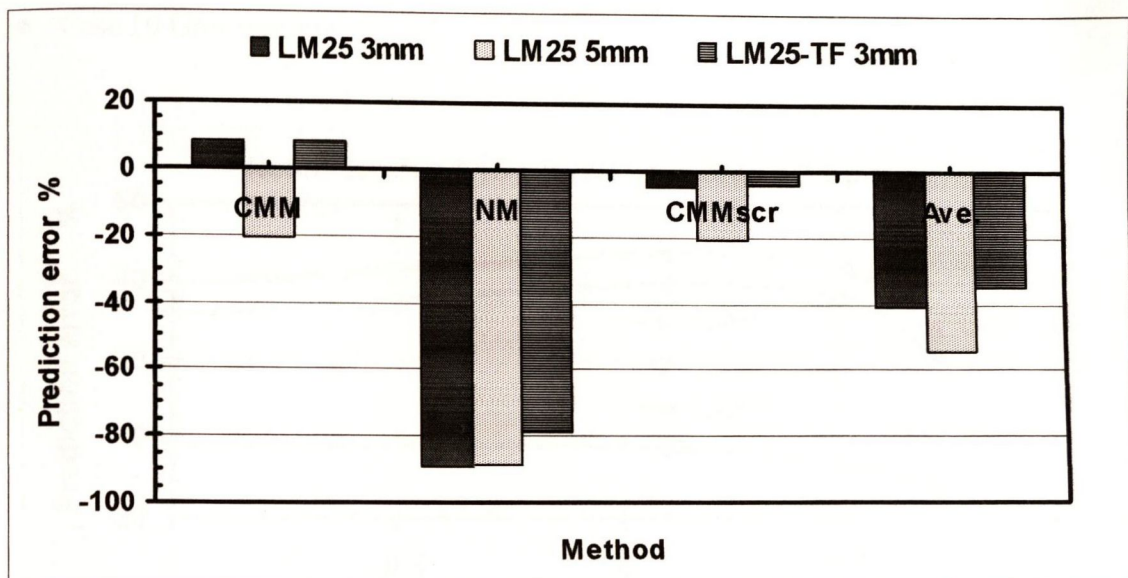


Fig. 6.5.9(b) prediction error on LM25 and LM25-TF SENP sample

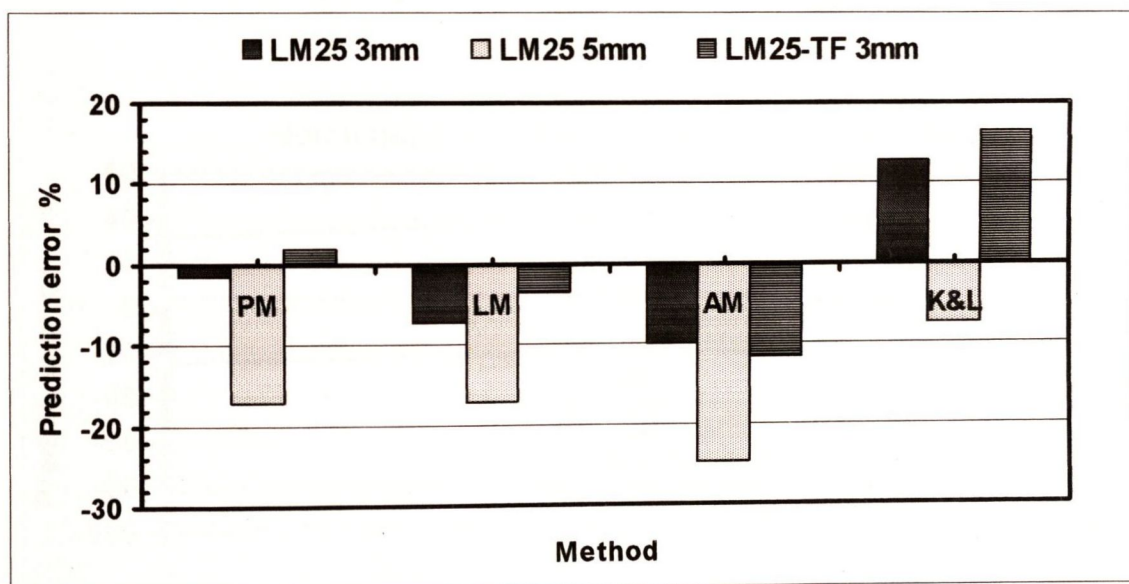


Fig. 6.5.9(c) prediction error on LM25 and LM25-TF SENP sample

6.5.3 Verification of cast iron samples

◆ Case 10 Grey cast iron

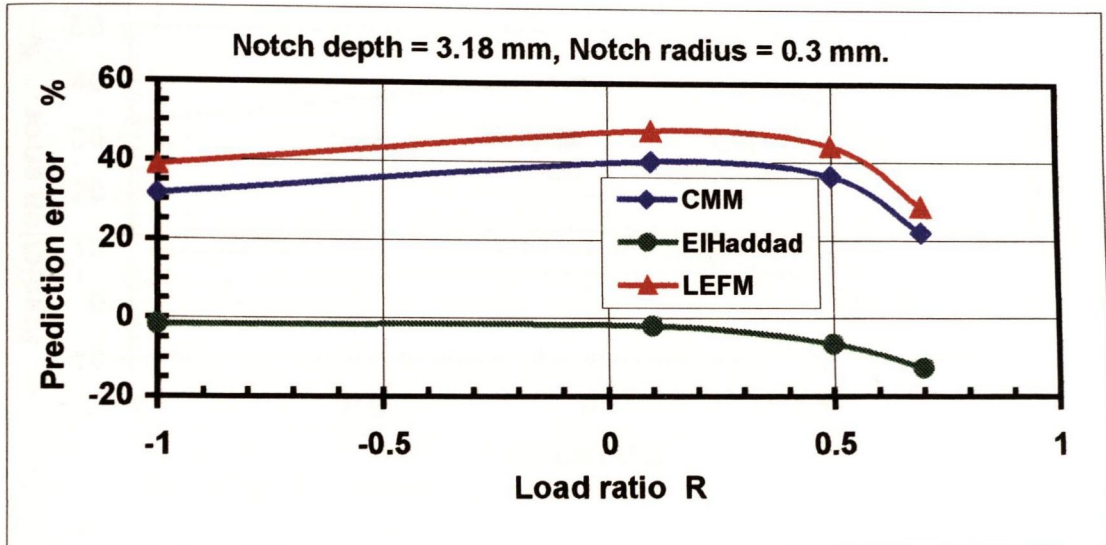


Fig. 6.5.10(a) Prediction error on Grey Cast Iron CNB samples

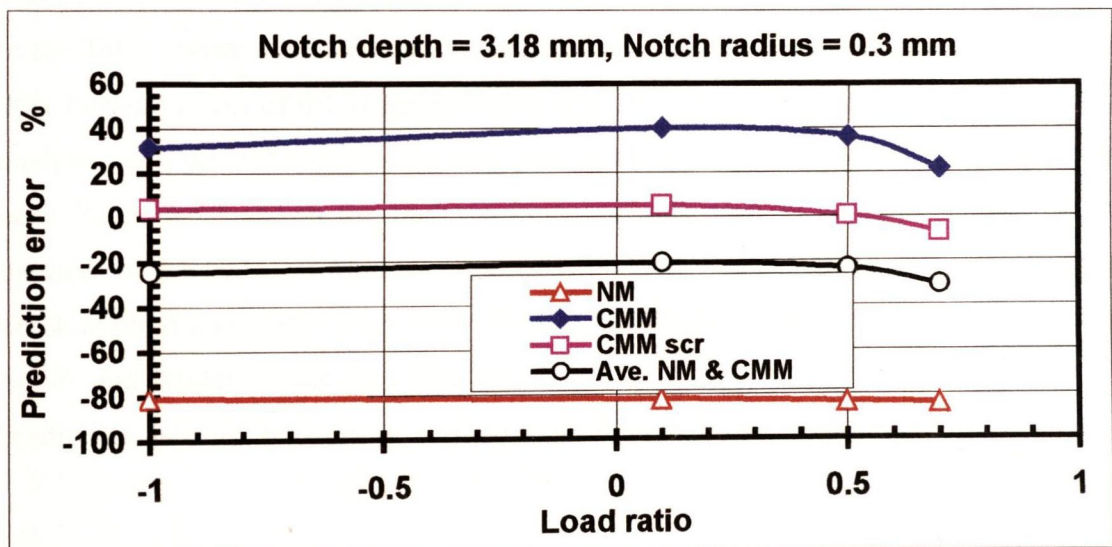


Fig. 6.5.10 (b) Prediction error on Grey Cast Iron CNB samples

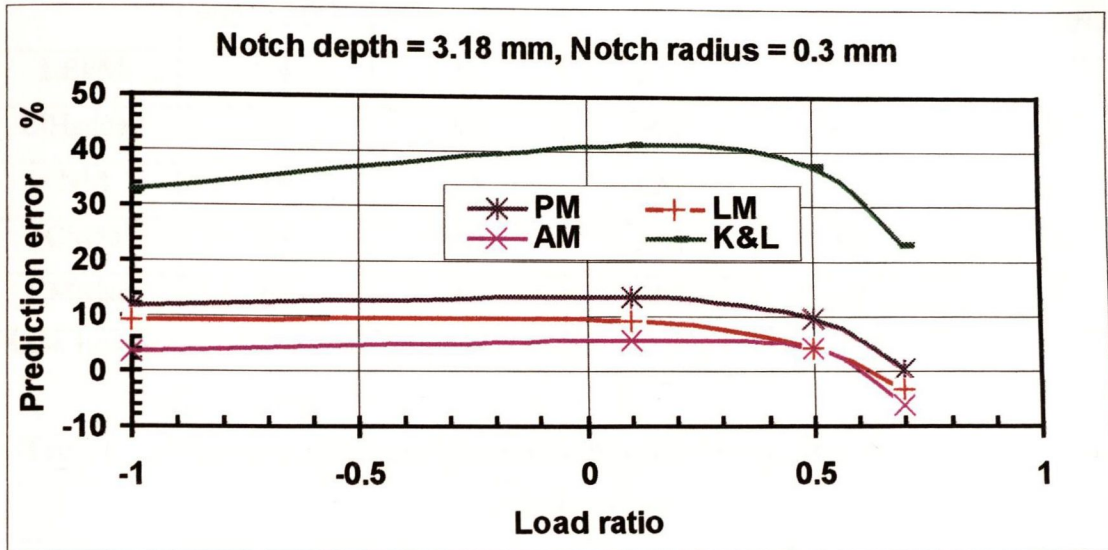


Fig. 6.5.10 (c) Prediction error on Grey Cast Iron CNB samples

6.5.4 Summary of verification

Table 6.5.1 summarises our findings from all the data analysed. Two categories are defined in the Table: better than 20% and better than 30%. Our goal was to make predictions within 20% because errors of this magnitude will arise anyway in the experimental work and stress analysis, so it was felt that one couldn't distinguish between an error of 20% and an error of zero. Table 6.5.2 shows the findings from methods used in conjunction with the notch method. In the table, an estimate from each method was compared with the one from the notch method and higher ones were chosen as final predictions. This technique is based on the Smith and Miller model (see Chapter 2). The last three in the table show very good predictions because they can be used for both short and long crack problems.

Table 6.5.1 Summary of the accuracy of the various methods of prediction

Method	Percentage accurate within 20%	Percentage accurate within 30%	Method	Percentage accurate within 20%	Percentage accurate within 30%
LEFM	44	53	Ave.*	51	70
ElHaddad	79	93	PM	94	100
NM	18	25	LM	81	100
CMM	49	66	AM	92	100
CMMscr	65	86	K&L	57	81

* Ave. represents the method of averaging NM and CMM

Table 6.5.2 Summary of the prediction accuracy of methods used in conjunction with the notch method

Method	Percentage accurate within 20%	Percentage accurate within 30%
LEFM and NM	42	56
CMM and NM	63	80
ElHaddad and NM	87	100
CMMscr and NM	68	96
Ave., NM and CMM **	81.4	98

** Three methods, Ave., CMM and NM, were combined for use.

6.6 Discussion

Geometrically, all notches in these ten sets data can be divided into three categories: small notches, long crack like notches and blunt notches. Around 20% of notches were blunt notches; these were all predicted well using the notch method. The boundary between small notches and long crack like notches was not clear; methods for long crack like notches could also give a good prediction on small notches in some cases. As the figures and Table 6.5.1 show, the new critical distance methods (PM, LM and AM) were clearly the best performers, with accurate predictions in about 90% of cases and no errors above 30%. These methods can handle any size of notches.

The ElHaddad method is capable of good accuracy in most cases, with accurate prediction in about 80% of cases and only 7% errors above 30%. The method can be used for both small and long crack like notches. However, it produced too conservative predictions on blunt notches.

LEFM and its FEA-friendly version, CMM, showed around the same results, with accurate prediction of 44% and 49%, 53% and 66% error above 30%; a slight difference existed, as we mentioned in Chapter 4, CMM was better on notched specimens. These methods can be used for long crack like notches. The advantage of using the CMM method is that the method converges very easily, as we mentioned in Chapter 3, in contrast to the critical distance methods - especially PM - which require finer meshes to pick up changes in stress at the critical distance. NM also requires a fine mesh, but CMM may still be the best option for large, crack-like notches in complex components.

The short-crack corrections of CMM are CMMscr and Ave., which showed good performance in most cases with small notches. The old Klesnil and Lucas method was almost as good, though it had a significant number of high errors.

It is interesting to look in more detail at the datasets, in order to appreciate trends in the predictions. Figs. 6.5.1 is typical of the kind of data from which Smith and Miller [1978] developed their approach: notches of relatively large D (compared to a_0) in which K_t is varied by changing r . Sharp notches are well predicted by LEFM and blunt notches by NM: using the highest of the two predictions is a successful strategy. Figs. 6.5.1 shows, as expected, that the FE-based CMM gives almost the same prediction as its analytical equivalent (LEFM) and the short-crack corrections (ElHaddad and CMMscr) tend to reduce the predicted fatigue limit, but only by a small amount here because D is large. All these can be seen in Figs. 6.5.2-3 in spite of the different geometry and load type.

As Fig. 6.5.1(c) shows, the point and area methods tend to give similar predictions: AM was expected to be 10% lower but in fact this rarely happens. LM gives slightly higher predictions and was a trend throughout the datasets. It was closely matched by K&L, which

is to be expected since both are based on the averaging of stresses over a line, though the line length and the method of determining stress differ significantly.

Fig. 6.5.4,5,8 show typical behaviour of small notches. A common character in those specimens was that the notch depth was equal to the root radius. ElHaddad and CMMscr are useful (and necessary) corrections to the crack-based theories. Ave. NM&CMM was very successful in these cases and can be extended to complex components because nominal stresses are not required. PM, AM and LM continue to work well but K&L can be poor. The largest errors generally occur for very small notches, in those methods which do not incorporate the size effect.

Figs 6.5.8-9 show predictions from aluminium alloys of varying strength levels. Lower-strength materials tend to have higher values of a_0 , thus extending the range of notches for which size effects are important. Fig.6.5.10 shows the material with the largest a_0 value found: a grey cast iron. This dataset also shows predictions at various R ratios.

The crack and notch methods cannot usefully be considered in isolation, since they are intended to be used in conjunction, as Smith and Miller proposed. LEFM & NM together constitute the original Smith and Miller approach, whilst CMM & NM is the FEA-friendly version. Both give good predictions in a majority of cases but experience large errors when dealing with notches that are small in size. This problem is almost alleviated by the use of short-crack corrections. Table 6.5.2 also shows good predictions using three combination methods, ElHaddad & NM, CMMscr & NM and Ave. & CMM & NM, with accurate predictions in over 68% of cases and about 2% errors above 30%. The strategy of using the higher of the two predictions is successful for these methods, except Ave. & CMM & NM.

Ave. & CMM & NM represents a package containing three methods: Ave., CMM and NM. This package was found to be valid for any kind of notches: small notches, crack-like notches and blunt notches as shown in Table 6.5.2. An additional requirement to the strategy is that one should know whether a given notch is a small notch or not.

Predictions showed no particular bias with regard to material type, loading type, R ratio or notch shape: Fig. 6.5.2 shows the same trend as in Fig. 6.5.1, in spite of the different geometry of specimens; Fig. 6.5.3 shows the prediction on another type of load – rotating bending; Fig. 6.5.6-7 show the predictions on variable load ratio. The two parameters of D and ρ were the only significant variables.

6.7 Conclusions

- 1) High cycle fatigue failure in notched specimens can be predicted based on linear elastic stress analysis. The fatigue properties of materials, threshold stress intensity ΔK_{th} , fatigue limit of plain specimens $\Delta\sigma_o$ and material constant a_o , are basic parameters for prediction. The two parameters, notch depth D and notch root radius ρ , are the only significant variables.
- 2). Critical distance methods – the point, line and area methods, based on the use of a_o , are very successful in predicting the fatigue limits of notched specimens from elastic FE analysis. They are able to handle notches of all sizes and shapes in a wide variety of materials, R ratios and load types. Their only significant disadvantage is the need for a relatively fine FE mesh.
- 3). The crack modelling method combined with the notch method can also be used successfully in most cases. This analysis can be carried out using coarser meshes and so may be more practical in complex components. Problems occur when notches are small in size. These problems can be solved mostly by using its revised version, CMMscr. However the solution is limited to specimens or components with simple geometry.
- 4). The combination of the ElHaddad method and notch method is capable of predicting the fatigue limit of notched specimens. This combination method is able to handle notches of all sizes and shapes in a wide variety of materials, R ratios and load types. Problems may occur when applying it to components with complex geometry.

5). The method of averaging predictions from the crack modelling method and notch method can be used for small notches. The method can be extended to complex components with short crack effects.

Chapter 7 Prediction of The Fatigue Failure in Engineering Components

A very important conclusion from the last chapter was that high-cycle fatigue failure could be predicted using linear-elastic analysis essentially. All the methods used for verification of notched samples did not deal with plasticity. In this chapter, the new techniques were employed on engineering components. All these components except the marine component were currently used in Rover vehicles. The new methods were compared with a traditional stress-life approach, which is the same as the notch method (NM).

7.1 Marine Component

The first component chosen for fatigue analysis was a large casting used in marine applications, which was made from grey cast iron. Previous work was successfully performed on the fatigue prediction using the Crack Modelling Method [Taylor, 1996]. Here the Point Method and the Average Method were used for comparison.

7.1.1 Fatigue failure description

In service this component had failed by fatigue; cracking initiated from a right-angle corner which had a fillet radius of 0.3 mm. In an attempt to prevent fatigue, this radius was increased by a factor of 10, to 3.18 mm, but fatigue failure still continued to occur. An alternative approach, in which the original small fillet radius was unchanged but the service loads were reduced, was successful in preventing fatigue. Fig. 7.1.1 shows the σ - r curve from the hot spot for these three design conditions: S1 refers to the original design; S2 refers to the increased root radius and C shows the reduced loading conditions on the original radius. The stress value that is plotted is the 1st principal stress at the point of maximum load in the cycle. In Table 7.1.1, the plain specimen fatigue limits in range $\Delta\sigma_0$, the threshold stress intensity factor ΔK_{th} , and the material constant a_0 were listed at different load ratios [Taylor, 1996; Taylor and Wang, 1999].

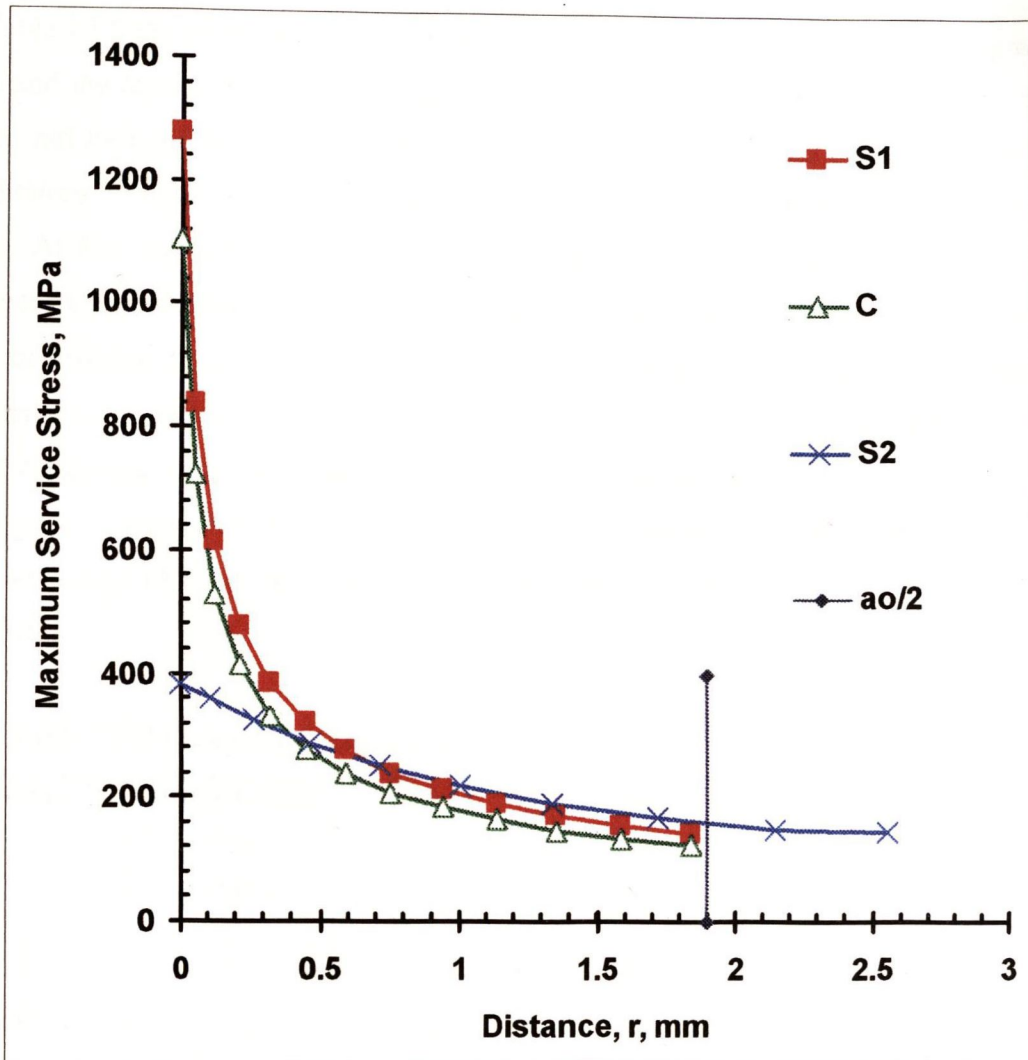
Fig. 7.1.1 σ - r curves on the large casting component

Table 7.1.1 Material property of marine components

Condition	Load ratio R	$\Delta\sigma_o$ in MPa	ΔK_{th} in MPa m ^{1/2}	a_o in mm
S1 (sharp fillet, high service loads)	0.56	62.4	6.83	3.81
S2 (blunt fillet, high service loads)	0.56	62.4	6.83	3.81
C (sharp fillet, low service loads)	0.65	53.4	5.93	3.93

7.1.2 Prediction results from CMM, PM and NM

In Table 7.1.2 the prediction results using CMM, PM and NM are listed, comparing with test data and the threshold. Because of limited stress data, the Line Method and Area Method could not be used for examining the fatigue failure. Both PM and CMM gave very good predictions on both the sharp and blunt fillets. The estimates using NM are also listed in the table. At this stage, we did not know the loads applied to the FE models, so we could not evaluate the prediction errors. However, CMM showed higher estimates in each case than NM comparing $\Delta\sigma_{PRED}$ with $\Delta\sigma_0$ (in Table 7.1.1) and ΔK_{FE} with ΔK_{th} , so we chose CMM results as final predictions as discussed in the last chapter and it was proved this choice was right comparing with the fatigue limits of components. Also because these predictions are very close to those from PM, one can say that these problems are long crack-like problems. The advantage of using two different methods together is that the prediction results can be verifiable.

Table 7.1.2 Comparison of prediction results with test data on marine components

Name	Fatigue limit σ_{max} in MPa	PM σ_{PRED} in MPa	NM $\Delta\sigma_{PRED}$ in MPa	Threshold ΔK_{th} in MPa m ^{1/2}	CMM ΔK_{FE} in MPa m ^{1/2}
S1	142	150	282	6.83	7.82
S2	142	160	85.5	6.83	6.30
C	152	135	195	5.93	5.03

From Fig. 7.1.1, we can see that fatigue failure of the component depended of the stress value at $a\sqrt{2}$ but not at the hot spot. The material constant a_0 of these two load ratios were around the same. The stress values at hot spot was decreased much from Condition S1 with sharp fillet to Condition S2 with blunt fillet, but no big change at $a\sqrt{2}$ and the fatigue limit was not increased even the fillet radio was 10 times larger than original. This implies that the fatigue limit of the component cannot be improved by simply increasing the fillet radio. The material in the component was low notch-sensitive material. For these kinds of material, a reasonable solution could be (a) reducing loads or (b) changing another material with higher fatigue limit.

NM showed too conservative predictions in each case, even on the blunt fillet, S2. The reason is that this traditional method only examines the stress at hot spot, which is not suitable for low notch sensitive materials, such as grey cast iron, since very high stresses can be tolerated by a component provided they are restricted to small regions of the component - leading to a so-called "stress-gradient effect". However, it plays a very important role if using CMM. Without comparing with the NM estimate, we did not know whether these geometries could be modelled as cracks or not; we did not know whether using CMM here was suitable or not. So NM was useful even if it could not give a proper prediction.

7.1.3 Conclusions

1. The stress concentration in the component subjected to high-cycle fatigue loads can be modelled a crack and CMM is able to predict the fatigue failure on this low notch-sensitive material, grey cast iron. PM can be used for the components as well and the method gave a clear explanation of why the failure could happen and solved the problem which had confused people when using the traditional method. CMM and PM came from different theory but showed the same prediction result. It implies the result is reliable.
2. NM showed too conservative estimates. This method was not available for the marine components made of grey cast iron. However it is helpful for judging whether a given geometry is crack-like or blunt notch-like, which is necessary if using CMM.

7.2 Crankshaft

7.2.1 Introduction

Taylor and his colleagues performed a fatigue analysis on a crankshaft under bending and torsion reversed loads [Taylor *et al.*, 1999; 1997]. The crankshaft, which was in commercial use in Rover vehicles, was made of spheroidal graphite (SG) cast iron. They carried out fatigue tests with a load ratio $R = -1$ and FE analysis. They made a prediction using the Crack Modelling Method, which agreed very well with the experimental data.

7.2.2 Material and experimental data

From the literature, the threshold stress intensity factor, ΔK_{th} , is $23.46 \text{ MPa m}^{1/2}$, $\Delta\sigma_o$ is 392.01 MPa therefore the value of a_o is 1.14 mm . The fatigue limits of the component were 12 kN load range for bending and 3.2 kNm for torsion. Fig. 7.2.1 shows the whole component. Fig. 7.2.2 shows details of the loading and clamping; bending and torsion loads were applied in such a way as to cause failure in the bearing closest to one end of the shaft. The components were clamped in the same manner for both types of loading; for the bending test the load was applied vertically downward and the vertical plane containing the loading clamp was constrained to remain vertical. For torsion loading the load was applied at the same location and the three clamps were constrained to remain coaxial.

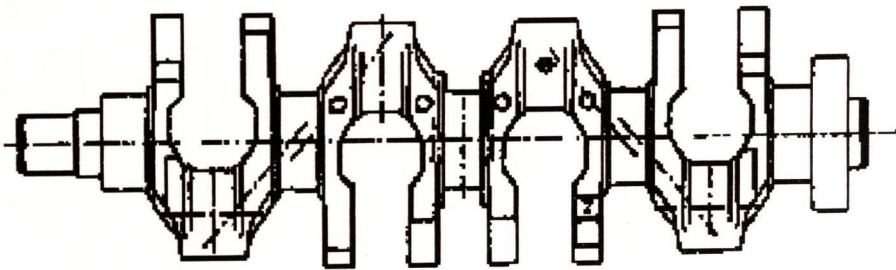


Fig. 7.2.1 The crankshaft component

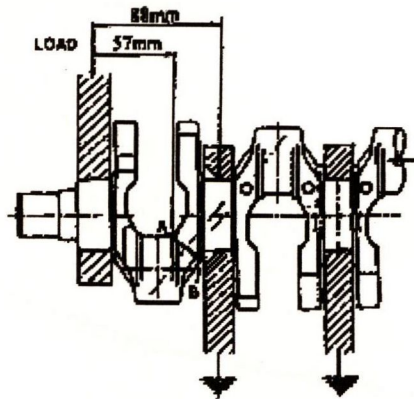


Fig. 7.2.2 The method of clamping and loading. The clamp on the left is loaded downwards to produce bending or rotated to produce torsion.

Fig. 7.2.3 shows schematically the appearance of fatigue cracking after testing in bending and in torsion. In bending (left) the crack grows from A to B in a plane normal to the diagram. In torsion cracks initiate at A and A' and grow at approximately 45° to the mid plane.

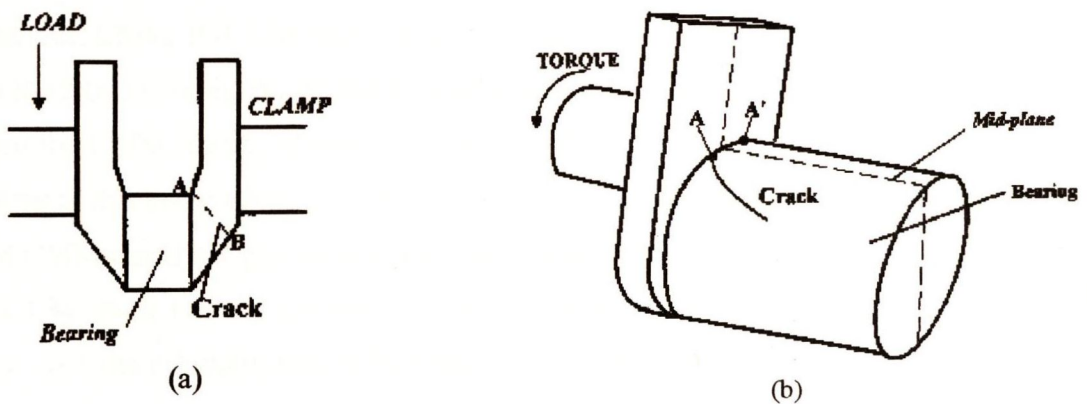


Fig. 7.2.3 Illustration of failure modes: (a) in bending (b) in torsion

The S/N data, the details of FE analysis and the place where fatigue failure occurred can be found in the literature. Fig. 7.2.4 shows the $\Delta\sigma-r$ curves from the hot spot.

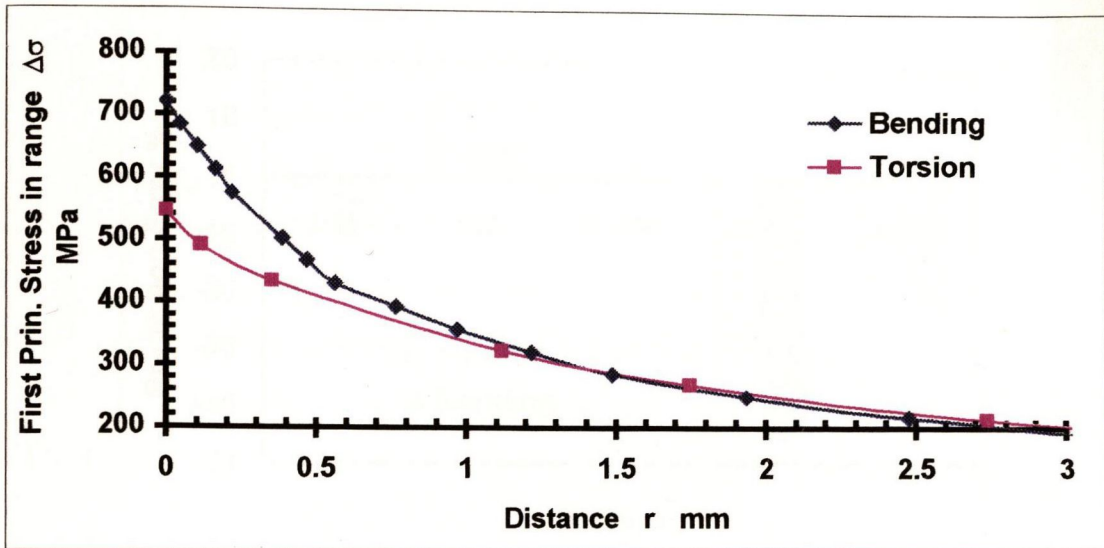


Fig. 7.2.4 Stress/distance curves of a crankshaft under bending and torsion loads at the fatigue limit.

7.2.3 Prediction result

Five methods, CMM, PM, LM, NM and Ave., which were available for the component, were tried for the fatigue prediction. CMM showed higher estimates than NM in both two cases, so we chose the CMM results. However we were not confident the method was good for the component at this stage, since the problem could be long crack-like and short crack-like as well and CMM could not give an accurate prediction if it was a short crack-like. So we used PM and LM; both method showed around the same estimates. Then we compared the estimates with the estimates from CMM and Ave.. It was found that the difference between PM, LM and CMM was smaller than that between PM, LM and Ave.. So it was confirmed that the given problem could be modelled as a long crack but not short crack

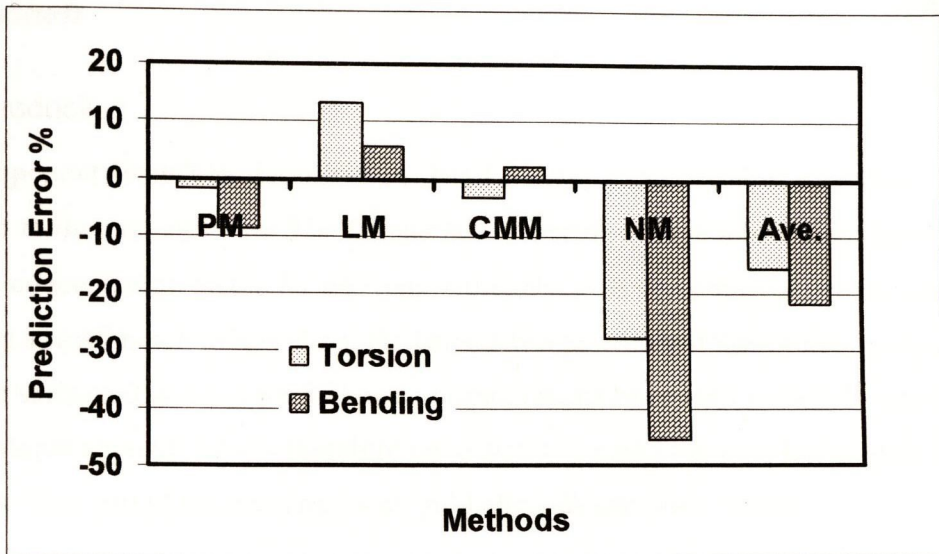


Fig. 7.2.5 Prediction error of the crankshaft in bending and torsion

The prediction errors are listed along with the CMM result in Fig. 7.2.5. Three methods — PM, LM and CMM — all gave good predictions; NM and Ave. gave poorer predictions which were too conservative, especially NM. The situation of the crankshaft was similar to the component in the last section.

7.2.4 Conclusions

1. PM and LM, which were able to predict the behaviour of notched specimens, were able to analyse the automotive crankshaft component made of SG iron. They showed a good agreement with test data under torsion as well as bending loads, which implies that the methods can be used with various types of loading.
2. CMM was able to analyse the same component as well so stress-concentrations of this kind can be modelled as cracks. NM show too conservative estimates but is necessary if using CMM.

7.3 Camshaft

7.3.1 Introduction

This component (which is described in detail below) had a number of different features compared to the previous two. The fatigue failure occurred from a relatively blunt notch — the stress concentration factor, K_t , was approximately 2. It was not clear whether this type of notch was a small notch or not. Also, the fatigue failure occurred from a notch which was on an as-cast surface. It was known that as-cast components have hard surface layers which can change fatigue strength. It was therefore necessary to extend the new techniques to include this effect. This part of the work has been published [Wang *et al.*, 1999]

7.3.2 Experimental details

Tables 7.3.1,2 show the material properties and composition of the material, which was a typical grey cast iron. The threshold stress intensity factor at $R=-1$ was found to be $\Delta K_{th} = 15.94 \text{ MPa m}^{1/2}$ [Taylor, Hughes, and Allen, 1996].

Table 7.3.1 Mechanical properties of grey cast iron

Young's Modulus	170 GPa
Poisson's ratio	0.29
Yield stress	202 MPa ($\sigma_{0.2}$)
Ultimate strength	249 MPa

Table 7.3.2. Composition of grey cast iron (% Weight)

C	S	Mn	Si	Ni	Cu	P	Cr
3.3	0.09	1.5	1.8	0.07	0.2	0.03	0.05

Fig. 7.3.1 shows a general view of the camshaft component, which contained a number of geometric features. The fatigue tests were done at Rover. The component was clamped at one end as shown, and loaded either in bending or torsion (both at $R=-1$), to produce failure at a chosen location, as shown in the detail in Fig. 7.3.1. Two designs were tested: the first had an as-cast notch, 1mm deep, 1.5mm root radius; in the second design, machining was used to remove the cast surface, deepening the notch to 1.75mm with 1.63mm root radius. The K_t

factors for these notches were 2.1 in bending (for both notch depths) and 1.6 for the as-cast notch in torsion. The S/N data for the material was obtained using standard hourglass specimens loaded in axial tension/compression at $R=-1$. Vickers hardness was measured using macro- and micro-indents, to record its variation as a function of distance from the surface.

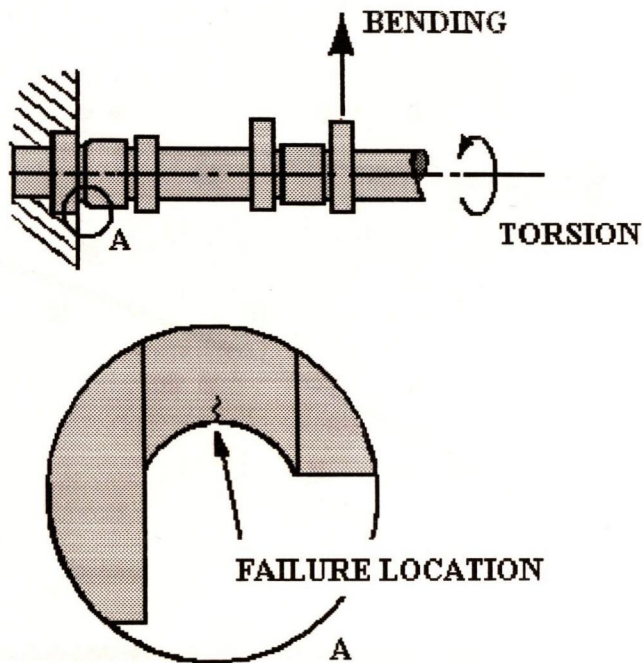


Fig. 7.3.1 Camshaft component, showing loading and details of the notch which caused failure

7.3.3 Results

Figs. 7.3.2-4 show test results in the form of S/N curves, plotting applied load range for the component tested in bending (Fig.7.3.2), torque range for the torsion testing (Fig.7.3.3) and stress range for the plain specimens (Fig.7.3.4). The material fatigue limit, defined at 10^7 cycles, was 190 MPa. The results showed a degree of scatter which is typical for this material, giving variations on the load (or stress) axis of 10-20% from the mean.

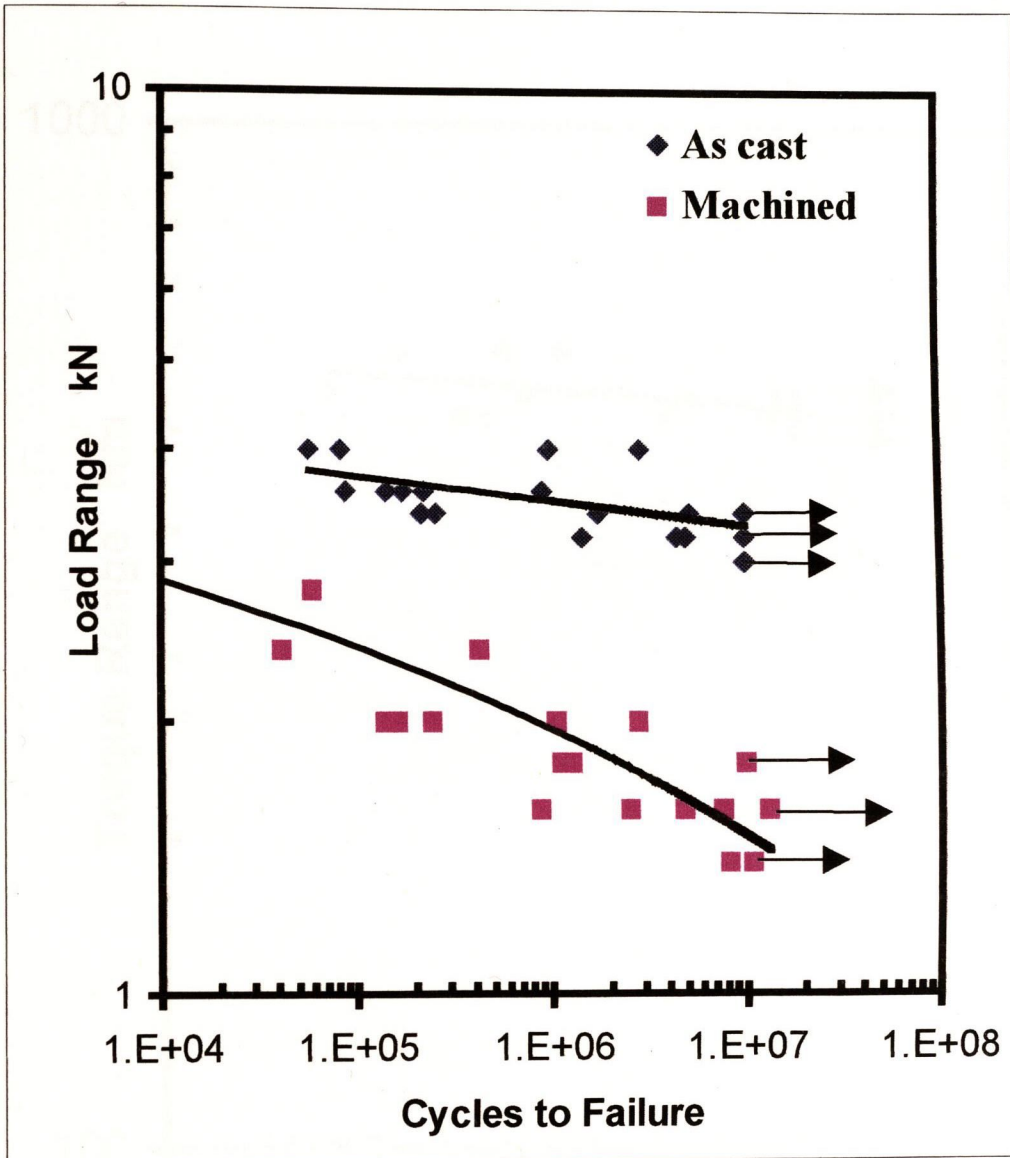


Fig. 7.3.2 Camshaft bending test results: (a) as-cast notch (b) machined notch.

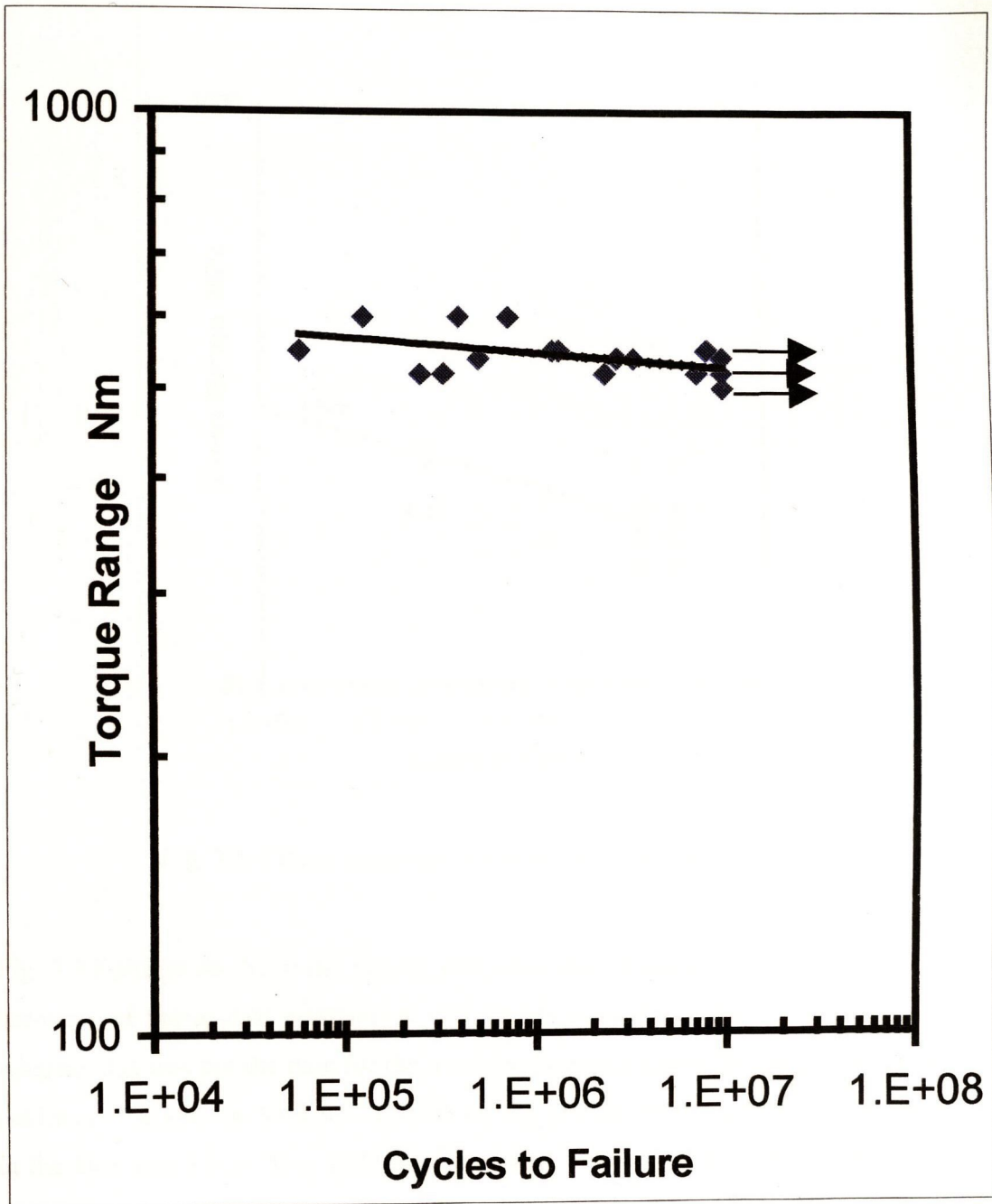


Fig. 7.3.3 Camshaft torsion test results (as-cast condition)

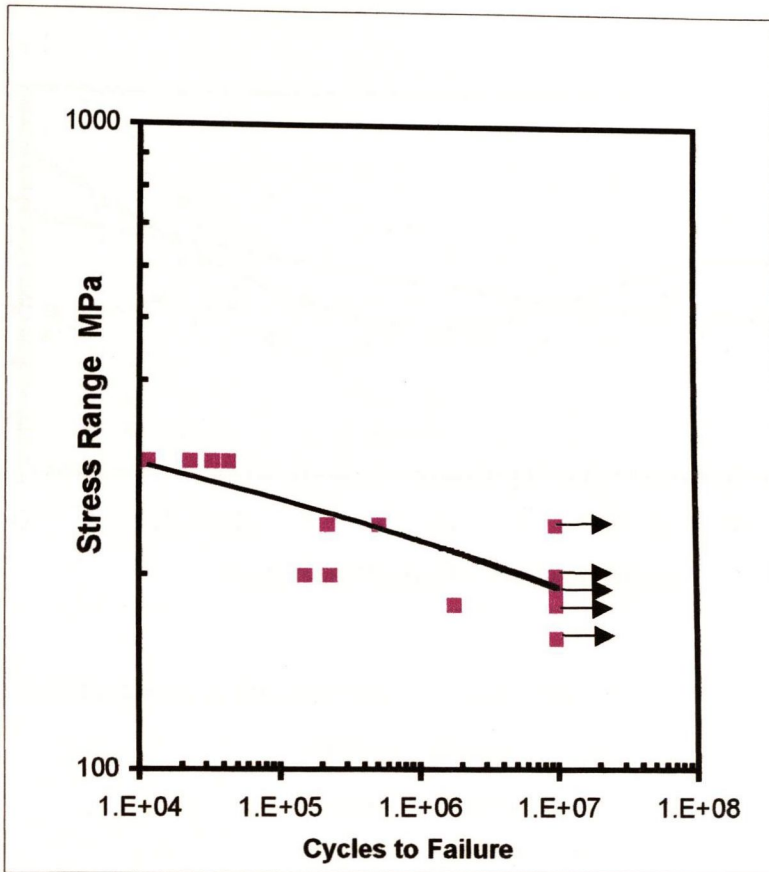


Fig. 7.3.4 Plain specimen bar tension/compression test results

Fig. 7.3.5 shows the hardness results; it is clear that, despite some scatter, the micro-indent hardness of the as-cast component was higher near the surface, especially within 1mm, whereas this was not the case for the machined component or for the macro-indent hardness readings. The average Vickers-hardness on the as-cast surface was 395.5. The average value in the bulk was 326.6. This difference appeared to arise due to a change in the amount and morphology of the cementite phase; it was thus detected by the micro-indents, which were always placed in the matrix (pearlite/cementite) and not in the graphite nodules. The average value for the machined condition was 319.3, which is not significantly different from the as-cast bulk value.

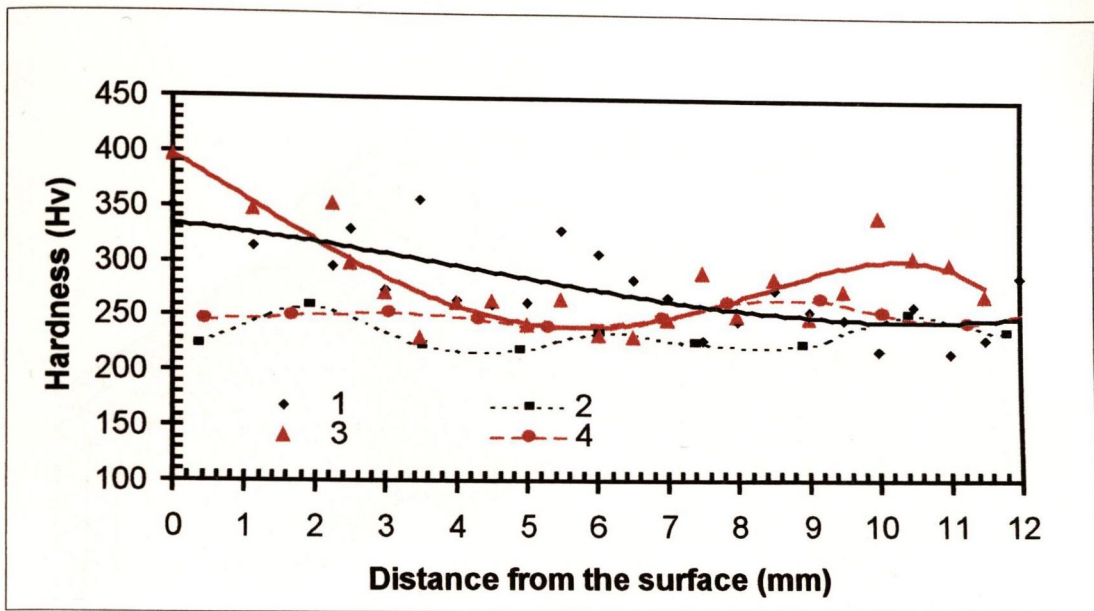


Fig. 7.3.5 Vickers-hardness of the camshaft: (1) micro hardness on the machined surface
 (2) macro hardness on the machined surface
 (3) micro hardness on the as cast surface
 (4) macro hardness on the as cast surface

7.3.4 Finite element analysis

ANSYS software was used to create a finite element model; a quarter model was used (Fig. 7.3.6) because the component is axially symmetrical apart from the cam lobes which do not carry much stress. The bending and torsion loading was treated as a symmetrical or asymmetrical load, respectively. The models were meshed using 3-D parabolic tetrahedral elements. Element size close to the notch was about 0.75 mm.

A linear elastic analysis was used. In each case the highest stress occurred at the notch tip. Fig. 7.3.7 shows the 1st principal stress plotted as a function of distance, r , measured from the notch tip along a straight line drawn in the direction perpendicular to the 1st principal stress direction at the tip (see Fig. 7.3.6). The loading in each case corresponds to the experimental fatigue limit of the component.

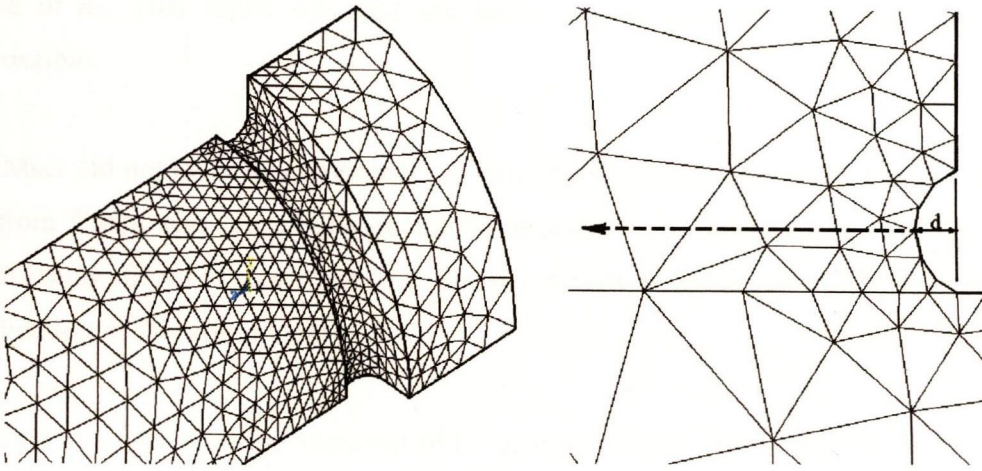


Fig. 7.3.6 The finite element model, showing in detail the mesh around the notch tip. The arrow shows the line on which the stress-distance curve was measured.

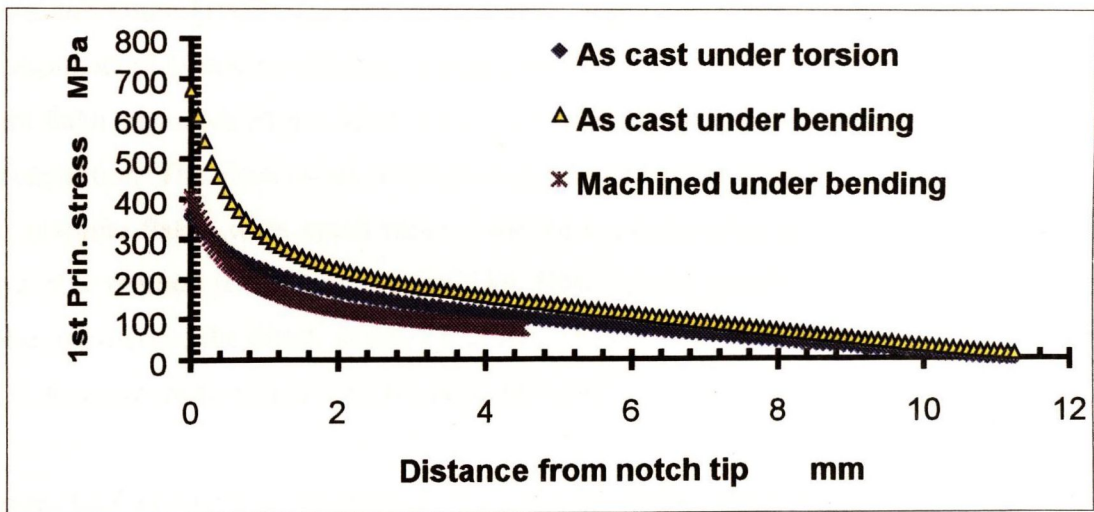


Fig. 7.3.7 FEA results: σ - r curves for each case at the experimental fatigue limit.

7.3.5 Prediction of fatigue limit

Not all of the ten methods could be used for predicting the fatigue failure of the camshafts. LEFM and ElHaddad could not be used directly because there were no available equations

for the loading circumstances, bending and torsion. K&L method was unavailable for the given problem because the notch tip radius at the failure location was less than the material value of a_0 . This result was that the factor K_f was less than 1, which was definitely impossible.

CMMscr did not make any difference compared with CMM. The reason was that the value of a_w from CMM was large because the component is in bending (see Chapter 4) and the modification factor is very close to 1. So six methods were left, which might be available for application to this components.

In order to understand the character of the given problem, NM and CMM were used first. It was found that the predicted fatigue limit from CMM was larger than that from NM. This implied that the problem definitely could not be treated as a blunt notch as it looked like. It might be a short crack or a long crack problem.

Ikawa and Ohira [1967] reported that graphite in grey cast iron was a highly branched and interconnected formation within a eutectic cell cluster, these cell structures were composed of sharp flake edges which provided paths of easy fracture in addition to regions of high stress concentration. The observation of the microstructure has confirmed this and it was also found that graphite flakes were much more interconnected near the surface. So CMM would be applicable method for solving the problem. However the possibility of short crack problem still existed since the notch depth, D , is very close to the value of a_0 . If the deduction was right, Average method would give a good estimate.

Figure 7.3.8 shows the comparison of prediction errors using these six methods. For the machined camshaft under bending load, the predictions from the Point Method and the Area Method agree very well with the experimental data. CMM's prediction is acceptable with a little over 20% error. LM shows about 30% error. NM and Ave. give an underestimated prediction. For the camshaft with the as-cast surface, under bending load, the prediction was not good and needed to be improved. It is necessary to consider the surface effect, even though the prediction for torsion loading was acceptable.

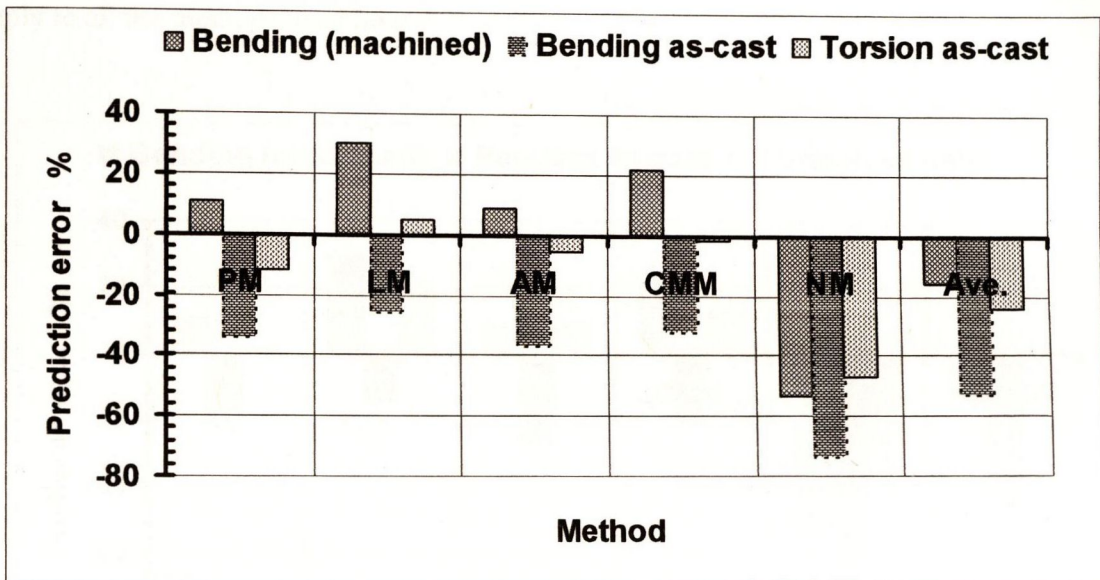


Fig. 7.3.8 Prediction error on the camshafts without considering the surface effect

Fig. 7.3.9 shows revised predictions in which a correction factor was introduced to allow for the surface effect noted above. This correction was made by using the methodology of Murakami and Endo [1986 and 1989], who proposed a generalised method for the analysis of small surface defects and notches. They proposed that, for steels, the fatigue limit could be predicted by assuming that the notch was a crack: the size parameter they used was "area" - defined as the area of the defect projected normal to the stress axis. They proposed equations for the fatigue limit and threshold for notches in all steels (see Chapter 2), as follows:

$$\Delta\sigma = 1.43(H_v + 120)(\sqrt{\text{area}})^{-1/6} \quad (7-1-1)$$

$$\Delta K_{th} = 3.3 \cdot 10^{-3}(H_v + 120)(\sqrt{\text{area}})^{1/3} \quad (7-1-2)$$

Here H_v is the Vickers micro-hardness. Since in a case such as the present one where the notch geometry was kept constant and the hardness changes, both the threshold and the

fatigue limit should increase in proportion to $(H_v + 120)$ which, given the hardness values quoted above, implied an increase of a factor of 1.15 for the as-cast case. This increase would apply to all the methods used here.

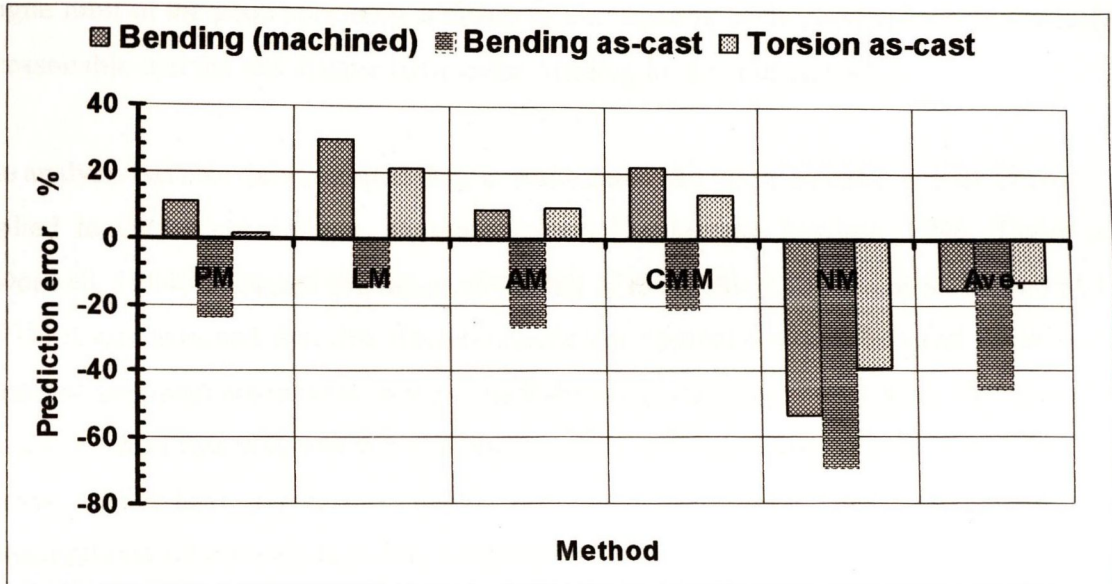


Fig. 7.3.9 Prediction error for the camshafts including the surface effect

7.3.6 Discussion

As Fig. 7.3.9 showed the PM and AM, along with the correction for surface hardness, give good predictions with the error within 20% in the case of bending (machined) and torsion (as-cast). In the case of bending (as-cast), these two methods give the prediction error within 30%. The prediction from LM was relatively non-conservative, except in the case of bending (as-cast). This implies that the method overestimated the fatigue strength sometimes and this problem was one which merited further investigation.

For the same situation such as with the as-cast surface, the prediction for bending is conservative compared with torsion. This result may be explained as follows. During the fatigue test, fatigue failure could occur at any place around the root of the camshaft notch under the torsion load because the shear stress goes to the maximum value on the outside of

the circle. That gave more opportunities for the initiation of a crack, compared with the situation of bending load. Under bending load a crack can initiate only at two opposite spots where the 1st principal stress goes to the maximum value. So there was more volume of material involved under the torsion load than under the bending load. In fact, the condition of fatigue limit of the plain specimen is closer to the situation of the torsion load. In general, it is reasonable that the real fatigue limit under bending load could be higher.

The analysis has also demonstrated that, in some cases, the crack-modelling method could be applied to very blunt notches. Previous papers [Taylor and Lawless, 1996; Taylor and O'Donnell, 1994] discussed the range of validity of the method: following Smith and Miller [1978] it was assumed that this fracture-mechanics approach would be valid for relatively sharp notches, with the maximum-stress method being valid for blunter ones. However, for a material such as cast iron, which has a particularly low notch-sensitivity, the crack-modelling method would have a greater range of validity, being preferred for many of the stress concentrations which were found on components.

Also the Average Method, which was designed for the short crack problem, showed good prediction, with the error being about 20% for two cases. And the predictions for all three cases were conservative. This implies that the equivalent crack length of the notched camshaft is around the length of a_2 in the Kitagawa and Takahashi curve (see Chapter 2). Sometimes (e.g. bending machined, torsion as-cast) the CMM and Ave. could be used simultaneously and both of them would give reasonable predictions.

7.3.7 Conclusions

- 1) PM, LM and AM were able to predict the behaviour of this component. They showed a good agreement with test data in two different design cases under both bending and torsion loading.
- 2) CMM was also successful. Failure occurred from a very blunt notch ($K_t = 1.6-2.1$) but even so the CMM gave better predictions than the use of NM. This implies that the method is suitable for a very wide range of features in materials of low notch-sensitivity, such as this grey cast iron.

- 3) A simple method based on hardness measurements was successful in allowing for the existence of a hardened surface layer. This provides some support for the approach of Murakami and Endo.

7.4 Al-alloy Components

7.4.1 Introduction

Cast aluminium alloy is quite popular for use in automotive industries. The fatigue design of these alloy components is a very important part of the whole design, which is directly connected with safe life and reliability of the vehicles and economic interest of industries. This section is concerned with the prediction of fatigue failure in engineering components that were made of a cast aluminium alloy, LM25. Some methods, such as LEFM, ElHaddad and K&L, could not be employed because corners instead of notches caused stress concentrations where fatigue failure occurred in these components. Another thing that had to be done was the estimation of the threshold stress intensity factor for long cracks because the long-crack threshold was not known for these materials. Two automotive components were examined here: a C-shaped bracket and a pump bracket, both of which are used in Rover vehicles.

7.4.2 Experimental details

The components were made of a cast Al-Si alloy, LM25, in the TF heat treatment, which means solution treated and precipitation treated [Smithells *et al.*, 1992]. Young's modulus $E = 71$ GPa, Poisson's ratio $\mu = 0.34$ and ultimate strength UTS = 275 MPa. From the literature there was no record that was found about the value of the material threshold ΔK_{th} under the load ratio $R = -1$. Due to the limited number of test bars available in the TF form, sample bars made of the same material but in the as-cast form were also used. These bars (18x10x170mm) were either plain or sharply notched through-thickness on a single edge (see Fig. 7.4.1a). The angle of the V-shaped notch was about 60°. Finite element analysis showed that K_t for the 3 mm notch was 15.54. The K_t value for the 5mm notch will be larger. At this stage, we did not know the critical value, K_t^* of the factor for this material (see Section 2.2.1

in Chapter 2), but we presumed that it was less than 15.54, so it was expected that these sharply notched bars would behave as cracked ones.

$$K_t = 1 + 2\sqrt{\frac{D}{r}} \quad (7-4-1)$$

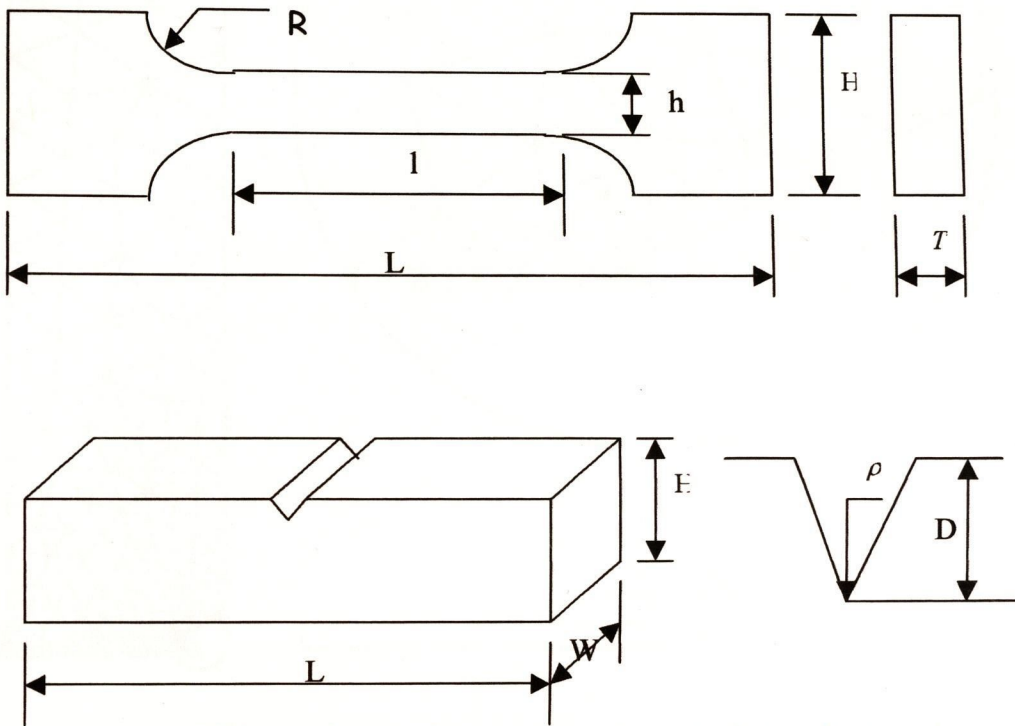


Fig. 7.4.1a Plain specimen and notched specimen for fatigue limit testing

The fatigue limit was defined at 10^7 cycles under the load ratio $R = -1$. Only one notch depth was tested because we just had a few bars in the TF form and they were quite small, so the notch depth in these bars had to be relatively shallow (3mm). The as-cast alloy was tested to give a more complete picture of the behaviour of the material, using notch depths of 3mm and 5mm. The hardness of the material in both heat treatments was measured. Fig.7.4.1b shows the FE model with the load conditions and the detail of the notch tip.

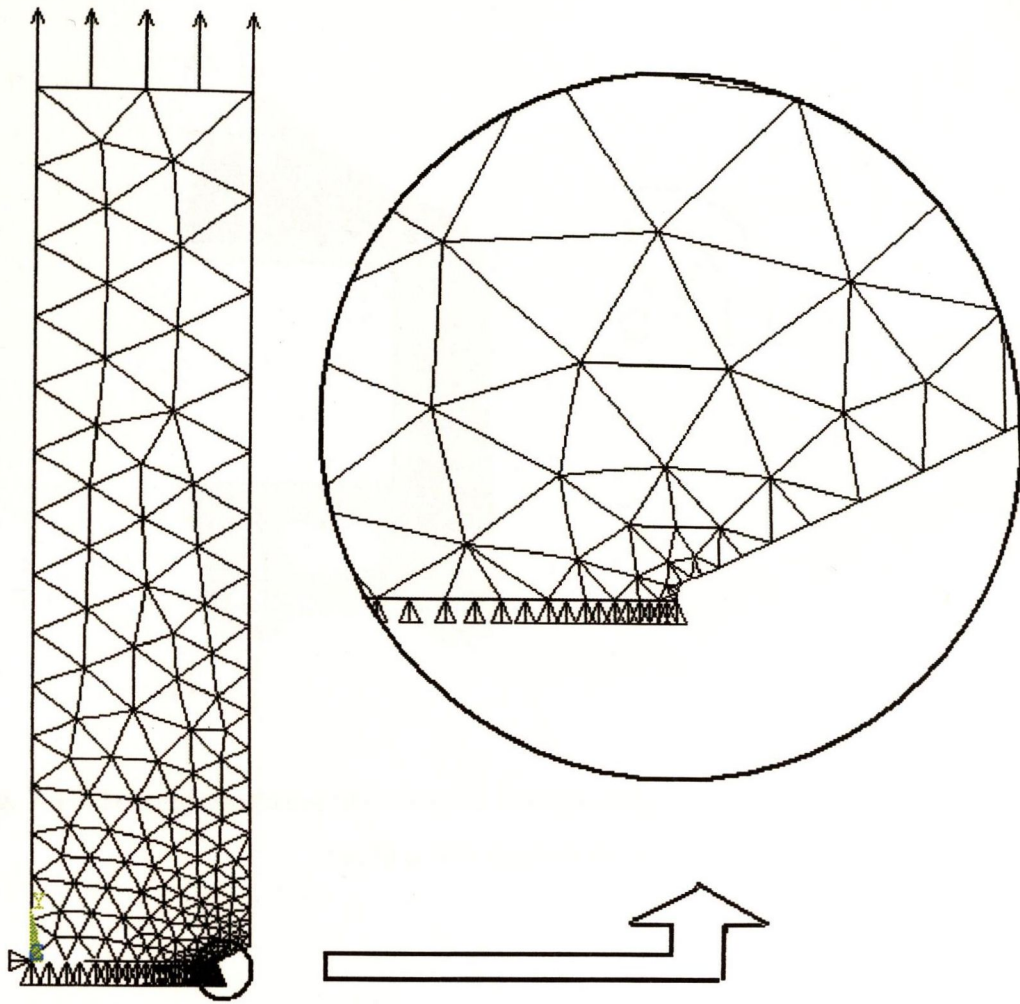


Fig. 7.4.1b FE model for sharply notched specimen bar

Figs 7.4.2 and 7.4.3 show the loading arrangements for the two components. Rover also modelled the C-shaped bracket and pump bracket using FEA. Subsequently the author made a refined-mesh FEA for the C-shaped bracket. The load ratio of the fatigue test R was -1 . The fatigue failure occurred on the upper corner for the C-shaped bracket and near the end of the thin wall for the pump bracket, as marked in the figure. Figs 7.4.4 and 7.4.5 show the FE models.

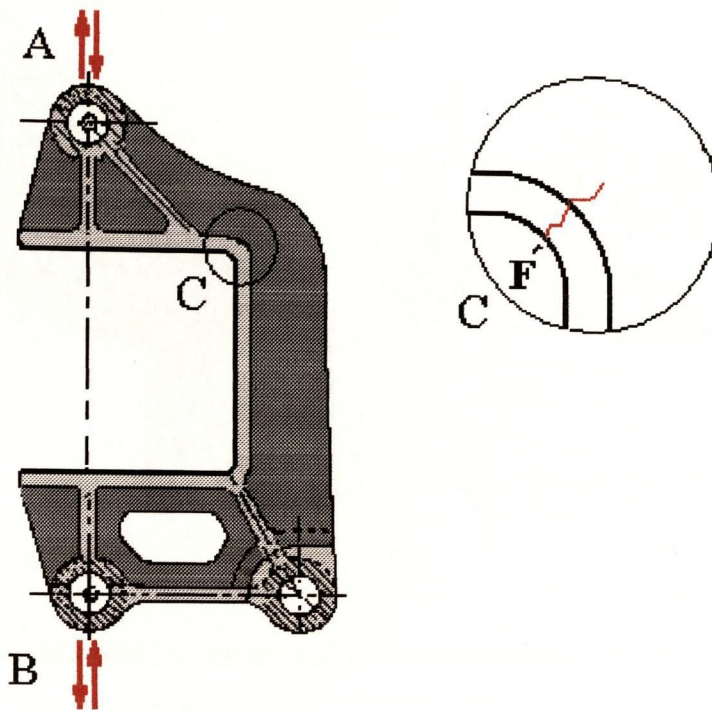


Fig. 7.4.2 Testing condition of C-shaped bracket; fatigue failure occurred at F'. Tensile loading was applied along AB.

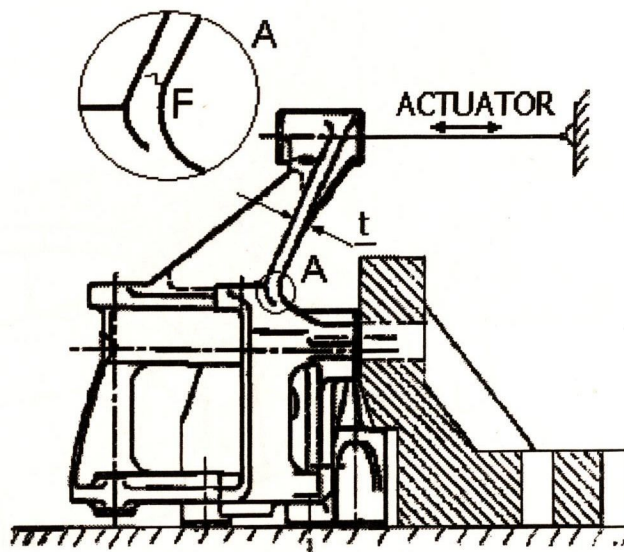


Fig.7.4.3 Testing condition of pump bracket; fatigue failure occurred at F.

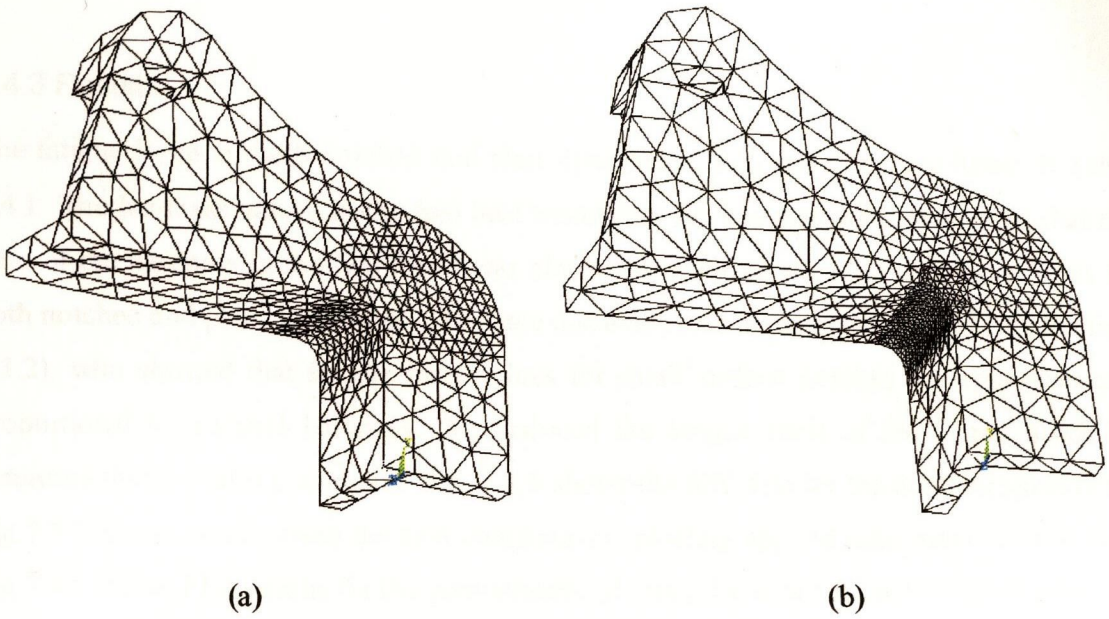


Fig. 7.4.4 FE model of the C-shaped bracket: (a) coarse mesh (b) fine mesh. The fine mesh has density increased by a factor of three near the corner.

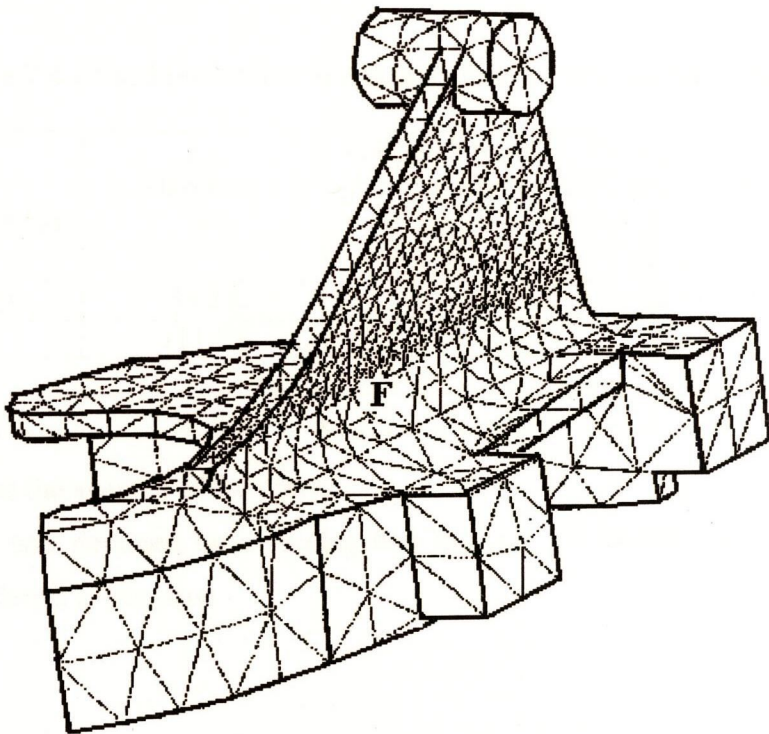


Fig. 7.4.5 FE model of the pump bracket

7.4.3 Results

The fatigue limits of both notched and plain specimens, $\Delta\sigma_o$ and $\Delta\sigma_{on}$, are listed in Table 7.4.1. The hardness values in the two heat treatments are listed as well. We found that the ratio of the hardness in the two forms was almost the same as the ratio of fatigue limits on both notched and plain specimens. The same discovery was made by Murakami (see Section 2.3.2), who showed that fatigue limit values for small surface notches are approximately proportional to material hardness. We deduced the fatigue limit of the 5 mm notch by assuming that the ratio is constant. Fig. 7.4.6 shows the S/N data for the notched specimens. Fig. 7.4.7 shows results from the two components, plotting applied load range in this case. Fig. 7.4.8 shows FEA results for the components, plotting the variation in maximum principal stress with distance from the hot spot (the σ - r curve).

Table 7.4.1 Hardness values and fatigue limit for the two heat treatments

Heat treatment	Hardness Hv	Fatigue limit of plain specimens $\Delta\sigma_o$ MPa	Fatigue limit of 3 mm notch $\Delta\sigma_{on}$ MPa	Fatigue limit of 5m notch $\Delta\sigma_{on}$ MPa
As cast	58.87	77.48	42.5	36
TF	111.73	140	81	66.6**
Ratio	1.9	1.8	1.9	1.9*

* This value is the average of the others.

**The value was deduced by assuming that the ratio of fatigue limit between two heat treatment forms is constant.

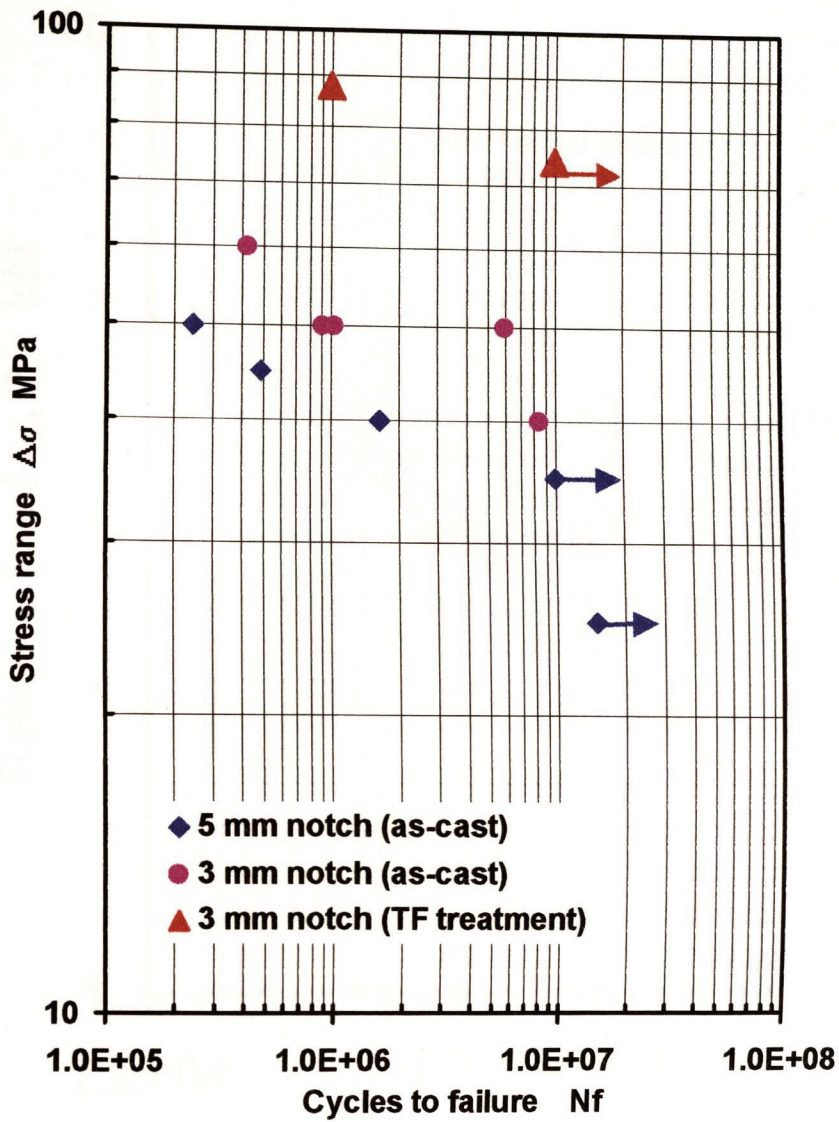


Fig. 7.4.6 S/N data of sharply notched specimens

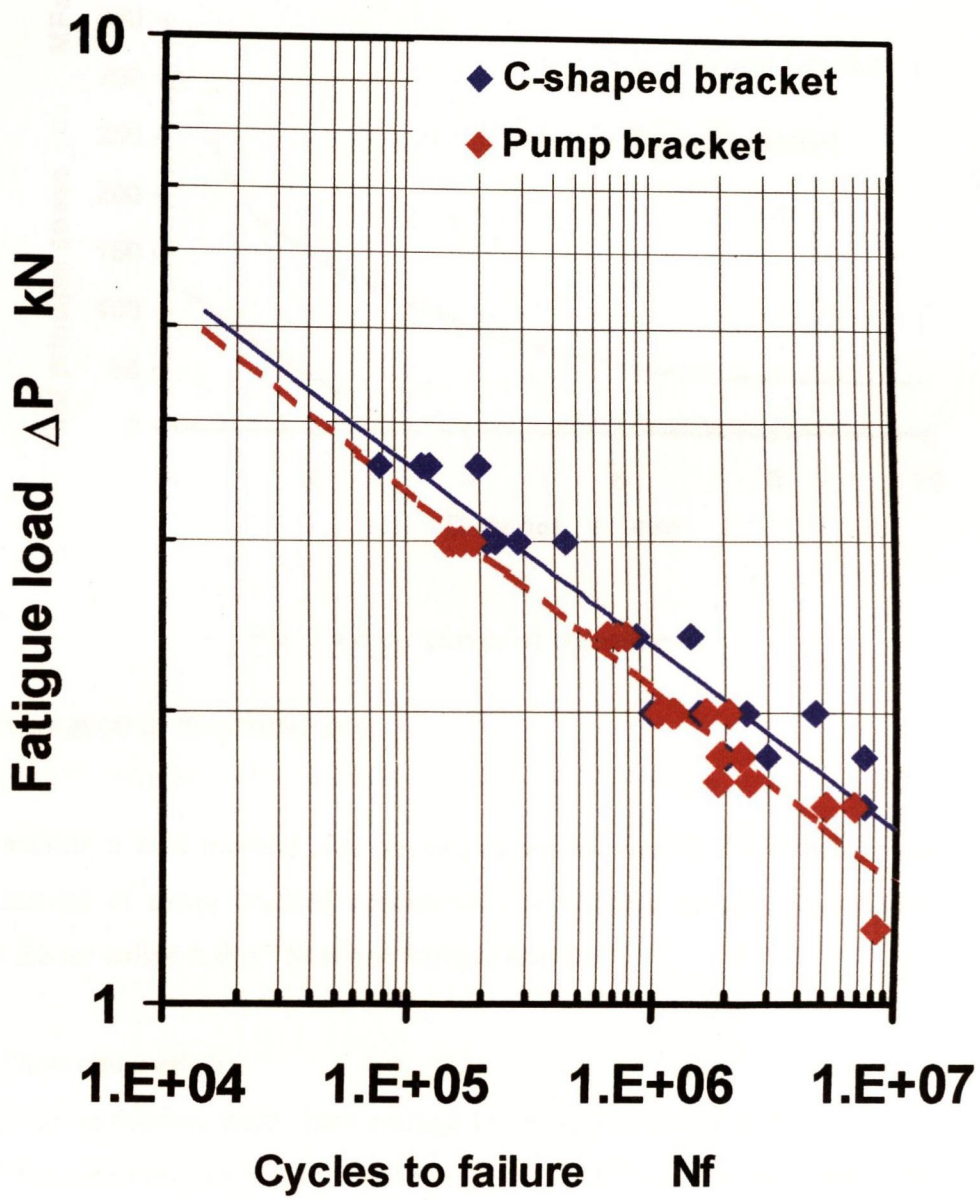


Fig. 7.4.7 S/N data of components

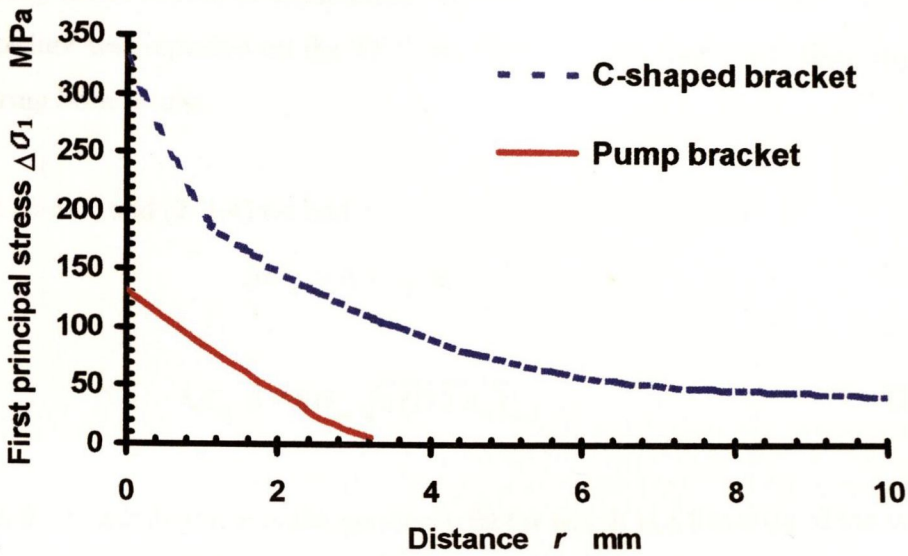


Fig. 7.4.8 σ - r curves of components

7.4.4 Estimation of threshold ΔK_{th}

In this section a new method was developed for estimating the threshold stress intensity factor. Instead of using cracked specimens, the notched samples were employed in the method. So we called it the “Notched Sample Method”.

7.4.4.1 Short crack effect

Although these notches were sharp enough to be crack-like, the method of LEFM could not be used for obtaining the threshold of the material, ΔK_{th} , as we expected. The calculation confirmed that there was a strong short-crack effect which made a big difference between the two notch depths when estimating the threshold value. Because notch depth was close to the value of a_0 , the short crack effect was inevitable.

7.4.4.2 Procedure

The following procedure was adopted for making the predictions. Firstly, the as-cast material was assessed, finding the value of a_0 which gave the best predictions for the two notched specimens. Then the value of the threshold ΔK_{th} was worked out by using the value of a_0 .

The geometry factor should be considered because the size of the specimens was small. The same procedure was repeated on the TF form. After that, the final prediction was confirmed by comparing both results.

From Eqs. (2-3-3) and (2-3-4) we had

$$\Delta K_{th} = \Delta \sigma_o \sqrt{\pi a_o} \quad (7-4-1)$$

and

$$\Delta K_{th} = F \Delta \sigma_{on} \sqrt{\pi(D + a_o)}, \quad (7-4-2)$$

where D is the notch depth; F is the geometry factor which is a function of the ratio of notch depth and sample width [Murakami *et al*, 1987].

7.4.4.3 Prediction results

The results for each step are listed in Table 7.4.2. We fitted the two notches by averaging the a_o value and used the average value to work out the threshold value. Finally we found that the ratio of the thresholds was identical to the ratio which was measured in hardness value.

Table 7.4.2 Threshold prediction of LM25

As cast form		TF form	
a_o in mm	ΔK_{th} in MPa m ^{1/2}	a_o in mm	ΔK_{th} in MPa m ^{1/2}
1.87	5.94	2.09	11.33

Further confidence for these two threshold values can be obtained by comparing them with results from the literature. Whilst no results were found for exactly the same alloy and heat treatment, data were found for closely-related materials [Wigant, 1987; Usami, 1981]: an alloy of similar composition tested in the T6 heat treatment gave a threshold of 6.0MPam^{1/2} at R=0.1, implying a threshold of about 12MPam^{1/2} at R = -1, and an as-cast material with a slightly higher Si content recorded a threshold of 4.8MPam^{1/2} at R = 0.1.

7.4.4.4 Kitagawa and Takahashi curves of LM25

Fig.7.4.9 shows the results in the form of Kitagawa and Takahashi curves. The ElHaddad model gave good descriptions of both heat treatment forms. According to the model, the

value of a_0 is 2.08mm for the TF form and 1.87mm for the as cast form. The threshold value so deduced was then used to make predictions for the components.

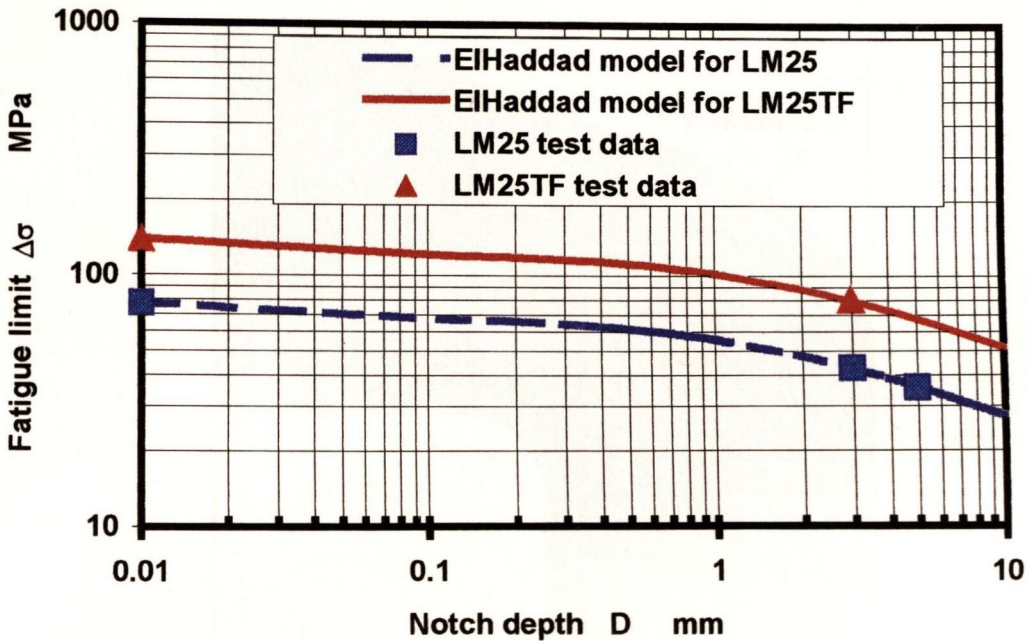


Fig. 7.4.9 Kitagawa and Takahashi curves for LM25TF and LM25

7.4.5 Fatigue failure prediction

7.4.5.1 Definition of σ - r curve path

The C-shaped bracket was a typical 3D engineering component so the situation was different from 2D problems or axially symmetrical 3D problems. For 2D problems, the surface of a fatigue crack is represented by a line. So we called the line a path. CMM and LM examine the lines on which fatigue cracks might grow. PM examines a certain point on the line. AM examines a semi-circle around the path as well. The critical values of fatigue parameters should be found on the path in which fatigue crack growth will occur.

For 3D problems, the surface of the fatigue crack may not be planar. Unfortunately, no method was developed for examining a curved plane yet. However we assumed that all the methods which work well in 2D problems could be applied to 3D problems. Fig. 7.4.10 shows the vector plot of the 1st principal stress on the corner. So the path direction should be

normal to the 1st principal stress that can be seen in the figure and the ΔK value from this path should be lowest.

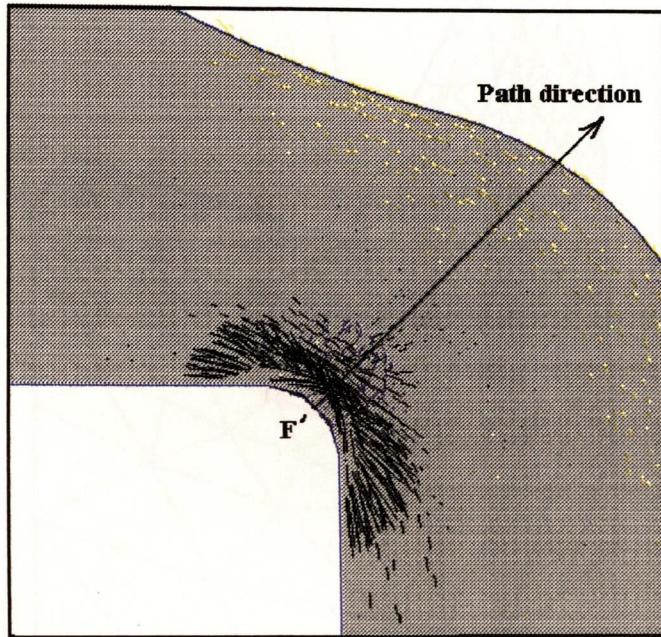


Fig. 7.4.10 Vector plot of the 1st principal stress on the corner of the C-shaped bracket and the path direction

Several directions starting from the hot spot F' were chosen in order to find the best σ - r path as shown in Fig. 7.4.11. The predicted ΔK values from CMM are shown in Fig. 7.4.12. The final path was on the direction of $\alpha = 0^\circ$ and $\beta = 45^\circ$, which gave the lowest ΔK value of $11.09 \text{ MPa m}^{1/2}$. This path was also used in PM and LM because it also gave the lowest $\Delta\sigma$ value. Actually there were several paths which gave ΔK values very close to the lowest, as shown in the figure. This implies that CMM is not sensitive to the path direction.

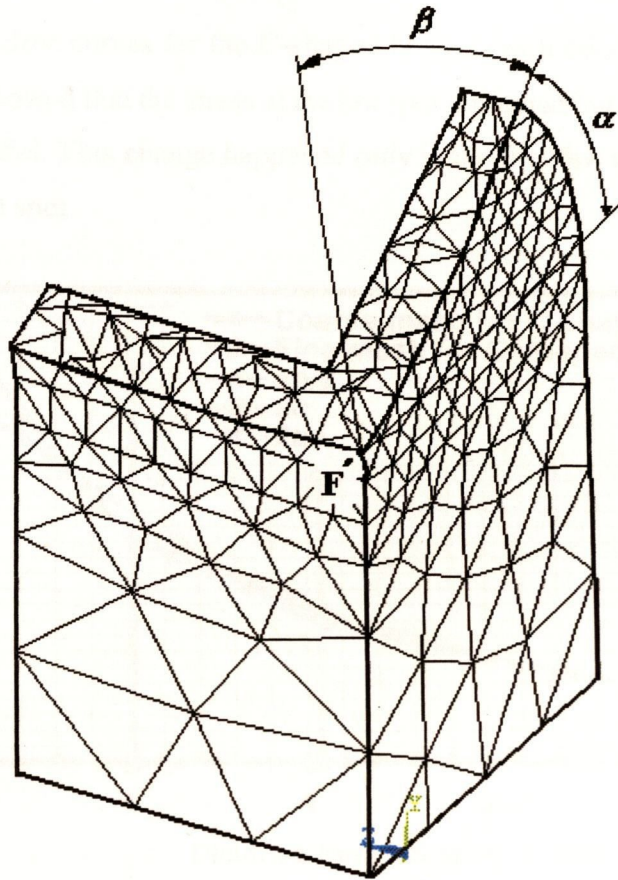


Fig. 7.4.11 Schematic illustration of searching correct path for CMM

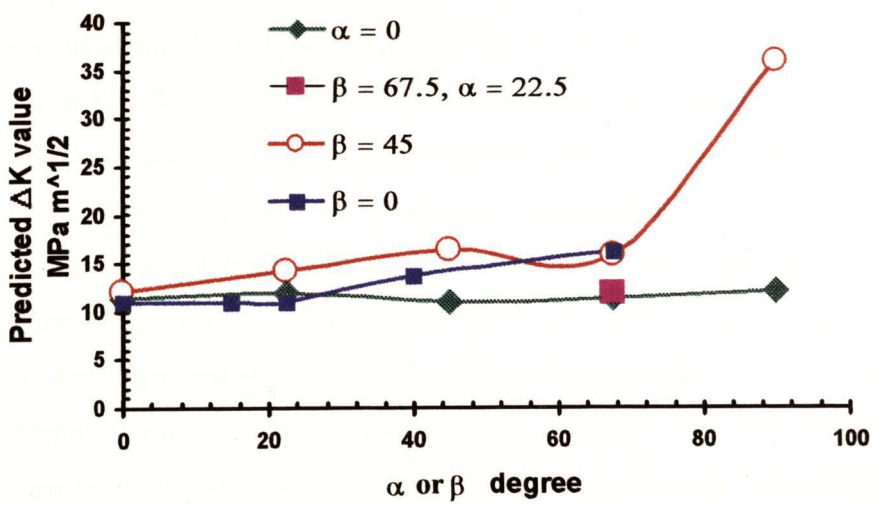


Fig. 7.4.12 Predicted ΔK on each path using CMM

7.4.5.2 Prediction results and discussion

Fig. 7.4.13 shows $\Delta\sigma$ - r curves for the C-shaped bracket, with coarse and fine meshes. The fine mesh model showed that the stress at the hot spot increased but then came down quicker than the coarse model. This change happened only in the first few millimetres and vanished further from the hot spot.

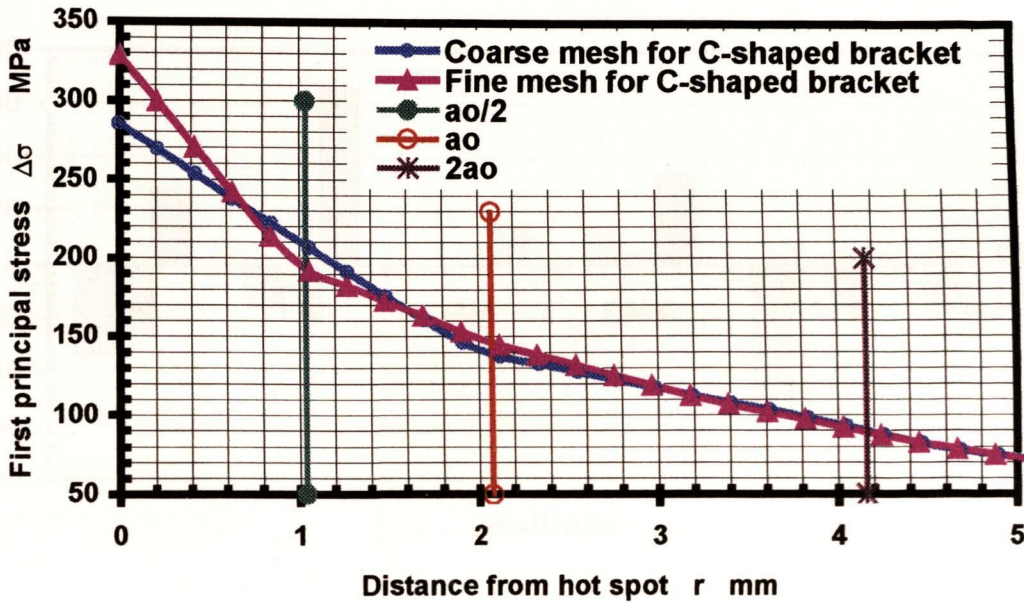


Fig. 7.4.13 Comparison of σ - r curves between the re-meshed model and original one

Six methods were used for the fatigue failure prediction on the Al-alloy components. The results are shown in Fig. 7.4.14. For the C-shaped bracket, CMM gave the best prediction among these methods, overestimating the fatigue limit slightly, which is within experimental error. The re-meshed model improved the prediction. LM, underestimating the fatigue limit slightly, also gave good predictions. The re-meshed model did not change the result very much. This confirmed the inference that LM is less sensitive to the mesh density than the others. However, the improvement can be observed in PM's prediction. The mesh density factor d_r (see Chapter 3) was 0.8 in the coarse mesh model and 1.75 in the fine mesh model which was still less than the required one. Even though the prediction error was still greater than 20%, it appears that the prediction will converge to the test data if the mesh is fine enough, i.e. $d_r = 5$. NM showed a poor estimate on the coarse mesh and even poorer on the

fine mesh, as expected. Even the average method shows a better result than the Notch Method, although the error was over -20%. It implies that the geometry feature was crack-like, instead of blunt-notch like, and could not be treated simply using conventional methods. AM was not available at this stage.

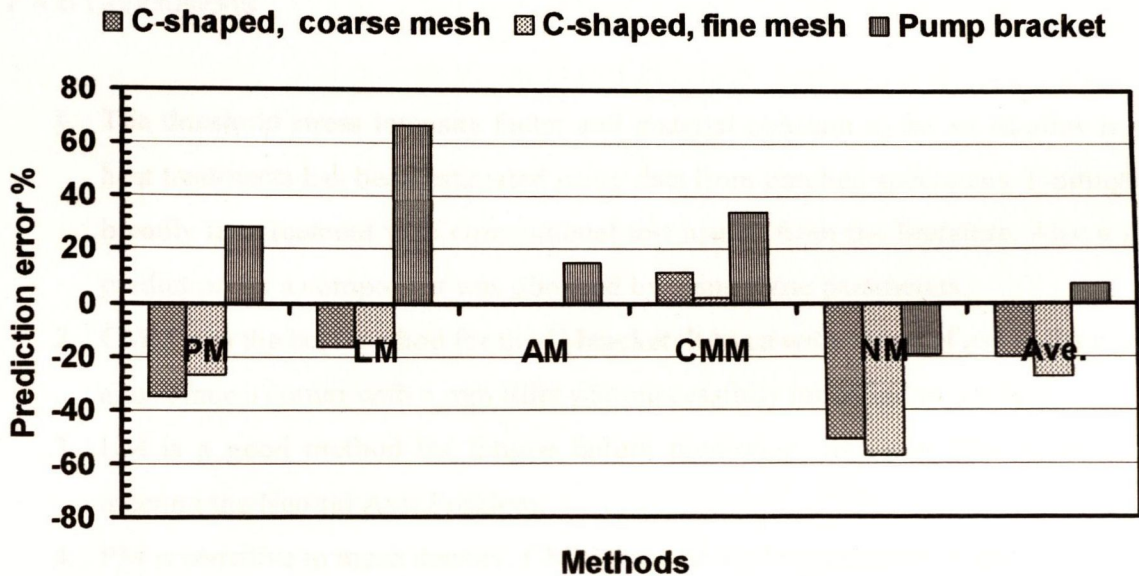


Fig. 7.4.14 Prediction errors on the Al-alloy components

For the pump bracket, NM gave a good estimate, with an error about -20%, as expected. The K_t value was 1.1, very low and stress gradient was due to the bending only, so the problem could not be modelled as a crack. Furthermore it was acceptable that CMM was not suitable here. For this component, Ave. showed a very good prediction, with a slight overestimation of the fatigue limit. It implies that the problem had a short crack effect.

The geometry limited the usage of LM for this component. The fatigue failure occurred at the end of a thin section, with a thickness of only 5.88mm and under bending loads, shown in Figs 7.4.3 and 7.4.5. The value of a_0 was 2.01 mm, so the length of $2a_0$ was very close to the neutral axis on which the bending stress was zero. We called it the "Neutral Axis Problem". The mesh density may be the reason that the PM showed a poor prediction. Unfortunately a refined-mesh model was not available for this component, so we could not make a comparison of two mesh densities. However AM overcame all these difficulties; it examined

an area, not a point, so the method was less sensitive to the mesh density than PM; it only needed a distance of a_0 , a half of the length in LM, so it avoided the effect of the Neutral Axis Problem. These are why AM showed a very good prediction, with an error less than 20%.

7.4.6 Conclusions

1. The threshold stress intensity factor and material constant a_0 for an Al-alloy in two heat treatments has been estimated using data from notched specimens. Findings are broadly in agreement with conventional test results from the literature. Also a good prediction for a component was obtained by using these parameters.
2. CMM was the best method for the C-bracket. It has a wide range of use in the cast Al-alloy since a corner with 5 mm fillet was successfully modelled as a crack.
3. LM is a good method for fatigue failure prediction. Its usage was limited when meeting the Neutral Axis Problem.
4. PM is sensitive to mesh density; CMM and LM are less sensitive to mesh density.
5. AM is a good method. It is less sensitive to mesh density and the Neutral Axis Problem. To develop a new technique for applying the method to a real 3D problem is a further work of merit.
6. NM was sufficient for the low- K_t feature for which the stress gradient was due to bending only.

7.5 General Conclusions for the Application to Engineering Components

1. PM, LM, AM and CMM were generally able to predict the behaviour of engineering components. These methods are suitable for a very wide range of features in materials of low notch-sensitivity, such as the grey cast iron and Al-alloy.
2. The Point Method needs a fine mesh density. The proper density is a function of the ratio of a geometry feature and the material constant a_0 and can be confirmed by checking the convergence of the two different mesh densities.

3. For some components like the pump bracket, the fatigue failure occurred at a thin section under bending or torsion loads and the thickness of the section or beam is relatively small compared with the value of a_0 . The Neutral Axis Problem will be met. In this case, AM showed its advantage to LM.
4. A general methodology is needed for deciding which method(s) to use in a particular situation. This is discussed in the next chapter

Chapter 8 Discussion, General Methodology and Conclusions

8.1 Discussion

8.1.1 Overview of Chapters 6 and 7

The critical distance methods (the point, line and area methods) showed the best adaptability for fatigue failure prediction on all sizes of notched specimens, as stated in Chapter 6. Among them the point method is the best with accurate prediction of 94 % (the prediction error is within 20%) and no error above 30%; the area method is the second; the line method showed a slight overestimate on some data.

Predictions on engineering components showed the same results, which can be seen in Table 8.1. We analysed eight cases (components) in Chapter 7; the marine component was counted as three cases due to three fillet radii; for the camshaft, we counted as two cases due to two surface forms, i.e. the as cast form and machined from. The line and area methods could not be applied to every case because (a) we had limited data, for example there were not enough $\Delta\sigma-r$ data for applying these methods to the marine component; (b) the component was not valid for applying the method as we discussed on the pump bracket in that chapter; (c) the technique of how to apply the area method to a 3D problem needed to be developed. Whereas the critical distance methods show very good behaviour; the best one – the point method – gave accurate prediction of 63% and no error over 30%; the rest show the same results. Based on the work in the last two chapters, the advantages of PM over other methods can be summarized in two words: accurate and simple. We can say that critical methods can be used to predict the fatigue failure on both notched samples and engineering components. This is significant for academic researches and engineering application. Using CMM and NM together was also very successful.

The critical distance is only a function of material fatigue properties, i.e. material constant a_o .

It is independent of geometry. As the critical distances differ in each of these three methods, $a_o/2$, a_o , and $2a_o$ for the point, line and area methods respectively, the sensitivity of each method to FE mesh density is different; the point method requires a fine mesh, followed by the area method and the line method. For the notch specimens this requirement can be satisfied because the geometry is simple and most cases can be simplified to 2-D problems. Also this difference can be an advantage when facing engineering components; the point method is better than the line method for a thin beam or wall subjected to a bending load because the $2a_o$ distance may be over the neutral axis and then the method will be invalid as happened for the pump bracket. However the line method is better than the point method when the FE method is coarse as happened for the C-shaped bracket.

Surface effects should be considered when appropriate, such as the camshaft in the as cast form. We made corrections by measuring the hardness from centre to surface and the prediction results proved that the method could be used for components with surface treatment. Quantitative correction and ease of use are the advantages of the method. For LM25, we measured the threshold stress intensity factor by testing single notched specimens with two notch depths. If the fatigue limits of specimens with two notch depths are known, the threshold can be evaluated using the critical distance methods: the stress-distance curves, $\Delta\sigma-r$, will intersect at one point which should be equal to $a_o/2$. And one can evaluate the threshold knowing a_o and the fatigue limit of plain specimens. In practice, an accurate result may not be obtained by only using one method because of numerical analysis errors. So using several methods and averaging the results may be a good solution. For sharply notched samples with regular geometry, the ElHaddad method is good for the short-crack correction as applied to LM25 specimens. If using critical distance methods, it is not necessary to sharply notch the specimens since these methods can be used for blunt notches as well.

Table 8.1 Summary of the prediction accuracy on components using different methods used

Method	Percentage accurate within	Percentage accurate within
	20%	30%
PM (8 cases)	63	100
LM (3 cases)	50	100
AM (3 cases)	67	100
CMM (8 cases)	63	88
NM (8 cases)	13	25
Ave. NM&CMM (8 cases)	50	75
CMM, NM (8 cases)	75	100

8.1.2 Critical distance methods

The critical distance methods developed here examine stresses in the focus regions. These methods evaluate average stresses which represent some kind of energy density. For blunt notches, small notches or long crack-like notches, however, if this energy density on the focus region is over a certain level, fatigue failure will occur. At this stage, the material constant a_0 is related to the ability of material to resist fatigue failure at notches; a material with a higher a_0 value has strong fatigue failure resistance, i.e. it has a low notch-sensitivity.

The advantage of these methods is that we need not divide the whole fatigue life into several phases, such as crack initiation, short crack propagation and long crack propagation. It is still a commonly held view that fatigue life of a material, of component or structure can be divided into an initiation phase, a short crack propagation phase and a long crack growth phase. For engineering components, defects, such as surface scratches, grain boundaries, triple points and surface inclusions, are inevitable; and any kind of defect, however small, is a stress concentration that can readily give birth to a crack. So the crack initiation period can often be neglected. However even then the prediction is still complex: short crack propagation can be studied with Microstructural Fracture Mechanics and long crack growth with Elastic Plastic Fracture Mechanics; many parameters and complex non-linear stress

analysis are needed. All these directly limit its application for engineering components.

We used the Rankine theory of maximum principal stress, MPS, in all cases including notched samples and components. MPS is suitable for the situation in which the Stage II crack dominates and cracks in notched specimens subjected to tension-compression or components with graphite flakes show tensile opening (or Stage II) type propagation [Miller, 1999]. All forms of loading, however simple or complex, induce a three-dimensional strain pattern which in fatigue loading leads to specific Stage I and Stage II cracking systems. Stage II cracks, for all loading modes, only grow on a plane whose normal is parallel to the direction of MPS. For Stage I dominance, as in torsion, the Tresca maximum shear stress theory is superior. However, should a material have grains with numerous slip systems then at higher stress levels the von-Mises criterion is more meaningful especially for multi-plane fracture materials. Our methods can be applied to Stage I cracks with some modifications, as discussed in Chapter 6.

8.1.3 Crack Modelling Method combined with the Notch Method

The use of CMM combined with NM was the best from Table 8.1. The materials in these components were cast iron and cast Al-alloy, which have low notch-sensitivity. The values of a_0 were large relatively. However the short crack effect was not strong in all these components. The reason may be that the defect effect was strong. The defect, such as graphite flakes in cast iron and pores in cast Al-alloy, combined with geometry feature, turning the problem into a long crack one. For the present work, we used MPS because of Stage II cracks. However it is possible to extend the method to Stage I cracks by examining shear stresses, as noted above.

For materials like mild steel, short crack effects may be strong when the fillet radius in a component or notch tip is small, as it was in Chapter 6, so it depends on the geometry of components and materials. The average method may be a good choice: it still keeps the advantage of the crack modelling method and can be applied to small notches. Due to the absence of the experimental data, we did not test the method on a component made of mild

steel. But it should work because it worked well on notched specimens.

All the methods used in the present research are based on linear elastic stress analysis. The fact that accurate predictions were obtained for notched samples and engineering components by using these methods supports the assumption that high-cycle fatigue is a linear elastic problem basically. This is very good for engineering applications, especially for components at the design stage. There were some methods developed recently for predicting high-cycle fatigue failure [Ting and Lawrence, 1993; Chien and Coffin, 1998], which were based on plastic models and considered short fatigue crack growth in the vicinity of the notch. They showed good prediction on notched specimens and notched components, which had small notches or long crack-like notches. However these methods were limited when applied to engineering components: since using the elastic stress concentration factor, K_t , nominal stress was inevitably concerned; for a component with simple geometry, this nominal stress is valid but not for complex geometry like the C-shaped bracket. Additionally, plastic analysis will result in huge cost of fatigue analysis for large and complex components such as a crankshaft, or for a blunt notch which can be simply predicted using the notch method. The present research overcame these difficulties and can satisfy the requirements of the state of art, to obtain the right design first time.

8.2 General Methodology

All the methods discussed in this thesis have advantages and disadvantages. It is hard to say which method is better or worse without considering a particular circumstance. They can be used independently. But a better way is to use them together in order to get an optimum prediction. It is easy to use all available methods because all of them need the same source data and material properties basically. A general methodology should be developed including the use of each method. This should cover three regions: geometry of long crack-like, short crack-like and blunt notch-like features. For an engineering component, if we know what kind of the problem we have, we know where to get the solution. The following section proposes a general methodology of this type.

The accurate prediction relies on a proper FE mesh density. Coarse meshes will usually result in higher ΔK_{FE} when using CMM; and this will underestimate the fatigue limit. It happens when using critical distance methods, CDM, i.e. the point, line and area methods. Coarse meshes will result in lower $\Delta \sigma_{FE}$ when using NM and so will overestimate the fatigue limit of a component. However the requirement of mesh density from CMM is easily satisfied: the method will predict an accurate result in its regime for any reasonable mesh. So CMM should be the first choice.

For an engineering component with stress concentration, the general methodology starts with the comparison of prediction results from CMM and NM. If the estimate from CMM equals or is close to the estimate from NM, i.e. $CMM = NM$, a prediction can be made from the estimates. It implies that the equivalent crack length of the geometrical feature equals or is close to the parameter a_2 on the Kitagawa-Takahashi diagram. While if $CMM < NM$, the feature behaves as a blunt notch and the prediction can be made using the NM estimate.

The situation needs to be considered when $CMM > NM$: the feature can behave as a long crack or as a short crack. If the feature has short crack behaviour and CMM is used for prediction, it will tend to underestimate the fatigue limit. So it is necessary to judge the character of the feature. At this stage, critical distance methods are invoked. Due to the fact that these methods are sensitive to FE mesh density, the first thing one should do is to check whether the given FE mesh is fine enough to apply these methods or not. There are two ways to examine the mesh density: one can directly measure the radial density, which was defined as $d_r = a_0/l_r$; l_r is the average element length along the radial direction. Experimentally, d_r should be larger than 5 for PM. Additionally, one can compare estimates from these methods. Since the critical distance in each method differs from the others, the requirement for the mesh density is different: PM needs the finest mesh relatively; AM is less sensitive and LM is even less. If each estimate is identical or around the same, it means that the mesh is fine enough. Here it should be mentioned that LM tends to slightly overestimate the fatigue limit compared with the others, as happened in notched specimens, shown in Chapter 6. If there is a big gap between each estimate, it implies that the present mesh does not meet the requirements of at least one method; the best way is to re-mesh the model and carry out the

analysis again until the expected results are obtained. However, sometimes for some reasons, re-meshing is impossible or very difficult. Using the highest estimate is a good strategy for getting an approximate answer: a coarse mesh will result in an underestimate of the fatigue limit for each of those methods in general; while a mesh is coarse for PM but may not be coarse for AM or LM; so if $AM > PM$ or $LM > PM$ and the difference is bigger, it means that the mesh is coarse for PM but not for AM or LM. Another possibility may appear that is $PM > LM$ or $PM > AM$. In this case, one should examine the stress – distance curve, $\Delta\sigma-r$; if the stress goes down to a negative value in a distance of a_o or $2a_o$, it means that the curve passes across the neutral axis. This happens when a thin beam or thin section is subjected to bending loads and AM or LM cannot be used in this situation. Thus one can obtain a CDM estimate from the above procedure.

The next step is to compare the CDM estimate with the CMM one. If $CDM \geq CMM$, it is a long crack problem and CMM will produce the best prediction. If $CMM > CDM$, the geometry feature behaves as a short crack; CDM will be the best choice; if a proper mesh density for CDM could not be guaranteed, CMMscr can be used (but not for bending loads) and Ave. NM & CMM for irregular geometry are highly recommended. Fig. 8.2.1 shows a schematic illustration of the whole methodology.

Briefly, the methodology can be divided into three steps:

1. Comparing the predictions from CMM and NM, if NM is bigger than CMM, it is a blunt notch like problem and NM will be efficient; no fine mesh is needed at this stage.
2. If CMM is bigger than NM, it is a crack like problem, either a long crack or a short crack. Comparing CMM with CDM, if the results are close to each other, it is a long crack problem. CMM is the best.
3. For a short crack problem, CDM is the best. However if a proper mesh density cannot be achieved, CMMscr or Ave. NM & CMM can be tried.

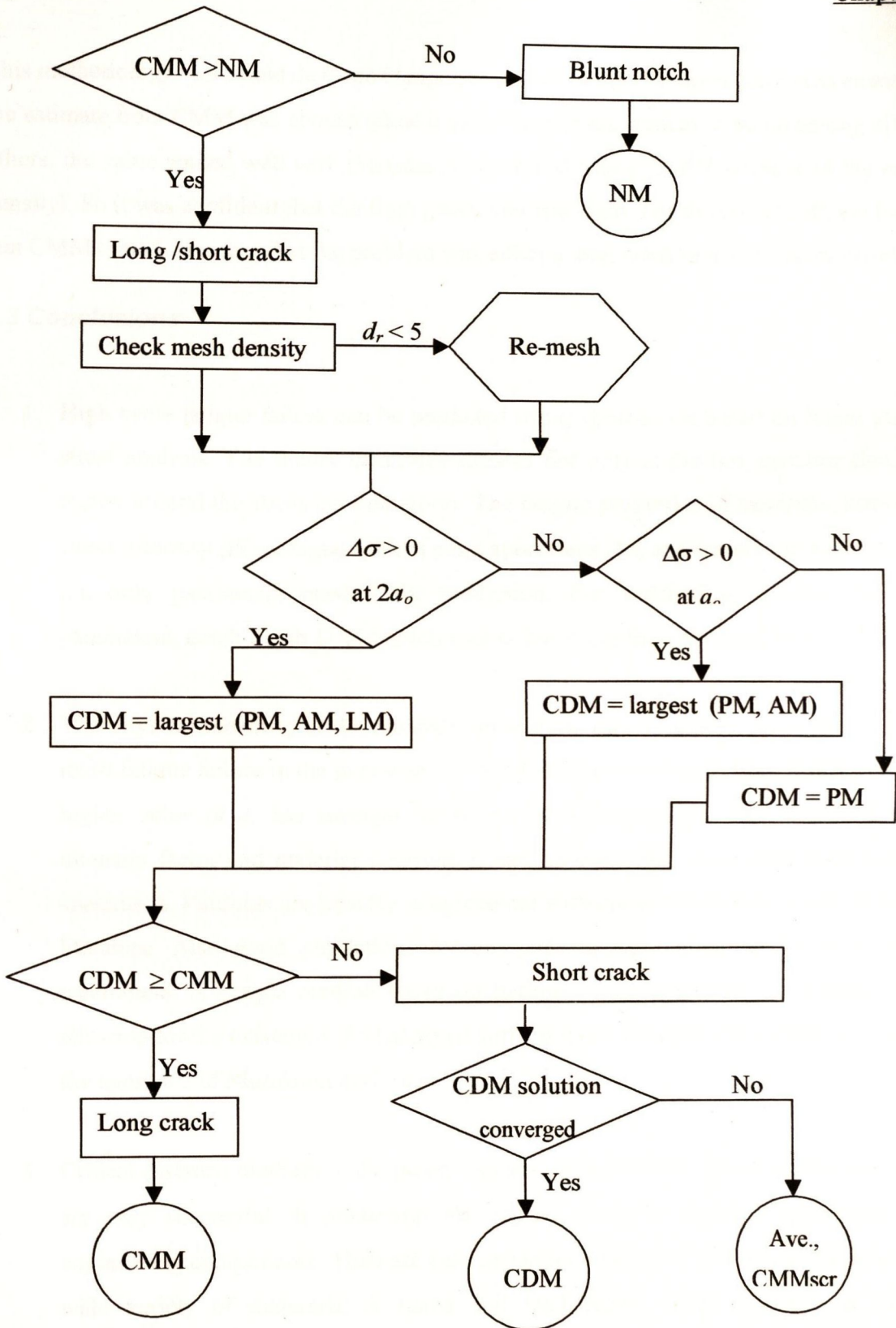


Fig. 8.2.1 Schematic illustration of the general methodology

This methodology was tested on these components. Taking the C-shaped bracket as example, the estimate from CMM was chosen since it gave the highest prediction value among all the others; the value agreed well with the estimate from LM (not with PM because of the mesh density). So it was confident that the final prediction was right. For the crankshaft, we found that $CMM > NM$, meaning that the problem was either a long crack or a short crack problem.

8.3 Conclusions

1. High cycle fatigue failure can be predicted using approaches based on linear elastic stress analysis. The theory examines stresses not only at the hot spot but also in a region around the stress concentration. The fatigue properties of materials, threshold stress intensity ΔK_{th} , fatigue limit of plain specimens $\Delta\sigma_o$ and material constant a_o , are the only parameters needed for prediction. For notched specimens, the two parameters, notch depth D and notch root radius r , are the only significant variables.
2. The physical meaning of the material constant a_o can be expressed as the ability to resist fatigue failure in the presence of a notch or stress concentration. A material with higher value of a_o has stronger resistance of fatigue failure. The threshold stress intensity factor and material constant a_o can be estimated using data from notched specimens. Findings are broadly in agreement with conventional test results from the literature. Also good predictions for components were obtained by using these parameters. A simple method based on hardness measurements was successful in allowing for the existence of a hardened surface layer. This provides some support for the approach of Murakami and Endo.
3. Critical distance methods – the point, line and area methods, based on the use of a_o , are very successful in predicting the fatigue limits of notched specimens and engineering components. They are able to handle notches of all sizes and shapes in a wide variety of materials, R ratios and load types. They are able to handle components with complex geometry as well. The only disadvantage of the point

method is the need for a relatively fine FE mesh and the disadvantage of the line method is the limitation on thin sections subjected to bending loads.

4. The crack modelling method is not sensitive to the path orientation, minimum distance, maximum distance and finite element mesh density. The path of the stress-distance curve should be normal to the maximum principal stress direction and the rule of lowest ΔK_{FE} can be used to find the path in complex situations. Any reasonable mesh density will make a reliable ΔK_{FE} possible.
5. The crack modelling method can be used for the short crack/notch problem after revision. Several modifications make the method available for different situations, such as different geometry and loads. Revised methods showed a good agreement with several sets of experimental data. Among them the average method is applicable on not only notched specimens but also engineering components with complex geometry. The method does not require special FE models or the material constant a_0 . A disadvantage of the method is that it is only suitable for the short crack problem.
6. A general methodology was developed, which uses the advantages of each methods mentioned in this research. The methodology is supposed to be used commercially for predicting the fatigue failure on engineering components subjected to high-cycle fatigue loads. The methodology considers every possibility which could be met when applying it to engineering components. The initial testing of the methodology has shown promising results.

References

ASME, 1989, *Boiler and Pressure Vessel Code*, Section 8, Rules for Construction of Pressure Vessels, New York: ASME.

ASTM Standards, of Annual Book, 1980, "Constant-Amplitude Low-Cycle Fatigue Testing", Part 10, Philadelphia, PA: ASTM E606-80

Brown, M.W. and Miller, K.J., (Editors), 1989, *Biaxial and multiaxial fatigue*, Mechanical Engineering, EGF publication.

Bueckner, H. F., 1970, A novel principle for the computation of stress intensity factors, *ZAMM* Vol. 50, No. 9, pp.529-546

Chermahini, R. G., et al., 1988, Three-dimensional finite-element simulation of fracture-crack growth and closure, in *Mechanisms of Fatigue Crack Closure* (Edited by J.C. Newman, Jr and W. Elber), *ASTM STP 982*, pp. 398-413

Chermahini, R. G., et al., 1989, Three-dimensional aspects of plasticity-induced fatigue crack closure, *Engng Fract. Mech.* **34**, pp. 393-401

Chermahini, R. G., et al., 1993, *Int. J. Fatigue* **15**, pp. 259-263

Chien, C.-H. and Coffin, L. F., 1998, A new method for predicting fatigue life in notched geometries, *Fatigue Fract. Engng Mater. Struct.*, **21**, 1-15

Dowling, N.E., Brose, W.R. & Wilson, W.K., 1977, Notched member fatigue life predictions by local strain approach, In *Fatigue under Complex Loading – Analysis and Experiments*, Warrendale: Society of Automotive Engineers, pp.55-84

Dugdale, D. S., 1960, Yielding of steel sheets containing slits. *J. Mech. Phys. Solids* **8**, pp.100-104

DuQuesnay, D. L., Topper, T. H. and Yu, M. T., 1986, The effect of notch radius on the fatigue notch factor and the propagation of short cracks, *The Behaviour of Short Fatigue*

Reference

- Cracks* (Edited by K. J. Miller and E. R. de los Rios), Mechanical Engineering Publications, London, pp.323-335
- Elber, W., 1970, Fatigue crack closure under cyclic tension, *Engineering Fracture Mechanics*, Vol. 2, pp. 37-45
- ElHaddad, M.H. and Miettinen, B.I, 1982, Fatigue thresholds (editors: J.Backlund, A.F.Blom and C.J.Beevers), **2**, 827
- ElHaddad, M.H., Dowling, N.F., Topper, T.H. and Smith, K.N., 1980, *Int. J. Fract.* Vol.16, pp.15-24
- ElHaddad, M.H., Dowling, N.F. and Topper, T.H, 1979, *J. Engng. Mater. Techn.*, **1**, 42
- ENDO, M., 1991, Fatigue Strength Prediction of Nodular Cast Irons containing small defects, *ASME Materials Division*, Vol. 28, *Impact of Improved Material Quality on Properties, Performance, and Design*, pp.125-137
- Frost, N. E., 1959, A relation between the critical alternating propagation stress and crack length for mild steel, *Proc. Inst. mech. Engrs.* **173**, 811-834.
- Frost, N. E., Marsh, K. J., and Pook, L. P., 1974, *Metal fatigue*. Oxford University Press, Ely House, London W.I, pp.130-156.
- Harkegard, G., 1981, An effective stress intensity factor and the determination of the notched fatigue limit, *Fatigue Threshold: Fundamental and Engineering Applications*, Vol. II (Edited by J. Backlund, A.F. Blom and C. J. Beevers), Chameleon Press Ltd. London, U.K., pp. 867-879.
- IKAWA, K. and OHIRA, G., 1967, Fatigue Properties of Cast Iron in Relation to Graphite Structure, *AFS Cast Metals Research Journal*, pp.11-21
- Irwin, G. R. J., 1957, *Appl. Mech. Tran. ASME*, **24**, 361.
- Kitagawa H. and Takahashi S., 1976, Applicability of fracture mechanics to very small cracks or the cracks in the early stage, *Proceedings of the Second International Conference on Mechanical Behaviour of Material*, Boston, pp.627-613

Reference

- Klesnil, M. K., and Lucas, P. L., 1980, *Fracture of Metallic Materials*, Elsevier, Amsterdam.
- Lukas, P., Kunz, L, Weiss, B and Stickler, R. 1986, Non-damaging notches in fatigue, *Fatigue Fract. Engng Mater. Struct.* **9**, 195-204.
- McClung, R. C., 1999, Finite element analysis of fatigue crack closure: a historical and critical review, *Fatigue 99*, China, publ. Higher Education Press (China) and EMAS (UK), **1**, pp. 495-502
- Miller, K. J. and Zaxhariah, K.P., 1977, *J. Strain Analysis*, Vol. 12(4), pp. 262-270
- Miller, K. J. and Rios, E. R. de los, (Eds.), 1986, *The Behaviour of Short Fatigue Cracks* EGF Publication 1, MEP, Institution of Mechanical Engineers, London
- Miller, K.J., 1993, The two threshold of fatigue behaviour, *Fatigue Fract. Engng Mater. Struct.*, **16**, 931-939
- Miller, K.J., 1999, A historical perspective of the important parameters of metal fatigue; and problem for the nest century, *Fatigue 99*, China, publ. Higher Education Press (China) and EMAS (UK), **1**, pp. 15-39
- Mitchell, M. R., 1979, SAE/SP-79/448, Publ. Society of Automotive Engineers (USA)
- Murakami, Y. and Endo, M., 1983, *Eng. Fract. Mech.*, **17**, 1
- Murakami, Y. and Endo, M., 1986, Effects of hardness and Crack Geometries on ΔK_{th} of small cracks emanating from small defects, *The Behaviour of Short Fatigue Cracks*, EGF Pub. L (Edited by K. J. Miller and E. R. De los Rios), Mechanical Engineering Publications London, pp.275-293
- Murakami, Y. and Endo, M., 1986, Effects of hardness and crack geometries on ΔK_{th} of small cracks emanating from small defects, *J. Soc. Mater. Sci. Japan*, **35**, 395 pp. 911-917
- Murakami, Y. and Endo, M., 1994, Effects of defects, inclusions and inhomogeneities on fatigue strength, *Int. Journal of Fatigue*, Vol. 16, pp.163-182

Reference

- Murakami, Y., *et al.*, 1987, Stress intensity factors handbook, Oxford, Pergamon.
- Murakami, Y., Kodama, S. and Konuma, S., 1989, Quantitative evaluation of defects of non-metallic inclusions on fatigue strength of high strength steels, *Int. Journal of Fatigue*, Vol. 11, pp. 291-307
- Neuber, H., 1958, *Theory of notch stresses*, Publ. Society, Berlin
- Newman, J.C. Jr., 1974, Finite-element analysis of fatigue crack propagation -- including the effects of crack closure. Ph. D Thesis, Virginia Polytechnic Institute And State University, Blacksburg, VA
- Newman, J.C. Jr., 1981, A crack-closure model for prediction fatigue crack growth under aircraft spectrum loading. *Methods and models for predicting fatigue crack growth under random loading*, Edited by J.B. Chang and C. M. Hudson, ASTM STP 748, pp. 53-84
- Newman, J.C. Jr., 1982, A nonlinear fracture mechanics approach to the growth of small cracks, *For presentation a the AGARD Specialists Meeting on Behavior of Short Cracks in Airframe Components*, Toronto, Canada
- Newman, J.C. Jr., 1994, A review of modeling small-crack behavior and fatigue-life predictions for aluminum alloys, *Fatigue Fract. Engng Mater. Struct.* Vol. 17, No. 4, pp. 429-439
- Paris, P. G. and Endoyan, F., 1963, A critical approach to crack propagation laws, *Trans. ASME, J. Eng. Ind.*, **85**, 528
- Peterson, R.E., 1953, *Stress Concentration Design Factor*, New York: John Wiley
- Peterson, R.E., 1959, Notch sensitivity. In *Metal Fatigue* (Ed. G. Sines & J. L. Waisman) McGraw Hill (New York) pp.293-306
- Peterson, R.E., 1974, *Stress Concentration Factor*, New York: John Wiley
- Pluvinage, G., 1997 Notch effects in high cycle fatigue. In *Proceedings of the Ninth International Congress on Fracture (ICF9)*, Pulb. Pergamon, 1239-1250

Reference

- Qian, J. and Fatemi, A., 1996, Mixed mode fatigue crack growth: A literature survey, *Engineering Fracture Mechanics*, Vol. 55, No. 6, pp. 969-990
- Rice, J. R., 1968, A path independent integral and the approximate analysis of strain concentration by notches and cracks, *J. Appl. Mech.*, Vol. 35, pp.379-386
- Rice, R.C. ed., 1988, *Fatigue Design Handbook*, Warrendal, PA: Society of Automotive Engineers.
- Ritchie, R. O. and Lankford, J. eds. , 1986, *Small fatigue Cracks*, Metallurgical Society, UK
- Schijve, J., 1994, Fatigue predictions and scatter, *Fatigue Fract. Engng Mater. Struct.* Vol. 17, No. 4, pp. 381-369
- Sheppard, S.D., 1991, *Trans ASME* 113, pp.188-194
- Siebel, E. and Stieler M, 1955, Dissimilar stress distributions and cyclic loading. *Z.Ver.Deutsch.Ing.* **97** 121-131.
- Smith, R. A. and Miller, K. J., 1978, Prediction of fatigue regimes in notched components. *Int. J. Mech. Sci.* **20** 201-206
- Smith, R. A., 1977, *Int. Journal of Fracture*, **13**, pp. 717-720
- Smith, R. A., 1982, Fatigue thresholds - a design engineer's guide through the jungle, *Fatigue Threshold: fundamentals and engineering applications*, (Editors: J. Backlund, A. F. Blom, and C. J. Beevers) EMAS, UK, pp.33-41
- Smith, R. A. and Miller, K. J., 1978, *Int. J. Mech. Sci.*, **20**, pp.201-206
- Smithells, Colin J., Brandes, Eric A., and Brook, G. B., 1992, *Smithells Metals Reference Book*, 7th ed, Oxford: Butterworth-Heinemann
- Suresh, S. & Ritchie, R. O., 1984, Propagation of short fatigue cracks. *International Metal Review* Vol. 29, pp.445-76.
- Suresh, S., 1991, *Fatigue of Materials*, Cambridge University Press, pp. 292-313

Reference

- Tanaka, K. and Akimiwa, Y., 1987, Notch geometry effect on propagation threshold of short fatigue cracks in notched components. *Fatigue '87*, Vol. II (Edited by R. O. Ritchie and E. A. Starke, Jr.), Third International Conference on Fatigue and Fatigue Thresholds, pp. 739-748. Charlottesville, Va.
- Tanaka, K. and Nakai, Y., 1983, Propagation and non-propagation of short fatigue cracks at a sharp notch. *Fatigue Fract. Engng Mater. Struct.* **6**, 315-327.
- Tanaka, K., 1983, Engineering formulae for fatigue strength reduction due to crack-like notches, *Int. Journal of Fracture*, **22**, R39-R45.
- Taylor, D and Lawless, S., 1996, Prediction of fatigue behaviour in stress-concentrators of arbitrary geometry. *Eng. Fract. Mechanics*, Vol. 53, pp.929-939.
- Taylor, D and Wang, G. 1999, Component Design: The interface between threshold and endurance limit, *Fatigue Crack Growth Thresholds, Endurance Limits, and Design, ASTM STP 1372*, J.C.Newman and R.S.Piascik, Eds., American Society for Testing and Materials, West Conshohocken, PA, US
- Taylor, D. and Knott, J.F., 1981, *Fatigue Fract. Engng Mater. Struct.* Vol. 4, p147
- Taylor, D. and M. O'Donnell, 1994, Notch geometry effects in fatigue: a conservative design approach, *Engineering Failure Analysis*, Vol. 1, No. 4, pp. 275-287
- Taylor, D. and Wang, G., 1999, A critical distance theory which unifies the prediction of fatigue limits, small cracks and notches, *Proc.Fatigue'99*, China, publ. Higher Education Press (China) and EMAS (UK), **1**, pp.579-584
- Taylor, D., 1989, *Fatigue Thresholds*, London: Butterworths
- Taylor, D., 1996, Crack modelling A technique for the fatigue design of components. *J. Engineering Failure Analysis*, Vol. 3, No. 2, pp. 129-136
- Taylor, D., Ciepalowicz, A. J., Rogers, P. and Devlukia, J., 1997, Prediction of fatigue failure in a crankshaft using the technique of crack modelling, *Fatigue Fract. Engng Mater. Struct.* Vol. 20, No. 1, pp. 13-21

Reference

- Taylor, D., Hughes, M. and Allen, D., 1996, Notch fatigue behaviour in cast irons explained using a fracture mechanics approach, *Int. J. Fatigue* Vol. 18, No. 7, pp. 439-445
- Taylor, D., Wang, G., Devlukia, J., Ciepalowicz, A. and Zhou, W., 1997, The analysis of stress concentrations in components: a modified fracture-mechanics approach, *Modern practice in stress and vibration analysis*, Gilchrist (ed.), Balkema, Rotterdam, pp. 355-358
- Taylor, D., Zhou, W., Ciepalowicz, A.J. and Devlukia, J., 1999, Mixed-mode fatigue from stress concentrations: an approach based on equivalent stress intensity, *Int. J. Fatigue*, **21**, 173-178
- Ting, Jason C. and Lawrence, Frederick V., Jr., 1993, A crack closure model for predicting the threshold stress of notches, *Fatigue Fract. Engng Mater. Struct.* Vol. 16, No. 1, pp. 93-114,
- Topper, T.H., Sandor, B.I. and Morrow, J., 1969, Cumulative damage under cyclic strain control, *Journal of Materials* **4**, 189-99
- Wang G, Taylor D, Ciepalowicz, A. and Devlukia, J., 1999, Prediction of fatigue failure in cast aluminium alloy components using the crack modelling method, *Proc. Fatigue'99*, China, publ. Higher Education Press (China) and EMAS (UK), **2**, pp.735-740
- Wang, G., Taylor, D., Bouquet, B., Ciepalowicz, A. and Devlukia, J., 1999, Prediction of Fatigue Failure in a Camshaft Using the Crack Modelling Method, *Journal of Engineering Failure Analysis*, (In press).
- Westergaard, H. M., 1939, Bearing pressures and cracks, *J. Appl. Mech.* A, pp.49-53.
- Wieghardt, K., 1995, On splitting and cracking of elastic bodies, *Fatigue Fract. Engng Mater. Struct.*, Vol. 18, pp.1371-1405 (translated from *Z. Mathematik und Physik*, 1907, Vol.55 (1-2), pp.60-103.
- Wu, X.R. and Newman, J.C. Jr., 1993, A small-crack effect assessment for 7075-T6 and LC9cs aluminium alloys, *Fatigue* **93**, pp.371-376

Reference

Yu, M. T., Topper and Au, P., 1984, The effects of stress ratio, compressive load and underload on the threshold behavior of a 2024-T351 aluminum alloy, *Fagugue '84* (University of birmingham, UK), Vol. 1, pp.179-186.